BAPVC BAY AREA PHOTOVOLTAIC CONSORTIUM

Bay Area Photovoltaic Consortium Project Catalogue 2016

Acknowledgment: "This material is based upon work supported by the Department of Energy through the Bay Area Photovoltaic Consortium under Award Number DE-EE0004946.

Cover Photos: Thomas Hymel and Ruby Lai, graduate students in the Yi Cui Group at Stanford, are handling silicon while using an ALD (atomic layer deposition) machine in the process of an experimental silicon solar cell fabrication *(cover image)*. Ruby Lai, graduate student and Hye Ryoung Lee, postdoc, members of the Cui Group *(back cover)*.

BAPVC Project Catalogue

2016

BAPVC Member Companies

SUNPOWER®

ALTADEVICES

Sivapower

TABLE OF CONTENTS

Introduction

Yi Cui, Co-Director Stanford
Ali Javey, Co-Director U. C. Berkeley
John Benner, Executive Director

About the Bay Area Photovoltaic Consortium (BAPVC)
BAPVC is a consortium led by Stanford University (SU) and University of California Berkeley (UCB) joined by three leading DOE labs—Lawrence Berkeley National Laboratory, SLAC National Laboratory, and the National Renewable Energy Lab. BAPVC's success is attributed to its three pillars of support.

Three Pillars

- **Industry** sets research agenda, assures relevance, provides path to commercial impact, contributes funding
- **Universities** and **National Labs** conduct innovative research, provide workforce development
- **US Department of Energy** provides leadership, support and guidance

The consortium is funded by the U.S. Department of Energy, industry members and the participating universities. DOE provided an initial funding of $25 million over five years (2011–2016) as part of the SunShot Photovoltaic Manufacturing Initiative (PVMI) to provide a source of research funding for all universities across the United States. During the past year, this award was extended by 18 months through December 31, 2017 with the addition of $2 million funding.

BAPVC provides a vibrant forum for interaction among PV industry and academic experts to address the critical challenges in converting the U.S. leadership in PV R&D into leadership in PV manufacturing. Our thesis is that great innovation is more likely stimulated by the collective efforts of manufacturing and academic experts working together rather than direction from either community alone. In BAPVC, industry members deliver far more than guidance and advice, they are part of the management team. They review and down select proposals, review projects, and guide the university researchers is setting their research directions. The success of this approach is highlighted by the industry members in the guidance document they delivered for the current phase of BAPVC research:

> "The Bay Area Photovoltaic Consortium (BAPVC) has created the premier platform in the U.S. for collaboration between leading academic researchers and U.S. manufacturers in the photovoltaics (PV) field. The Industry Board attests that academic researchers value and trust the guidance provided by industry representatives, and respond constructively to its inputs. The Industry Board sees a high value in continuing this platform beyond the expiration of its current funding in 2016."

University-focused contributions to the goal of building a robust U.S. PV industry must be differentiated from other public and private programs to identify those aspects of the problem that universities are particularly well suited to solve. BAPVC achieves this by maintaining balance in the management between industry and university members. In this way, BAPVC conducts industry-relevant research and development that will impact high-volume PV manufacturing, produce a highly trained workforce, and speed up commercialization of cutting-edge PV technologies. BAPVC will develop and test innovative new materials, device structures, and fabrication processes necessary to produce cost-effective PV modules in

high volumes. The research aims to find technologies which can increase photovoltaic conversion efficiencies and simultaneously reduce manufacturing cost. Success in research is measured by transfer of the technologies for development in industry. In short, BAPVC conducts research and development in universities to produce technologies that industry members will use.

BAPVC Mission: Impactful research for a strong US PV industry

While many organizations likely share a similar mission, BAPVC is differentiated is several ways. First, as highlighted by the industry members, BAPVC has established an innovative and unique industry-university partnership that assures pragmatic relevance while maintaining academic freedom. On the research side, BAPVC is unique in its access to all U.S. Universities via annual national competitive procurements. Building on the capabilities of the founding research members – Stanford University, UC Berkeley, LBNL, SLAC, NREL – BAPVC engages an extraordinary PV community comprised of many of the nation's top researchers and most forward-thinking companies. It is the membership and participation of these leading companies that builds a strong research portfolio as they guide the technology scope, select projects and review progress. Finally, the administration of the program is very efficient in large part due to the selection of top talent for performing research and participation of leading industrial scientists to review progress. Most of the funding, both from DOE and industry members, supports research. With staff of only the Executive Director and only 0.5 grant administrator and 0.5 administrative assistant, 90% of revenues flow to research projects.

Just as the three pillars support BAPVC's success, the benefits of this success flow back to each. Corporate Members set the research agenda to focus on their needs. This provides accelerated access to innovative and impactful research; similar access for recruiting the students performing that research; and, networking with other corporate members, DOE, and National Labs. Universities and National Labs not only gain access to the financial support for research, but also access to PV industry and DOE insight on challenges, opportunities, and constraints that improves the relevance of their research. The early participation from corporate members provides a path to commercialization. The U.S. Department of Energy benefits directly from being a part of this remarkable government-industry-university partnership and the impactful research it produces. DOE also gains access to thought leaders who can help to define, communicate, and execute a national renewable energy agenda.

BAPVC Technical Scope

BAPVC projects have aggressive goals set to develop disruptive technologies. Such projects frequently present multi-faceted challenges needing collaborative, consortium-sized efforts to advance to the next technology readiness level. BAPVC brings together materials scientists, device engineers, manufacturing specialists and equipment suppliers to capture the revolutionary advantage of our technologies.

BAPVC research is composed of the following thrusts: 1) High performance and multijunction cells; 2) Silicon absorbers and cells; 3) Thin film absorbers and cells; 4) Photon management and transparent conductors; and, 5) Encapsulation and reliability. This catalogue includes a brief description of the thrust strategy followed by the annual reports for relevant projects.

BAPVC Research Agenda

BAPVC's industry members developed guidance for the next phase of BAPVC research that places much greater emphasis on exploration of technologies that will reduce the CapEx of PV manufacturing. New technologies with very low CapEx and production cost, based on defensible intellectual property created in the U.S., will enable renewed growth of a sustainable and competitive domestic PV manufacturing industry.

Research will focus on the development of PV devices, materials, manufacturing methods, and understanding of reliability that enable disruptively-lower costs and rapid scaling. A reduction in capex has extra leverage toward these goals because it reduces costs, enables cash-flow-positive growth at lower margins, and enables old-technology-capacity to be replaced by new capacity thus accelerating industry progress. High reliability and confidence in the reliability is required to be able to scale a new technology and have that product be financeable at low interest rates. A module which addresses these needs would have the following characteristics as targets:

- Very low CapEx intensity (target <$0.25/$W_p$ p.a.)
- High conversion efficiency (target >20%)
- Very low product manufacturing cost (<$0.25/$W_p$)
- Excellent environmental profile
- Long module lifetime (>35 years) with low degradation (target < 0.2%/year)

Achieving these goals requires new structures and approaches from those in production or in near term development within industry. Pathways to reaching these goals encompass research on both the traditional as well as new material classes that can challenge the dominance of incumbent PV technologies. Industrial R&D, in the face of decreasing profit margins, is confined by a 5-year development horizon to incremental improvements of the incumbent technology. BAPVC's industry members bring industrial expertise to the consortium to increase academic researcher's understanding of manufacturability. Guidance from industry assists BAPVC to identify avenues of investigation just beyond industry's own mission critical research while avoiding technologies that have been tested and discarded in the course of proprietary industrial research. BAPVC established a strong community that has bridged these two groups and created a working platform that enables truly disruptive research – performed in the leading academic and National laboratories, under the guidance of US PV companies.

High levels of teaming with good synergy and efficient organization will be required to meet these goals. Many BAPVC investigators are engaged in teamed efforts that crosscut the original five technology thrusts and thus are prepared to address these grand challenges.

Thrust: High Performance and Multijunction Cells

Key Challenges

The goal of this thrust is to explore new growth processes, material systems, and device architectures for offering high device efficiencies at low processing costs. In particular, two parallel approaches are being explored, one relying on reducing the processing costs of III-V single junction solar cells and the other exploring tandem device architectures based on Si bottom cells. The key challenge for the field is developing disruptive growth and processing technologies that would drastically lower the cost without sacrificing the device efficiencies. In parallel, tremendous opportunities are present in exploring tandem cells based on Si (or CIGS, CdTe, or III-V) bottom cells to enhance the efficiency of the existing PV technologies, but with careful consideration of the costs to ensure a balance approach is developed. Cost analysis, device modeling, and experiments are being performed in parallel in a collaborative manner to ensure success.

Existing Projects in our Thrust

- *High Performance, Low Cost, III-V Photovoltaics on Metal Foils,* Ali Javey (Berkeley)
- *Low Capex Solar Manufacturing Enabled by Perovskite Semiconductors,* Mike McGehee (Stanford)
- *Improving the Stability of Halide Perovskite Solar Cells by Atomic Layer Deposited Oxides,* Paul McIntyre (Stanford)
- *Integrated Approach to Fundamental Challenges in High-Performance Thin Film Photovoltaics,* Peter Bermel (Purdue)
- *Highly Mismatched GaSb-GaAs Thin Film Multijunction Solar Cells,* Seth Hubbard (RIT) and Diana Huffaker (UCLA)
- *Laser Liftoff of GaAs Thin-Films,* Bruce M. Clemens (Stanford)
- *Fast and Scalable Deposition of Crystalline MoOx for Si and III-V Photovoltaics,* Xiaolin Zheng (Stanford)
- *Ultra High Efficiency Thin Film Multi-junction Solar Cell,* Jim Harris (Stanford)
- *High Voc Solar Absorbers; the Missing Link for High-Efficiency, Spectral-Splitting, Solar Cells* Eli Yablonovitch (Berkeley)
- *Defect Identification and Mitigation in High-Lifetime Silicon Materials: Growth, Processing, Reliability,* Tonio Buonassisi (MIT)
- *Design Principles and Defect Tolerances of Silicon/III-V Multijunction Interfaces,* Tonio Buonassisi (MIT)

Potential New Areas of Interest

- More cost analysis of the explored research projects in collaboration with NREL. Currently 2-3 of the projects within the thrust have had cost analysis discussions with NREL. More projects can follow this path.
- Exploring the device processing and manufacturability of the new III-V growth technologies, such as the thin-film VLS process.

- Exploring surface passivation effects and back-contact reflectors for the new III-V growth technologies, such as the thin-film VLS process.
- Better understanding (experiments and modeling) of the types of defects that their correlation to performance for the new III-V growth technologies, such as the thin-film VLS process.
- Development of high bandgap (III-V, II-VI, perovskite or other) solar cells for performance in tandem devices
- Defect mitigation during silicon cell fabrication, for improved multijunction bottom-cell performance.
- Defect recognition and characterization in high-quality Czochralski silicon for high-efficiency PV devices.
- Light management in tandem and other high performance solar cells.
- Development of tunnel junctions, recombination layers, polymer electrolytes, or other transparent contacts that will enable current matching between silicon solar cells and a high bandgap solar cell.

BAPVC Annual Project Report

Project Title: High Performance, Low Cost, III-V Photovoltaics on Metal Foils
PI: **Ali Javey**
E-mail: ajavey@berkeley.edu

Summary:

Two main research directions were pursued under this project title: *1. Simple InP solar cells based on low-cost vapor-liquid-solid (VLS) growth; and 2. alternative contacting strategies for high efficiency c-Si solar cells.*

- **InP VLS cells**
  The VLS process allows the growth of large grain InP thin films on low-cost substrates with optoelectronic properties approaching those of epitaxial grown layers, enabling the fabrication of low cost InP thin-film solar cells with efficiencies >12%.

- **Dopant-free contacts for c-Si solar cells**
  Commercially available silicon solar cells utilize doped silicon layers to collect electrons and holes - an approach which is hindered by a number of optoelectronic losses. This project involves the trial an integration of other materials, for example metal oxides and alkali metal salts, as a substitute for the doped silicon layers – which do not incur the same losses.

Key Accomplishments:

In the realm of thin-film InP PV, the group has developed further methods for improving dopant profiles and microscale localized process control, implementing methods for in-situ doping of thin-films via phosphorization with spin-on diffusants as part of the required cap structure. The method demonstrates control over doping on the micron scale, through the growth of single crystal domains in close proximity that display high concentrations of both holes and electrons. (Figure 1). The optoelectronic quality of the material grown with in-situ doping via this method is comparable to single crystal wafers, and the material can be grown easily on an amorphous substrate with a nucleation layer or on metal substrates for direct cell contacts.

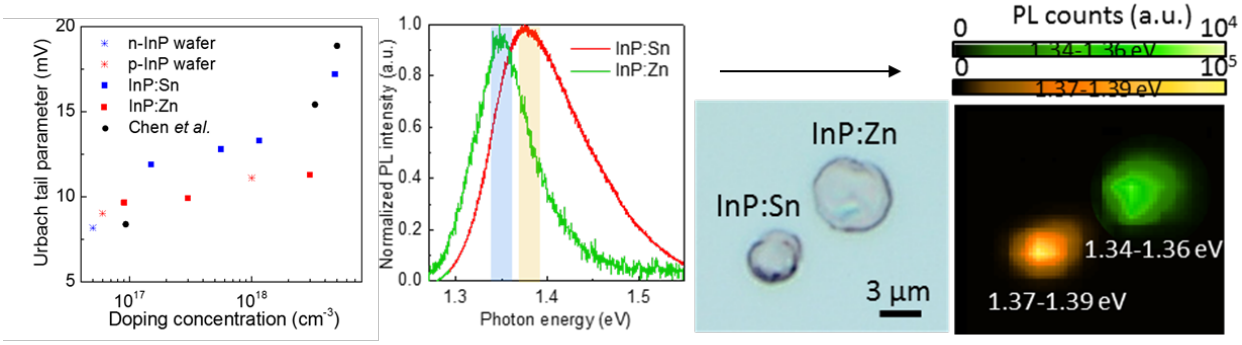

Figure 1. Demonstration of co-doping with a single growth run, via PL mapping and a Burstein-Moss shift. Urbach tail parameter of p- and n-type material with varied doping concentration, close to wafer values.

Under the research topic of alternative carrier-selective contacts for c-Si solar cells, a number of advances were made within 2016. Firstly, a low work function LiF based electron contact was developed to compliment the group's existing high work function MoOx based hole contact (See Figure 2). These advancements led to the development of high efficiency dopant free asymmetric heterocontact (DASH) silicon solar cells with efficiencies close to 20% - the first of their kind to demonstrate competitiveness with conventional processes. This low resistivity LiF based contact also allowed the fabrication a novel n-type partial rear contact cell (with an efficiency above 20%) without the need for localized phosphorus doping.

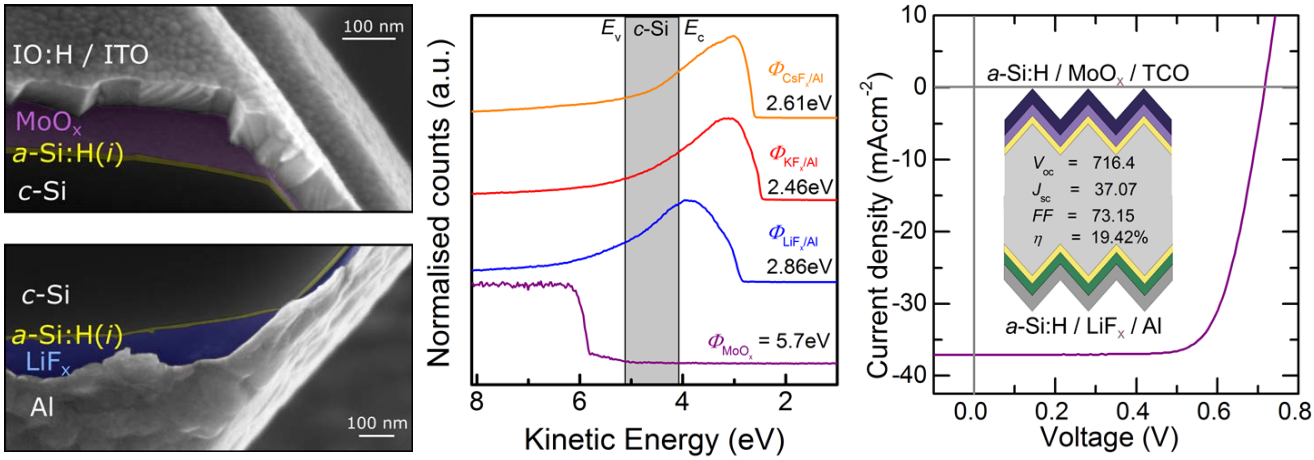

Figure 2. Cross section, contact work function measurements and *JV* curve of the DASH solar cell.

Future Work:

For further advances in high efficiency InP thin-film solar cells, the group will focus efforts on leveraging doping and process control methods required to fabricate more advanced structures on higher quality n-body films, that can obtain high theoretical V_{oc}.

As for selective-contact development, future research will focus on advancing towards a higher efficiency second generation DASH cell structure whilst simultaneously investigating the thermal and humidity stability of selective-contact candidates.

BAPVC Annual Project Report

Project Title: Low Capex Solar Manufacturing Enabled by Perovskite Semiconductors

PI: Michael McGehee (Stanford University)
coPIs: Zach Holman (Arizona State University), Paul McIntyre (Stanford University)
E-mail: mmcgehee@stanford.edu

Summary:

The team has dramatically improved the long-term stability of perovskite solar cells with the composition ABX_3, where A is a mixture of methyl ammonium (MA), cesium or formamidinium (Fa), B is a mixture of Sn and Pb and X is a mixture of Br and I by reducing the use of methyl ammonium, replacing metal electrodes with indium tin oxide and packaging the cells between two sheets of glass with a rubber edge seal. Semitransparent perovskite solar cells have a power conversion efficiency of 17% and do not suffer efficiency loss after 1000 hours at 85°C and 85% humidity or after 200 cycles between 85°C and -40°C. Mechanically stacked four-terminal tandem solar cells and monolithic two-terminal tandem solar cells have efficiency greater than 23%.

Key Accomplishments:

Holman's team at ASU has fabricated heterojunction silicon solar cells specifically for use in tandem solar cells with high bandgap perovskite semiconductors. The silicon cell fabrication process was adjusted to tune the silicon cells to the infrared spectrum that they receive in the tandem, as well as for compatibility with the spin-coated perovskite top cells. In particular, the a-Si:H layers were slightly thickened to enhance passivation and carrier collection (the resulting visible parasitic absorption is not detrimental in tandems), an excellent rear reflector comprising a silicon nanoparticle (SiNP) / silver stack was implemented, and the front surface was polished to allow for top-cell spin coating (the rear surface remained textured as usual to provide light trapping in the silicon cell). Additionally, the front ITO layer, which acts as the recombination junction in the tandem, was thinned to reduce infrared parasitic absorption since it does not need to play the role of antireflection coating in tandems and because, unlike in a single-junction silicon cell, the lateral conductivity of the front electrode need not be high.

McGehee's team at Stanford has developed the most efficient and stable semitransparent perovskite solar cells in the world. They were one of several research groups to realize that stability can be improved by replacing methylammonium with combinations of cesium and formamidinium. Our best results (17 % efficiency with a Voc of 1.1 V) have been obtained with the compound $Cs_{0.17}FA_{0.83}Pb(Br_{0.17}I_{0.83})_3$, which has a bandgap of 1.6 eV.

The most important innovation that was required to make solar cells with the excellent sub- bandgap transparency that is needed when the cells will be used as the top cell in a tandem was to find a suitable buffer layer to protect the perovskite during sputtering of indium tin oxide. In collaboration with Stacy Bent's group we developed a process for using atomic layer deposition to put down 4 nm of conformal SnO_2. This layer makes it possible for us to deposit a 150-nm-thick ITO electrode with a sheet resistance of 30 Ω/□.

Our best perovskite on silicon tandem cell has a V_{OC} of 1.65 V, a J_{SC} of 18.1 mA/cm^2, and a *FF* of 79.0%, resulting in an efficiency of 23.6% with a 1 cm^2 aperture area and no hysteresis. These results have been validated by NREL.

With funding from another SunShot grant, McGehee has collaborated with DuPont to develop a process for packaging perovskite solar cells and demonstrated that these cells do not suffer from efficiency loss after 1000 hours at 85°C and 85% humidity. The research funded by BAPVC is putting an emphasis on degradation that might occur at interfaces. Towards this end, the team has performed thermal shock tests to see if delamination occurs due to the relatively low fracture energy reported by Dauskardt (another BAPVC PI). Eight out of nine solar cells retained > 90% of their efficiency after 200 cycles between 85°C and -40°C at D2 Solar. The fact that no visual delamination was observed and no severe efficiency loss occurred is very encouraging.

If part of a module becomes shaded and does not generate current, the unshaded parts of the module will build up a tremendous negative voltage that will try to pass current through the shaded solar cell. If this reverse current causes part of the solar cell to break down, the current in that region can be high and cause permanent damage. For this reason, the team has performed preliminary experiments to see what happens in reverse bias with perovskite solar cells and found that damage does occur at low voltages of only -1.5 V in devices with metal electrodes. The team cannot say for sure what happens at this time, but the working hypothesis is that metal migrates all the way through the perovskite forming a shunt. The team has not yet had the opportunity to find out what happens when indium tin oxide electrodes are used. The team will thoroughly investigate this problem and use McIntyre's expertise on making stable interfaces to fix it.

Future Work:

The biggest opportunity for improvement lies in improving the voltage of the perovskite solar cell. When the 23.6 % efficient tandem was made, the single-junction perovskite solar cells on glass only had a power conversion efficiency of 15.5% and a voltage of 0.9 V. A 26 % efficient tandem should be made by the end of 2016 using the better perovskite cells made in October. The team will try to increase the voltage by another 0.2 V by raising the bandgap of the perovskite to 1.8 eV, which is the ideal value, by increasing the cesium and bromine content. Some goals are to:

- Deposit smooth 800-nm-thick films of $Fa_xCs_{1-x}PbI_yBr_{1-y}$ that have a band gap of 1.8 eV.
- Determine which electrode and contact materials (e.g. Ag, Au, Ni, NiO, ITO, FTO, AZO) will be stable indefinitely when in contact with the perovskite films.
- Develop a process for sputtering ITO at Stanford and explore other TCOs at ASU.
- Seal the solar cells using ionomer encapsulants with impermeable front and back sheets with guidance from the DuPont team in Sunnyvale and the PV Reliability lab at ASU. Perform industry standard reliability tests at ASU.
- Understand reverse bias breakdown and make the devices stable at -10 V.

BAPVC Annual Project Report

Project Title: Improving the stability of halide perovskite solar cells by atomic layer deposited oxides
PI: Paul C. McIntyre
E-mail: pcm1@stanford.edu

Summary:
Low temperature ALD-grown TiO_2-Al_2O_3 alloy films can improve the stability of perovskite solar cells significantly. By adding TiO_2 to Al_2O_3 in a supercycle ALD process, the electrical conductivity of the alloy can also be tuned over a wide range, showing potential for stability with limited impact on solar cell performance.

Key Accomplishments:
The structure of the devices prepared and studied in this project is shown in Figure 1A. PCBM and a ZnO nanoparticle layer are spin-coated on top of a perovskite ($MAPbI_3$) absorber layer in order to protect it degradation during the ALD process. Low temperature ALD-grown TiO_2 was found to not reduce the performance of perovskite solar cells; however, the stability enhancement of the solar cells during subsequent testing at elevated temperatures and in air is limited. On the other hand, low temperature ALD-grown Al_2O_3 improves the stability of perovskite solar cells considerably, but it has a high electrical resistance because of its large band gap. By making TiO_2-Al_2O_3 alloys, stability and device resistance can be tuned. Improved stability of perovskite solar cells is indicated by the results in Figure 1B. The absence of a PbI_2 peak in the x-ray diffraction pattern after 15 days heating in air at 100°C is an important indication that the oxide alloy layer protects the perovskite from deprotonation. Moreover, the I-V characteristics of the device are encouraging, as evident in Figure 1C.

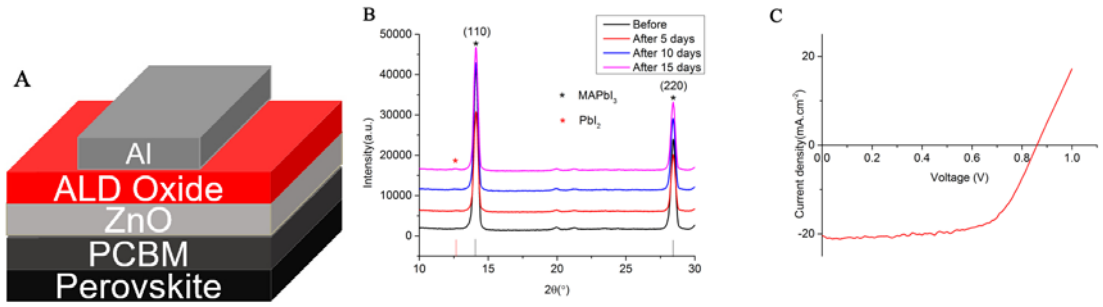

Figure 1 (A) Structure of the device. (B) XRD of perovskite with ALD protection layer in Muffle furnace which is set at 100 ℃ The control sample without ALD layer turns into PbI_2 after less than 1 day. (C) Forward bias to short circuit I-V curve of the best device fabricated before stability test. The Al:Ti ratio is about 1:3.

Future Work:
Future work will concentrate on optimizing the TiO_2-Al_2O_3 alloy composition to improve the stability and performance of perovskite solar cells. In addition, other perovskite systems (e.g. $Cs_{0.17}FA_{0.83}Pb(I_{0.83}Br_{0.17})_3$) and a larger range of ALD oxides will be considered in the future.

BAPVC Annual Project Report

Project Title: Integrated Approach to Fundamental Challenges in High-Performance Thin Film Photovoltaics
PI: Peter Bermel
Co-PIs: Mark Lundstrom, Ashraf Alam, Jeff Gray (Purdue University)
E-mail: pbermel@purdue.edu

Summary:
This project investigated two types of thin-film solar cells over the last year: vapor-liquid-solid grown indium phosphide heterojunction cells (in collaboration with Ali Javey), as well as thin-film cadmium telluride-based solar cells (in collaboration with Jim Sites).

Key Accomplishments:
VLS-grown indium phosphide cells from Ali Javey's group can be understood by collecting various characterization results (e.g., dark and light I-V measurements in Fig. 1), and establishing an HSPICE-based InP cell model, which can be used to accurately predict the I-V performance. It is likely that the degradation of the open-circuit voltage observed in experiment can be explained by features local to grain boundaries in TF-VLS grown InP solar cells.

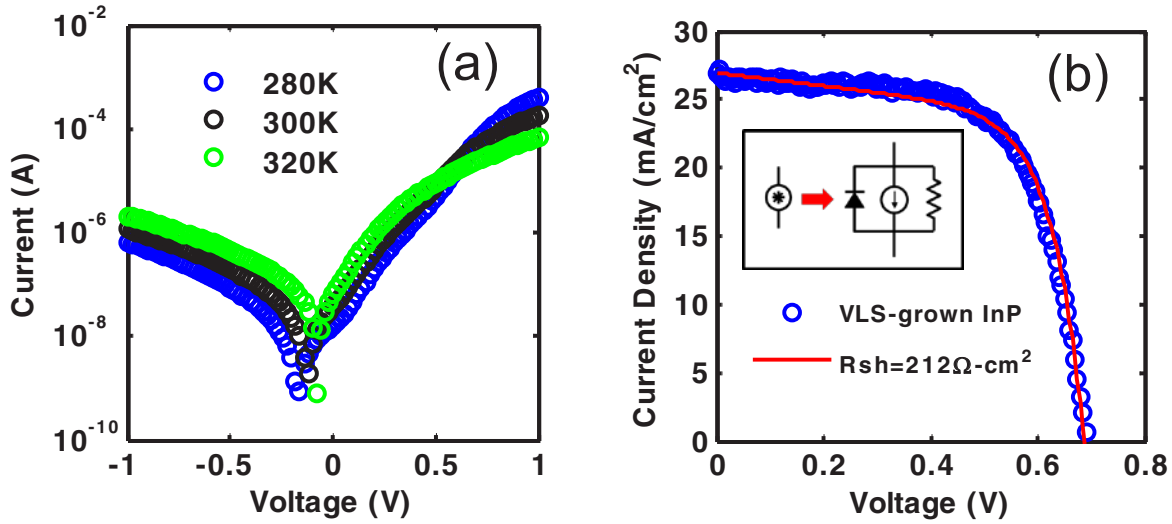

Figure 1: Measurements of VLS-grown InP solar cells: (a) Dark current versus voltage at 3 different temperatures; (b) Current versus voltage under AM1.5G solar spectrum (blue dots), compared to the model shown in inset (red line).

CdTe absorbers typically show very low radiative efficiency, generating relatively low PLE signals. Nevertheless, a PLE signal was successfully measured from a CdS/CdTe np heterojunction solar cell. Using numerical simulations combined with PLE, a recombination lifetime below 1 ns and an SRV between 10^5 and 10^6 cm/s were measured, which are consistent with previously published results for a crystalline CdTe wafer [1].

For the thin-film CdTe solar cell from Jim Sites group, an unusually-shaped PLE spectrum was measured (Fig. 2) that differs greatly from EQE measurements (Fig. 3). However, this unusual behavior can be explained precisely with detailed numerical simulations, which show that the observed peak is due to photon absorption in the CdS layer, followed by carrier diffusion and recombination at the junction. These results suggest that PLE may be a useful, contactless, in-line characterization tool for solar cells.

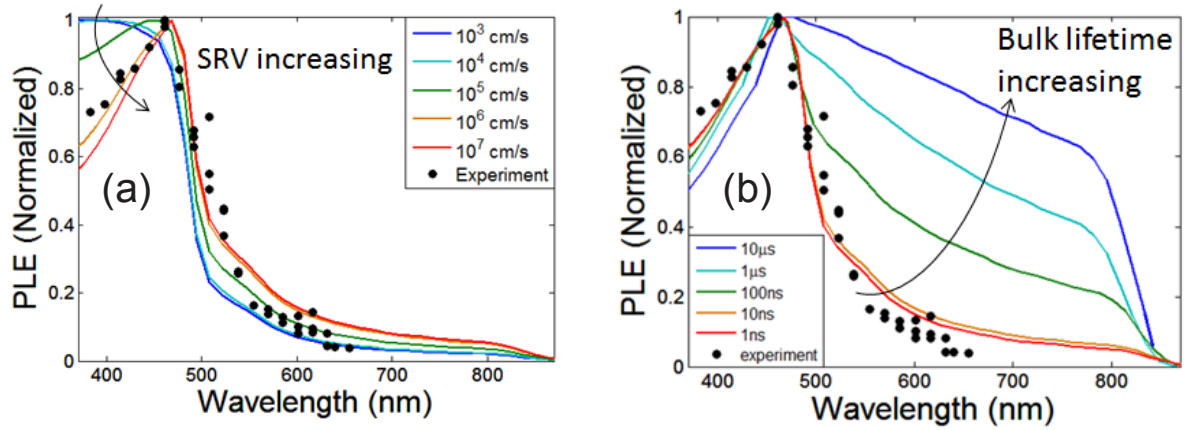

Figure 2: Measured photoluminescent excitation (PLE) spectrum (black dots) compared to: (a) Simulated PLE with different surface recombination velocities (color lines); (b) different bulk lifetimes in CdTe absorber layer (color lines).

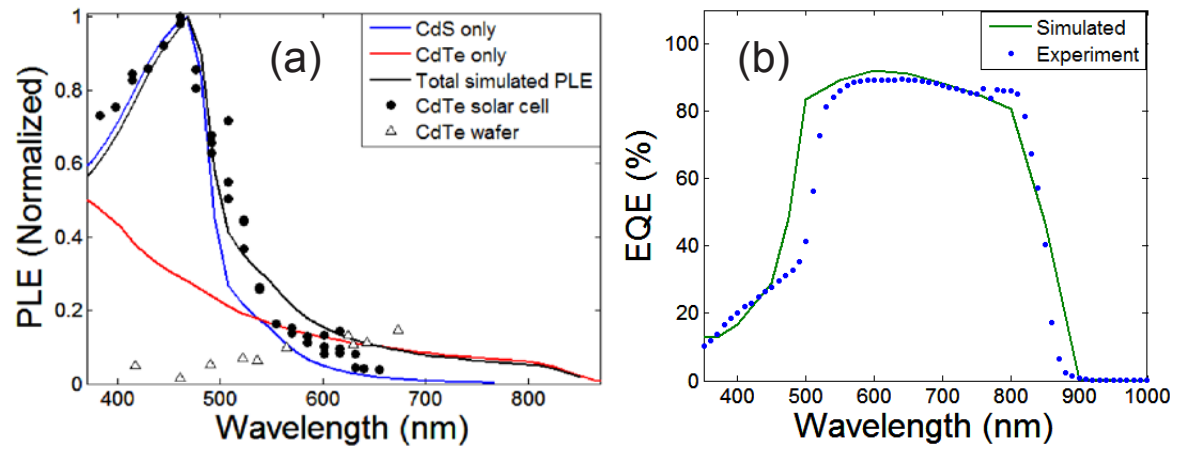

Figure 3: (a) Decomposition of simulated PLE with absorption of CdS only (blue line) and CdTe only (red line). The latter matches closely with CdTe solar cell PLE measurements (black dots). (b) Experimentally-measured EQE (blue dots) versus simulated EQE with same parameters (red line).

Future Work:

The next steps here include further experimental measurement of inhomogeneities and designing mitigation strategies to passive charged trap states in VLS-grown indium phosphide thin-films.

References:

[1] R. K. Ahrenkiel, S. W. Johnston, D. Kuciauskas, and J. Tynan, "Dual-sensor technique for characterization of carrier lifetime decay transients in semiconductors," *J. Appl. Phys.*, vol. 116, no. 21, p. 214510, Dec. 2014.

BAPVC Annual Project Report

Project Title: Highly mismatched GaSb-GaAs thin film multijunction solar cells
PI: Seth Hubbard (RIT) and Diana Huffaker (UCLA)
E-mail: smhsps@rit.edu, huffaker@ee.ucla.edu

Summary:

The interfacial misfit array (IMF) growth method can be used to grow the bottom subcell in multi-junction (MJ) Sb-based solar cells, with potential to eliminate the current standard metamorphic grade and open the door for 4-6 junction III-V solar cells with high efficiency (greater than 50%) and significantly lower manufacturing costs and capital intensity compared to current inverted metamorphic (IMM) technology. During this 1 year project, IMF was used to grow single junction GaSb solar cells on GaAs substrates as an initial study of the IMF technology. The IMF cell efficiency reached as high as 3.0% with a V_{OC} of 270 mV, compared to 5.8% and 370 mV for the homoepitaxial GaSb control cell. These results show excellent progress towards the goal of high-efficiency multijunction cells incorporating IMF GaSb.

Key Accomplishments:

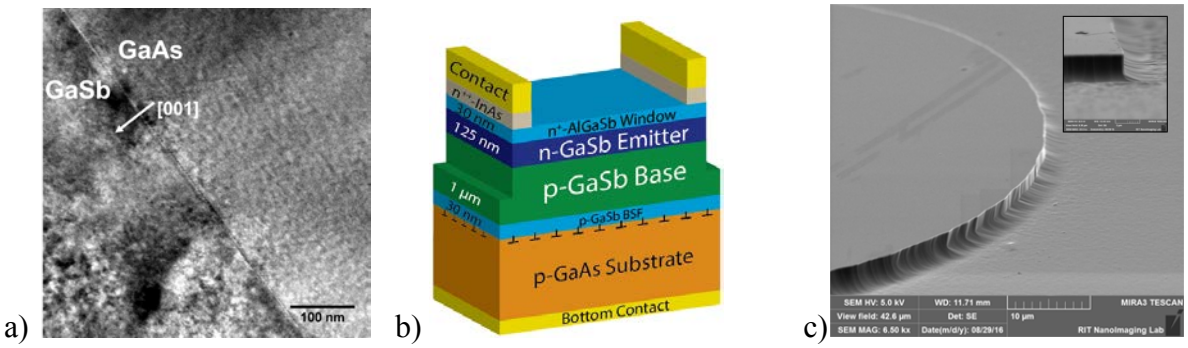

Figure 1: a) Cross sectional TEM of GaSb grown on GaAs using IMF growth method b) layer structure of the fabricated IMF solar cells. The inverted 'T' symbol represents the heteroepitaxial IMF layer. c) SEM image of a GaSb sidewall. The inset shows the sidewall profile of the etch.

GaSb single junction solar cells were grown heteroepitaxial on GaAs using IMF alongside homoepitaxial GaSb control cells. Figure 1a shows a cross-sectional TEM image of GaSb and GaAs. GaSb is fully relaxed at the interface and no threading dislocations are observed in the scanned area. Solar cells were designed, guided by modeling with Synopsys® Sentaurus™ TCAD and then grown via molecular beam epitaxy (MBE) in a Veeco Gen 930 solid-source reactor. The layer structure of the fabricated IMF cell is shown in Figure 1b. It is also well known that the GaSb native oxide forms nearly instantaneously upon exposure to air and consists of a mix of Ga and Sb oxide species and decomposed to elemental Sb, leading to sidewall shunting and surface recombination. In order to passivate the devices, a new wet etch solution had to be developed as etch solutions from the literature led to rough or scalloped device sidewalls. A citric acid, HF, and peroxide mixture was found to give consistent and smooth

sidewalls, as seen in Figure 1c. For passivation, a wet soak in ammonium sulfide after oxide removal in acidic solution has produced control cell shunt resistances of ~500 Ohm·cm^2, which is near the value needed to continue with a triple junction cell under 1 sun illumination.

Figure 2a shows 1-sun and concentrated AM1.5 light I-V results for the homoepitaxial and IMF solar cells (no anti-reflective coatings were used). At 1 sun, the homoepitaxial control cell was 5.8% efficient with a V_{OC} of 295 mV, which represents a high quality epitaxial GaSb solar cell. The W_{OC} (E_G-V_{OC}) for this device was 431 mV. The IMF cell was 0.7% efficient with a V_{OC} of 60 mV under 1-sun conditions, indicating the presence of non-radiative defects.

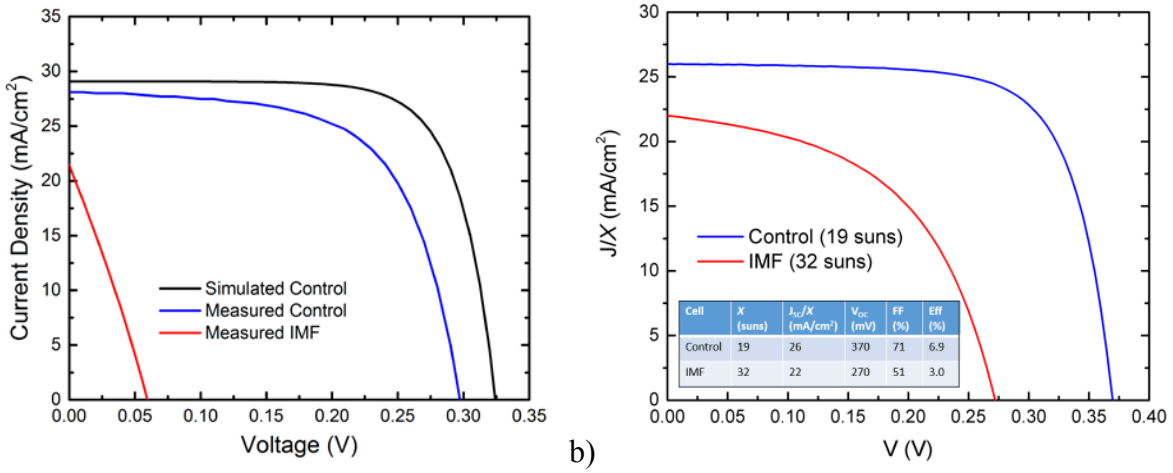

a) b)

Figure 2: Illuminated current-voltage results for the homoepitaxial and IMF cells under a) 1-sun AM1.5 illumination and b) mild concentration with current density normalized to 1-sun. No anti-reflective coatings have been used.

However, as seen in Figure 2b, the results improved significantly under mild concentration due to state filling at higher injection. At 19 suns, the GaSb control cell achieved 6.9% efficiency with an open-circuit voltage (V_{OC}) of 370 mV and a short-circuit current (J_{SC}) of 26 mA/cm^2. W_{OC} (E_G-V_{OC}) for this device was 356 mV. The IMF efficiency at 32 suns was 3.0% with a V_{OC} of 270 mV (W_{OC} of 456 mV), indicative of state filling as the predicted V_{OC} from dark current is 150 mV. To the group's knowledge, these results represents the highest reported efficiencies for both homoepitaxial and IMF GaSb solar cell to date and point to potential for application in an multijunction solar cells under mild concentration.

Future Work:

The group will continue to develop passivation methods for surface currents, including sidewall encapsulation by Al_2O_3 deposited via atomic layer deposition or by epitaxial regrowth of a high bandgap material. The IMF cell quality must be improved and the shunt resistance increased by an order of magnitude in order to be used in a multijunction cell at 1 sun intensity. Low temperature GaSb buffer layers will be incorporated to reduce bulk recombination in IMF samples. Alternatively, the IMF cells may be used under concentration as is or with slight improvements.

BAPVC Annual Project Report

Project Title: Laser Liftoff of GaAs Thin-Films
PI: Bruce M. Clemens
E-mail: bmc@stanford.edu

Summary: The group separated single-crystal InP thin-films from InP growth substrates using a process analogous to their work with GaAs except that an atomically coherent $In_{0.53}Ga_{0.47}As$ thin-film layer is used for the preferential infrared-laser absorber instead of $In_xGa_{1-x}As_yN_{1-y}$ ($x \approx 0.1$, $y \approx 0.04$). They found non-linear effects such as two-photon absorption reduce the energy deposited in the absorbing layer after the laser pulse has travelled through the single-crystal substrate. The group is addressing these effects by spatially-homogenizing the ~100 MW/cm^2 laser pulse, reducing the thickness of growth wafers, and using large-bandgap optical coatings to prevent plasma formation on the incident surface of the single-crystal substrate.

Key Accomplishments: Whereas this project initially focused on separating a GaAs epitaxial thin film from a GaAs substrate by selective excitation of a lattice-matched $In_xGa_{1-x}As_yN_{1-y}$ ($x \approx 0.1$, $y \approx 0.04$) interlayer with a near-infrared laser pulse, the group developed an analogous processs for InP (E_G=1.4 eV) using $In_{0.53}Ga_{0.47}As$ ($E_g \approx 0.8$ eV) as a coherently strained, single crystal absorbing layer for a Nd:YAG laser pulse. This process may be useful for production of InP-based solar devices, and furthermore the ease and reduced cost of synthesizing InGaAs, compared to InGaAsN, lends the system to research. InP single crystal thin-films have been transferred from their growth substrates to polymer substrates, and etching with engineered etch-stop layers (such as AlInAs) has been used to remove melt debris. These films have been cracked on the ~100 μm to 1 mm scale.

High-frequency spatial modes characteristic of the untreated ~1 J/cm^2 Nd:YAG laser pulses used for liftoff, as shown in Figure 1, can lead to points in the absorber remaining below the liftoff threshold which can mechanically stress and crack the film that is ejecting. Therefore, a pinhole spatial-homogenizer has been built which uses a vacuum chamber in conjunction with lenses and pinholes to filter out the high-frequency components of the laser for a Gaussian beam profile, but without leading to ionization losses characteristic of Nd:YAG pulses focused in air.

Non-linear absorption (NLA) in the InP substrate has a large effect on laser liftoff. Specimens which did not exhibit lift off with ~500 μm thick substrates have been shown to work by reducing this substrate thickness to 250 μm. The degree of NLA can be measured by comparing, pixel-by-pixel, the incident fluence and fluence transmitted through an InP wafer. Figure 2 shows the 2-D histogram for such a measurement. Despite incident fluences as high as 9 J/cm^2, transmitted fluences are not higher than 1 J/cm^2; increasing the incident fluence does not proportionally increase the fluence delivered to the absorbing layer.

The effects of non-linear absorption can be further reduced by depositing optical coatings, such as Al_2O_3, on the bottom of the substrate, shown schematically in Figure 3. Preliminary results indicate the addition of an Al_2O_3 coating reduces the damage to the InP substrate and increases the energy delivered to the absorber layer.

Future Work: Pinhole damage in the spatial-homogenizer will be addressed by modelling the laser pulse's propagation, transform, and masking in the spatial homogenizer to guide construction of a homogenizer that removes the high-frequency spatial components of the laser pulse without being irreversibly damaged after tens of laser pulses. This system will be used in conjunction with the Al_2O_3 coatings to maximize absorption and to minimize thermal gradients within the absorbing layer and ejected thin-film during liftoff, and therefore allow for the experimental determination of the minimum fluences and maximum crack-free areas for InP thin-film liftoff.

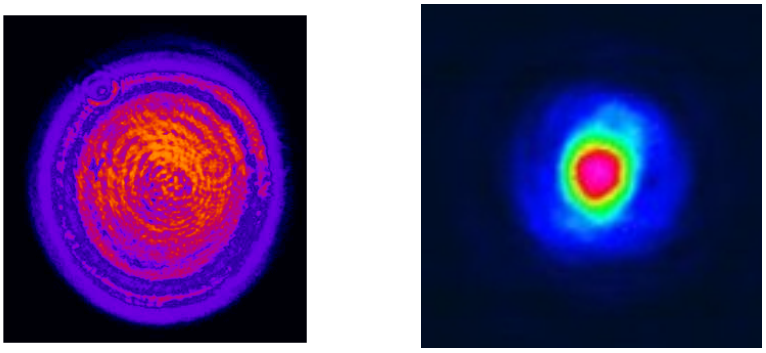

Figure 1: The untreated Nd:YAG pulse as imaged on a CCD. Higher order modes can be seen which lead to incomplete and uneven laser liftoff. The image on the right shows a pseudo-Gaussian profile obtained using a spatial filter.

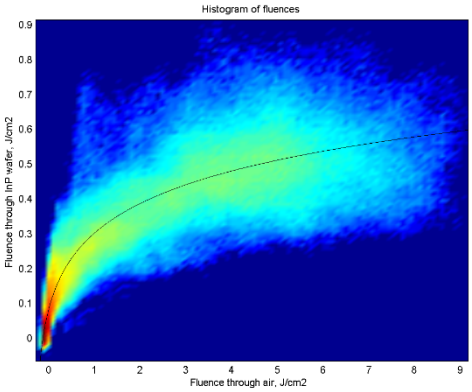

Figure 2: Histogram of fluences comparing two pulsed laser beam profiles: one through air, and one through an InP wafer. The black line is a possible fit for the data.

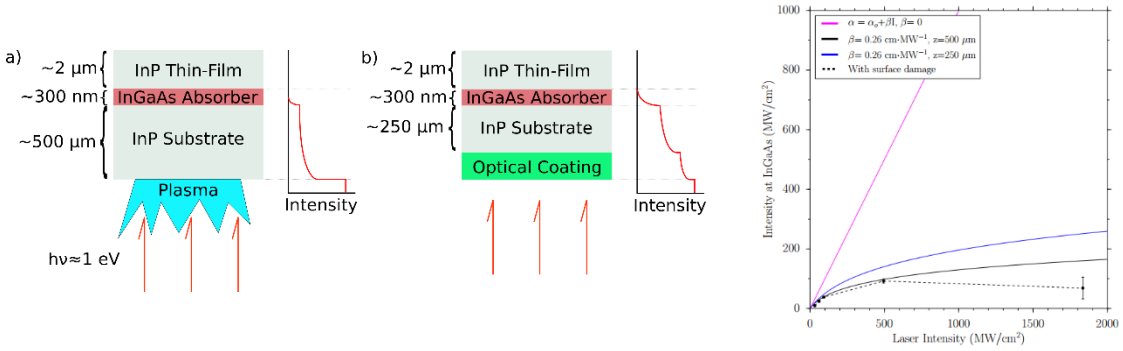

Figure 3: In a), an infrared laser pulse ($h\nu < E_{G,\,InP}$) is directed through the InP substrate and is absorbed in the InGaAs ($E_G \approx 0.8$), but energy is also absorbed via plasma and substrate TPA. In b), more energy is absorbed in the InGaAs because the optical coating prevents plasma formation and less TPA occurs in the thinner substrate. The right figure shows calculated and measured intensity at the InGaAs layer as a function of intensity at the substrate with no TPA, different substrate thicknesses (z), and experimental results above and below the plasma threshold.

BAPVC Annual Project Report

Project Title: Fast and Scalable Deposition of Crystalline MoOx for Si and III-V Photovoltaics

PI: Xiaolin Zheng, Mechanical Engineering, Stanford University
E-mail: xlzheng@stanford.edu

Summary:

High crystalline molybdenum oxide (MoO_3) can potentially enhance the performance of several solar cells currently investigated by BAPVC. Monolayer and few layers of crystalline MoO_3 thin film were successfully deposited by a low-cost flame-enhanced chemical vapor deposition technique in only 2 minutes. These flame-deposited MoO_3 film was demonstrated to be effective hole donors.

Key Accomplishments:

1. Monolayer and few layers of crystalline MoO_3 thin film were successfully deposited by a low-cost flame-enhanced chemical vapor deposition technique in only 2 minutes. The experimental setup for the flame synthesis of MoO_3 monolayer is schematically illustrated in Fig. 1a. The flame synthesis setup, from bottom to top, consists of a premixed flat flame burner, a molybdenum (Mo) metal mesh as the precursor source, and exfoliated thin Mica flakes supported on a Si/SiO_2 wafer as the growth substrate. The premixed flame provides O_2 and heat for the oxidation of Mo metal mesh and the evaporation of Mo oxide vapors. The Mo oxide vapors condense on the Mica/Si growth substrate placed downstream in the lower temperature region. In our setup, when we control the post-flame O_2 partial pressure to be low, monolayer crystalline MoO_3 is grown on top of the Mica surface with a growth time of 2 min. The SEM image (Fig. 1b) shows that large portion of the Mica surface (gray) is covered by MoO_3 (black) flakes. Further atomic force microscopy (AFM) measurement (Fig. 1c) shows that the as-grown MoO_3 layer has a uniform thickness of ~ 0.8 nm, which is a monolayer. Similarly, flame can be used to deposit WO_x thin film as well.

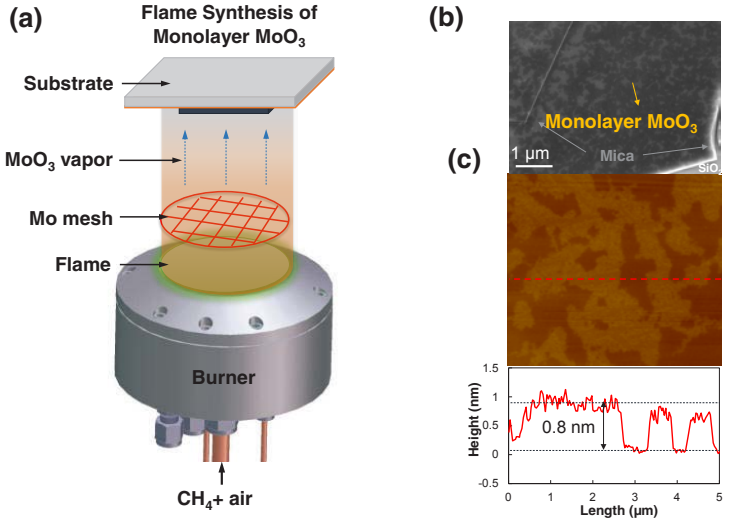

Figure 1. (a) Schematic of the experimental setup for flame synthesis of monolayer MoO_3. (b) SEM image and (d) AFM image of the monolayer MoO_3 on Mica. The AFM height profile shows that the thickness of MoO_3 is about 0.8 nm.

2. The flame-deposited MoO_3 film was shown to have lower contact resistance with Si wafers than flame-deposited WOx film. Specifically, we used the flame method to deposite MoO_x and WO_x thin films on Si (wafer resistivity = 0.5 Ohm·cm, wafer thickness = 0.04 cm) for a duration of 5 min. Then Pd/Al metal contact was deposited on top to extract the contact resistivity using the dot method (see Equation). Figure 2 shows that the extracted contact resistivity for MoO_x and WO_x are about 1.3 and 70.9 Ohm·cm^2, respectively.

The equation for the extraction method is as follows:

$R_{measure} = R_{contact} + R_{spread} = \rho_c/(\pi d^2/4) + (\rho/2d)B$**.**

$R_{measure}$ is the total measured resistance.

$R_{contact}$ is the resistance due to the potential barrier at the contact-semiconductor interface.

R_{spread} is the spreading resistance resulting from mental design, the current flow is perpendicular to current constriction in the contact area.

ρ_c is the contact resistivity

ρ is the resistivity of the wafer material.

d is the contact diameter

B is a factor that corrects for the finite thickness of the wafer layer. $B = 2/\pi \cdot \arctan(4t/d)$

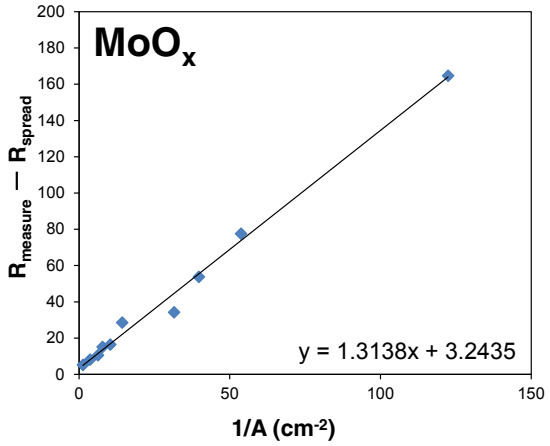

Contact resistivity (Ohm.cm²)	1.31
Correlation	0.995964379
Contact resistivity extraction ref	Shepela, 1972

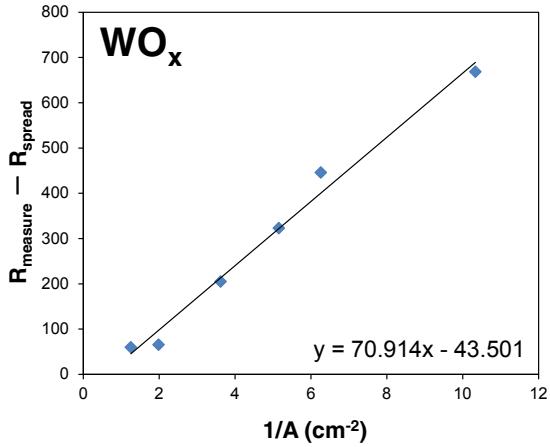

Contact resistivity (Ohm.cm²)	70.91
Correlation	0.993207424
Contact resistivity extraction ref	Shepela, 1972

Figure 2. Contact resistance of flame-deposited (a) MoO_x and (b) WO_x on Si wafers. MoO_x shows much smaller contact resistance.

Future Work:

Those high crystalline MoOx will be deposited on Si and InP solar cells and their effects as p-type contact will be investigated.

Project Title: Ultra high efficiency thin film multi-junction solar cell
PI: James S. Harris
E-mail: jharris@stanford.edu

Summary:

The Harris group proposed to develop significantly higher efficiency thin film multi-junction solar cells by combining multi-junctions and advanced nano-scale light management concepts in ultra-thin film devices that lend themselves to very large scale, low cost manufacturing. In the past year, they developed the processing and demonstrated selective carrier oxide tunnel barrier Ohmic contacts for both electrons and holes. Cells with oxide barrier contacts were fabricated and demonstrated an enhancement in V_{oc} in ultra-thin, c-Si solar cells. The also demonstrated world record solar to hydrogen generation (>30%) from water splitting utilizing multi-junction GaAs based solar cells that were developed as part of the BAPVC program. A white paper was submitted to DOE EERE and we were invited to submit a full proposal that is now pending review and a decision.

Key Accomplishments:

An ultra-thin-film 'nanowindow' solar cell (figure 1a, b) was developed that combines a nanostructured window layer on an ultra-thin-film (3µm) c-Si planar absorber/junction with carrier selective oxide barrier Ohmic contacts. A schematic diagram of the cell structure incorporating a photon management surface structure layer is illustrated in Figure 1 (a) and the band lineups with selective carrier Ohmic contacts in Figure 1 (b).

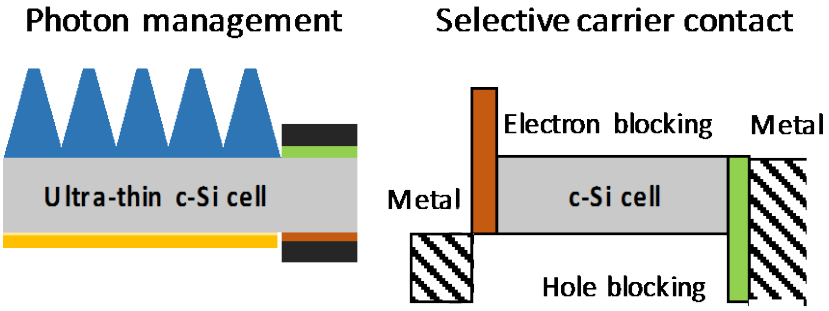

Figure 1. Ultra-thin c-Si solar cell with nanostructured photon management top layer (a) and selective carrier oxide tunnel barrier Ohmic contacts (b).

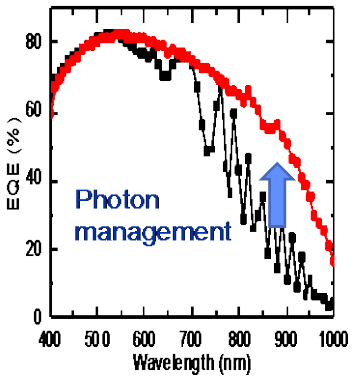

Figure 2. External quantum efficiency vs wavelength for a nanopatterned photon management c-Si solar cell

The improvement in external quantum efficiency due to photon management in the 700-1100nm range is clearly evident. If one can achieve the same external QE in a thinner cell, the carrier density can be increased resulting in an increase in V_{oc} and efficiency IF the Ohmic contacts don't create a sink for minority carriers, which the conventional p+ or n+ metal barrier contacts do. Ohmic contacts. and leads to an increase in V_{oc} and efficiency. An approach using thin oxide

barriers was proposed and investigated some years back, but control of the insulator was just too difficult. This past year, a new Atomic Layer Deposition (ALD) tool was installed in SNF that enables very precise control over insulator thickness. Deposition processes were developed to deposit sub-nm layers for TiO_x (hole blocking) and NiO_x (electron blocking). Four types of TLM contact structures were fabricated for both TiO_x and NiO_x and on n and p-type Si and measured to verify the electron or hole-conducting and hole or electron-blocking behavior respectively. An Al/n-Si and Al/p-Si were fabricated as control structures for comparison. Similarly for NiO_x, Pt/NiO_x/p-Si and Pt/NiO_x/n-Si were fabricated to verify the hole-conducting and electron-blocking behavior respectively, together with the Pt/p-Si and Pt/n-Si control structure.

The J-V characteristic for such a structure is illustrated in Figure 3 and shows an increase in Voc over the reference cell in spite of the fact that the current is still less than in the thicker cell. This

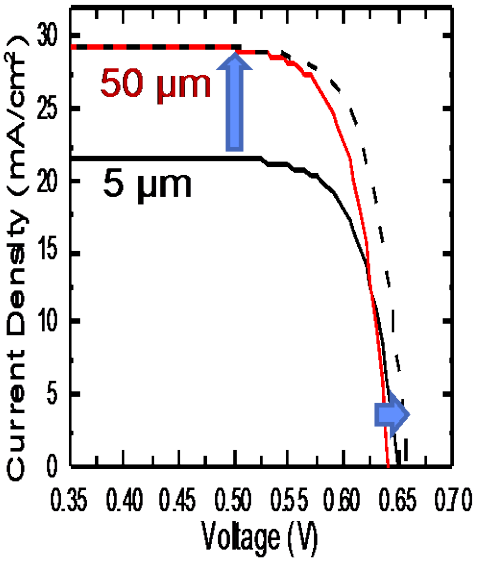

Figure 3. J-V characteristic of nanopatternd c-Si solar cells with selective carrier contacts.

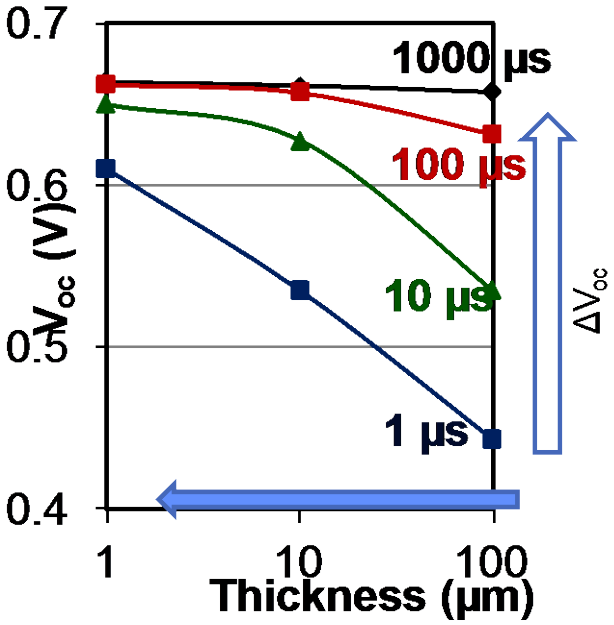

Figure 4. Voc vs cell thickness as a function of carrier lifetime.

demonstrates the voltage enhancement for thin-film c-Si solar cells due to vertical carrier confinement when selective carrier Ohmic contacts are used.

One of the exciting outcomes of this demonstration is that carrier lifetime becomes much less critical in ultra-thin c-Si cells since carriers only need diffuse 2-3µm vs 200µm or more in conventional cells. This idea was modeled to examine the V_{oc} vs. cell thickness as a function of c-Si lifetime between 1 and 1000µs and is illustrated in Figure 4. This result suggests that for cells thinner than 5µm, a carrier lifetime of 50µs or longer is adequate to reach the maximum in V_{oc} and efficiency. Si of this level of performance is far less costly, not only as a raw ingredient, but in process robustness so as not to degrade the original long lifetime used in the highest efficiency cells today.

Yusi Chen, one of the key contributors to the BAPVC project in the Harris Group the past 4 years completed his PhD in December. The title of his thesis is, "THIN-FILM CRYSTALLINE SOLAR CELLS FOR LOW CAPEX MANUFACTURING".

Future Work:

The Harris Group will continue to optimize a nanostructured single junction ultra-thin-film GaAs solar cells with a high short circuit current extraction of over 20mA/cm^2 with an overall energy conversion efficiency of over 18%. The record performance solar to hydrogen conversion efficiency places different boundary conditions on the optimum cell voltage to match the electrolyzer and a while a GaAs based multijunction cell was utilized to achieve this record, it was not optimized. They'll also fabricate multi-junction solar cells based on GaAs and Si, trying to achieve >25% energy conversion efficiency.

BAPVC Annual Project Report

Project Title: High V_{oc} Solar Absorbers; the Missing Link for High-Efficiency, Spectral-Splitting, Solar Cells
PI: Eli Yablonovitch; **Co-PIs:** Connie Chang-Hasnain and Ming Wu
E-mail: eliy@eecs.berkeley.edu

Summary:

High V_{oc} absorbers are required for future high-efficiency multi-junction cells. In this project we investigated whether bandgap micro/nanopillars could provide the wide bandgap function. The group investigated the characteristics of high bandgap micron-sized InGaP nanoneedles/pillars directly grown on lattice mismatched silicon substrates, and explored selective area growth for solar cell absorption enhancement. Our best result on single InP nanopillar solar cells was conversion efficiency of 19.6 % and an open circuit voltage of 0.534 V under AM 1.5 G, both records for InP directly grown on Si.

Nonetheless, we believe that the progress in transferrable thin film layers is more likely to be successful than nano-pillars. The emphasis has to continue to be toward E_g=2.2eV with V_{oc}=1.8Volts, since we already have good tandem solar cell candidates at lower bandgaps, like GaInP alloys at E_g=1.8eV and V_{oc}=1.45Volts. These GaInP films are routinely produced by epitaxial liftoff, which is capable of very low cost.

Key Accomplishments:

In this project we employed high quality III-V nanopillars synthesized on low cost substrates. The group demonstrated that a single InP nanopillar grown and fabricated on silicon substrate exhibits a record power conversion efficiency of 19.6% and an open circuit voltage (V_{oc}) of 0.534 V under AM 1.5 G illumination. This is the highest efficiency and V_{oc} ever achieved for an InP nanowire or nanopillar solar cell grown on a foreign substrate, which can be attributed to high-quality single-crystalline wurtzite-phased InP nanopillars grown using a novel regrowth technique to drastically reduce the dark current by three orders of magnitude. Taking advantage of dielectric antenna effect, effective external quantum efficiency is as high as 400% at 550nm and generally greater than 100% in the visible spectrum, beyond that predicted by Lambert-Beer law is achieved over a broad solar spectrum (Fig.1a).

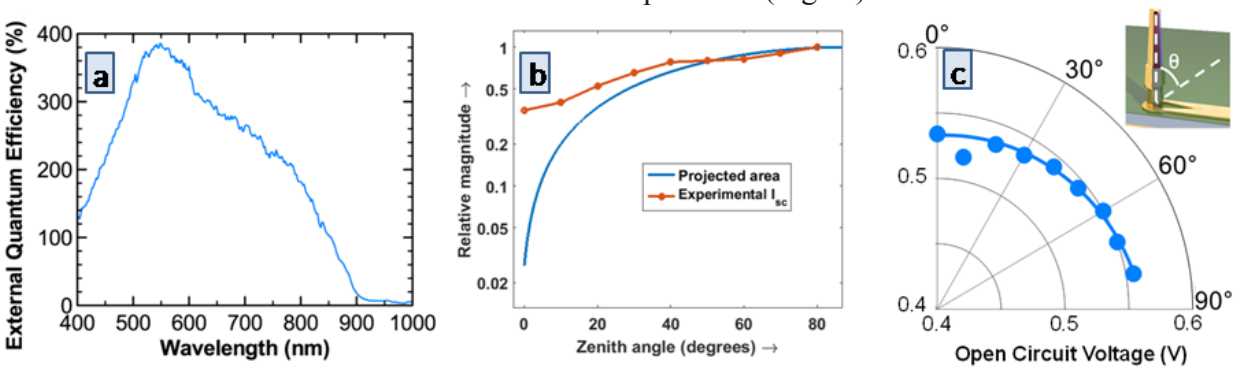

Figure 1. (a) Measured external quantum efficiency top-down illumination of a single InP nanopillar solar cell fabricated on silicon substrate. (b) I_{sc} as a function of incident angle under 1 sun (AM 1.5 G) IV characteristics of InP solar cell. (c) V_{oc} as a function of incidence angle.

Specifically in the surface normal direction, the field enhancement compensates the reduced of surface exposure area, resulting in a relatively smooth I_{sc} (Fig. 1b). Similarly V_{oc} is relatively insensitive to angle (Fig. 1c) all under 1 sun illumination.

It was also demonstrated, for the first time, single crystalline wurtzite InGaP nanoneedles with composition ordering directly grown on silicon substrate. By increasing Ga precursor flow it was possible to reach a wider bandgap of E_g~1.50eV at room temperature and E_g~1.58 eV at low temperature, for $In_{0.82}Ga_{0.18}P$ intrinsic micropillars on a silicon substrate (Fig.2a-b), regardless of the lattice mismatch constraint, also presenting Fermi-level splitting values larger than 0.95 eV under 1 sun from equivalent V-I characteristic (Fig.2c). Selective area growth of micro/nanopillars on a patterned silicon substrate improved the density from 65% to 95% (Fig.2d), which can be used to enhance the absorption of the nanostructures and future device performances.

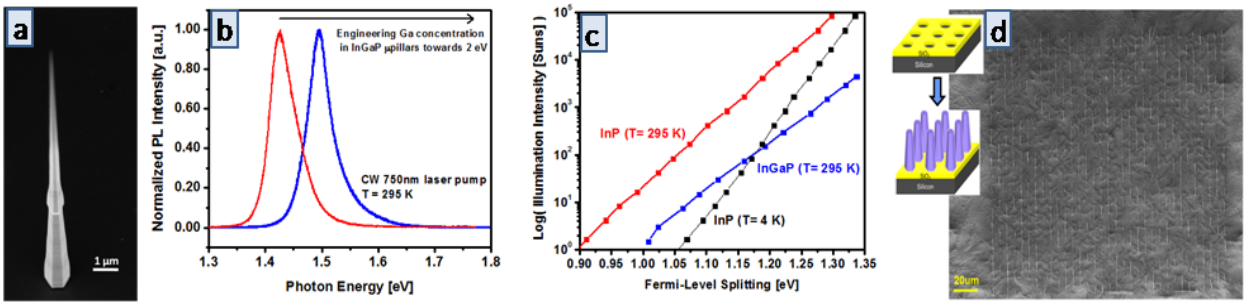

Figure 2. (a) Scanning electron micrograph of a micro-sized $In_{82}Ga_{18}P$ needle. (b) Ga content variation in InGaP towards 2 eV. (c) Comparison between Fermi level splitting from InGaP and InP micro/nanopillars. (d) High yield selective area growth of needles on a patterned silicon substrate.

Future Work:

We recommend abandoning the nano-pillar approach in favor of an epitaxial liftoff approach. These need to have higher bandgaps for multi-junction tandem cells with the highest bandgap layer E_g=2.2eV. Ga-rich $Ga_{0.75}In_{0.25}P$ layers remain a viable candidate, almost reaching a direct bandgap E_g=2.2eV. But these are not lattice matched to GaAs, and would require an engineered GaAsP substrate. Epitaxial liftoff would likely still be quite successful using AlAsP as the sacrificial layer. Now that large area epitaxial liftoff is in production for GaInP at Alta Devices Inc., there is a real need to extend this to wider bandgap materials. There is almost no competition or financial support for this approach, suggesting that funding should be diverted from other areas that are already well-funded.

One of these well-funded areas is the lead-halides sometimes called perovskites. While the E_g=1.60eV bandap lead-halides are beginning to perform well, especially in luminescence extrapolation of potential V_{oc}, the higher-bandgap, bromine-based, lead-halides, are not yet fulfilling their potential. Therefore we recommend materials development work on wide-bandgap, lead-halides, with E_g=2.2eV. The usual set of problems will need to be dealt with, including material quality, or luminescence efficiency, the need for good hetero-barrier electrical contacts, etc. One of the opportunities is the recognition that the lead-halides would likely be much more stable as single crystal films. Commercial epitaxial liftoff has shown that single-crystal films can be low-cost. It would be great to search for etching selectivity in heterogenous multi-layers that would allow epitaxial liftoff and separation of single-crystal lead-halide films.

BAPVC Annual Project Report

Project Title: Defect Identification and Mitigation in High-Lifetime Silicon Materials: Growth, Processing, Reliability

PI: **Tonio Buonassisi**
E-mail: buonassisi@mit.edu

Summary:

Interstitial metal impurities impact solar cell efficiencies at concentrations as low as 10^{10} cm^{-3}. Knowledge of the defect identity, concentration, and spatial location can inform targeted process modeling and design efforts. Existing methods for non-destructive defect identification are limited, *e.g.* metastable defect lifetime spectroscopy and synchrotron-based X-ray Fluorescence Microscopy. To advance our understating of the role of defects in silicon, the group has developed methods to robustly measure and extract the Shockley-Read-Hall lifetime for defect identification *via* temperature- and/or injection-dependent lifetime spectroscopy (TDLS, IDLS, and TIDLS). These techniques have been applied to understand the root cause of light- and elevated temperature-induced degradation (LeTID) in multicrystalline silicon. LeTID can cause about 10% relative performance degradation in passivated emitter and real contacted (PERC) solar cells. Uncertainty about the root cause of LeTID necessities process- and/or material-specific optimized of proposed engineering solutions, which can be costly and time-consuming. Pinpointing the root cause of LeTID is critical to developing targeted solutions that maximize device efficiency.

Key Accomplishments:

Injection-dependent lifetime measurements at temperatures between 25-200°C were measured with TIDLS tools available from Sinton Instruments (WCT-120TS) and the University of New South Wales. Both tools integrate a photoconductance coil with a temperature controlled cryostat and a standard Xenon flash lamp for illumination to measure spatially-averaged minority carrier lifetimes in silicon. In an exemplary experiment in collaboration with UNSW, two adjacent *p*-type multicrystalline silicon wafers were prepared as PERC semifabricates and fired at 950°C. To isolate the defect responsible for LeTID, one wafer was stored in the dark (undegraded) and one wafer was subjected to degradation conditions 65-75°C and 0.9-1.1 suns) for 168 hours (degraded). Measurements were acquired at sample setpoint temperatures 25°C, 50°C, 100°C, 150°C, and 200°C. Since the LeTID defect is known to be metastable at 200°C, room-temperature QSSPC measurements were completed after each elevated temperature measurement with a Sinton Instruments WCT-120. The results of these measurements are shown in Fig. 1. The

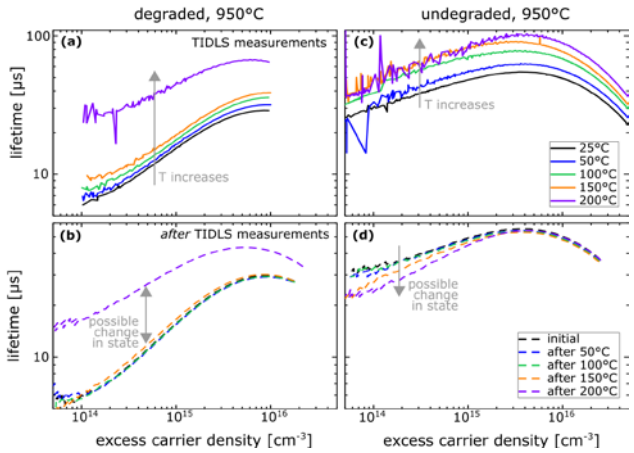

Fig. 1: (a) and (c): Injection-dependent lifetime measurements at setpoint temperatures 25°C, 50°C, 100°C, 150°C, and 200°C for the degraded and undegraded samples, respectively. (b) and (d): Room-temperature injection-dependent lifetime measurements performed after each elevated temperature measurement to demonstrate the stability of the LeTID defect.

lifetime changes in magnitude at 200°C, likely related to the metastable nature of the defect.

For each temperature, the injection-dependent Shockley-Read-Hall (SRH) lifetime is determined according to the inverse harmonic difference between the undegraded and degraded wafers. In this analysis, the LeTID is assumed to be an SRH defect, solely responsible for the difference in measured lifetimes. The SRH lifetime is then linearized, and a two-defect fit that minimizes the χ^2 error between the measured and fit SRH lifetimes is used to identify possible defect parameters. The electron-to-hole capture cross-section ratio (*k)* and electron capture time-constant (τ_{n0}), which is a function of electron capture cross-section (σ_n), defect concentration (N_t), and thermal velocity (v_{th}), are calculated as functions of possible defect levels within the bandgap.

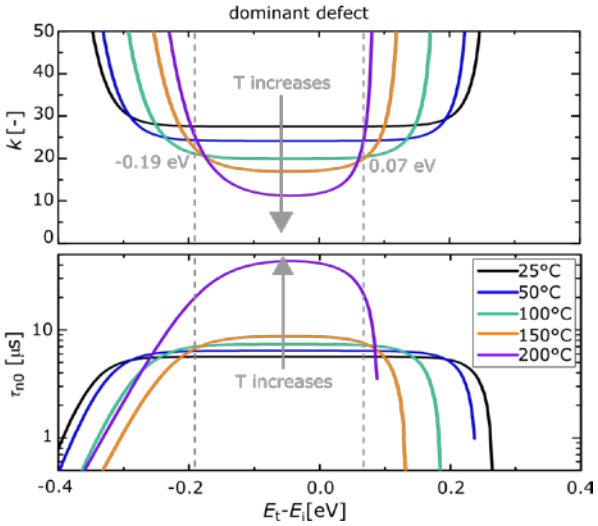

Fig. 2: Calculated LeTID defect parameters at each measured temperature, with no clear intersection point for all curves. (top): *k*-value (electron-to-hole capture cross-section ratio) as a function of energy level. (bottom): τ_{n0} (electron capture time constant) as a function of energy level.

The results of the fitting procedure are shown in Fig. 2. At every temperature, there is one defect that dominates the lifetime signature throughout the measured injection range and would therefore be dominant under solar cell operating conditions. If the *k*-value is not temperature-dependent, the true defect parameters can be determined from the intersection of the E_t-*k* curves. The standard deviation of the *k*-values at each energy level is a quantitative way to evaluate possible intersections, with the most likely intersection points corresponding to the minimum standard deviation. Two local minima can be identified: k = 24.2 at -0.19 eV (lower bandgap half) and k = 23.0 at 0.07 eV (upper bandgap half). The intersection at -0.19 eV is much sharper, with a lower standard deviation; therefore, this energy level is more likely to be the true energy level than the corresponding value in the lower bandgap half.

Future Work:

This report demonstrates the analysis method required to conduct TIDLS measurements. In the analysis presented above, the *k*-value is assumed to be constant with temperature; however, the lack of a clear intersection between curves at different temperatures suggests a possible *k*-value temperature-dependence. To further assess the defect responsible for LeTID, researchers will develop analysis methods to assess the possible *k*-value temperature dependence and then apply these to the measured data. In addition, TIDLS data should be compared across samples from multiple suppliers and processing lines to provide a complete picture of the LeTID defect.

BAPVC Annual Project Report

Project Title: Design Principles and Defect Tolerances of Silicon / III-V Multijunction Interfaces

PI: **Tonio Buonassisi**
E-mail: buonassisi@mit.edu

Summary:

The group performed atom probe tomography (APT) measurements on silicon and III-V material samples. APT provides a 3D map of the atomic composition of the samples, which improves our understanding of material composition on the atomic level. Highly impure silicon and InAlAs with embedded Ge Nanowires were characterized.

Key Accomplishments:

The group performed measurements of metastable materials that are intractable by other method. The internal structure and kinetics of formation was reconstructed from the gathered APT data. The group accomplished Measurements of performance-limiting defects in III/V materials (InAlP, figure 1), and developed APT protocols for these materials. The group also developed an improved theory of ionization states and the probability for arbitrary elements in a semiconducting matrix. Findings matched experimental data and allows defining broad standards for APT measurements, and determine real-world detection limits for impurities in Si (figure 2) and III/V compound semiconductors. Finally, the group accomplished measurements of buried III/V-Ge interfaces (figure 3).

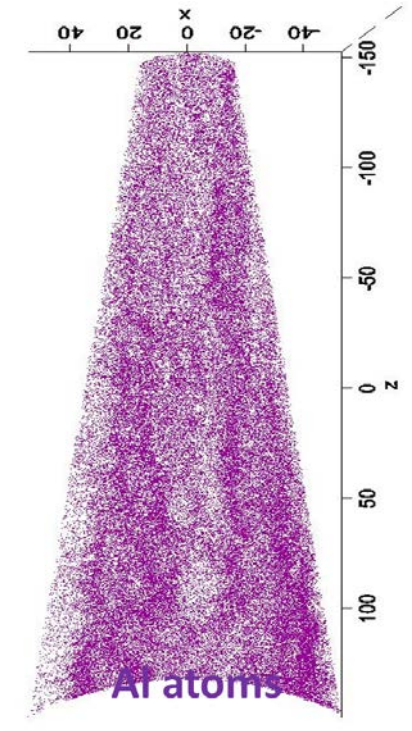

Figure 1: Map of aluminum atoms in a InAlP sample. The measurement provides information about variation in the elemental distribution due to spinodal decomposition.

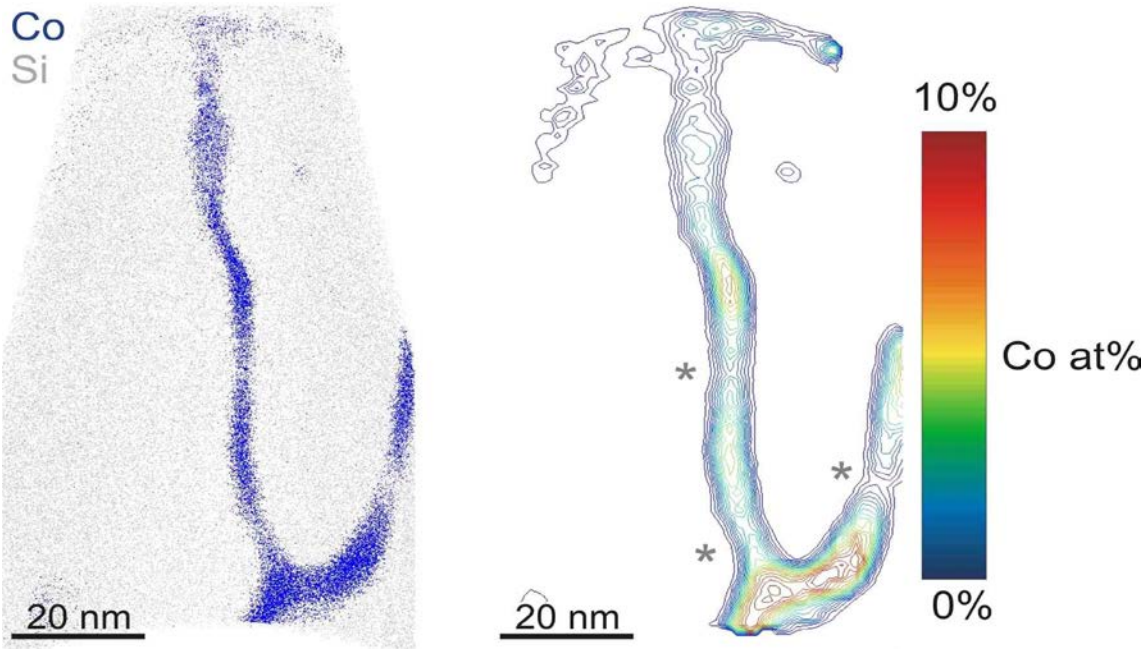

Figure 2: Atom Probe Tomography measurement showing the distribution of Co in Si.

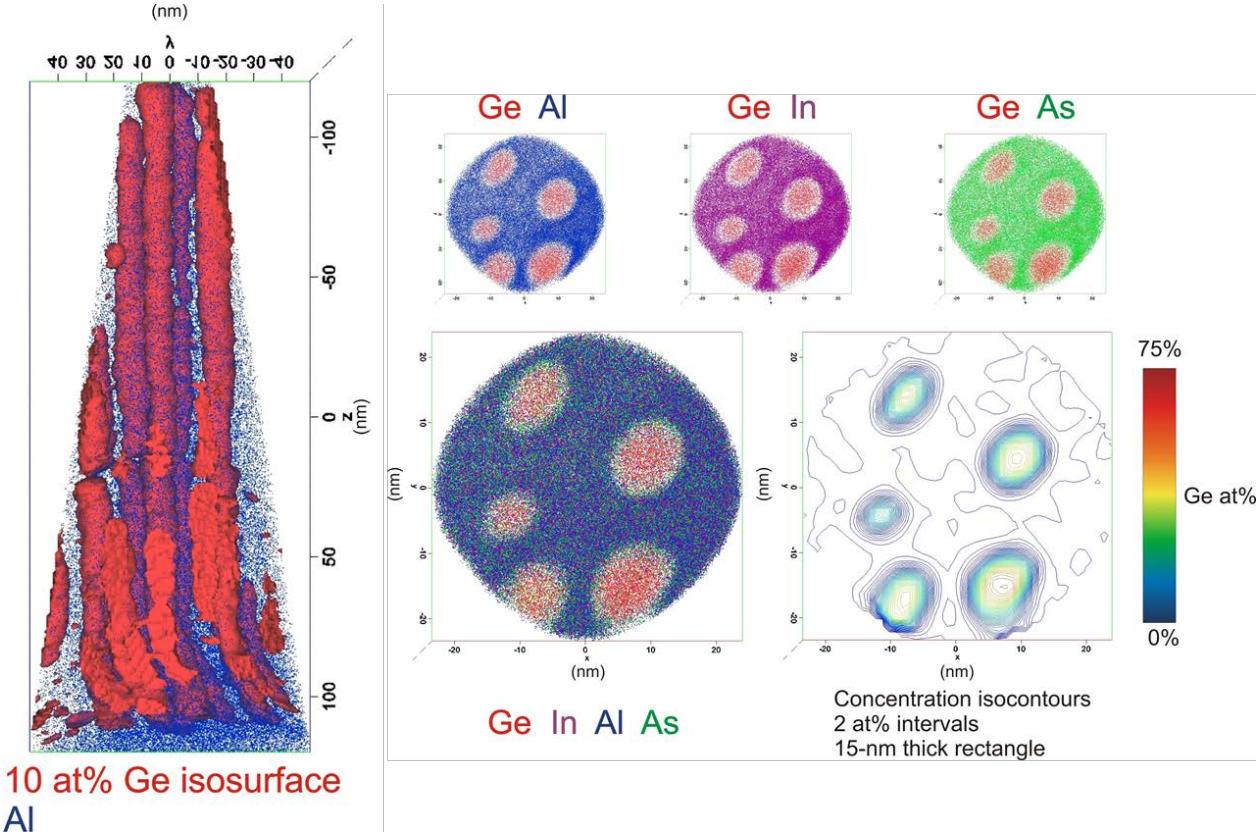

Figure 3: Elemental distribution of Ge Nanowires in a InAlAs matrix

Future Work:

The group plans to develop an advanced model for the description of phase segregation which explains the effects observed in the APT measurements. Further foundational work is required to accurately interpret atom probe tomography measurements at hetero-interfaces. Specifically, improved detector hardware, method for measurement of APT specimen evolution. Theory support would be helpful in development.

Thrust: Photon Management and Transparent Conductors

Key Challenges

The thrust spans two major areas: light management and transparent electrodes for solar cells. The key challenges are several folds:

1. Develop materials and structures to couple maximum sunlight into the solar cells and to achieve near-complete absorption of above bandgap photon with significantly reduced usage of absorber materials.
2. Develop low-cost highly transparent (~95%) and low sheet resistance electrodes (<5 ohm/sq) for solar cells with n- and p-type contact capability.
3. Develop process to implement the above materials and structures in practical scalable solar cell manufacturing.

Existing Projects in our Thrust

- *Perfect TCO for Full Spectrum Photovoltaics*, Wladek Walukiewicz (LBNL)
- *Earth Abundant P-Type Transparent Conductors,* Joel Ager (LBNL)
- *Optimal Integration of Transparent Electrodes and Photon Management,* Shanhui Fan (Stanford)
- *Large-Area, Fast, and Electric-Field Assisted Continuous Coating for Nanostructured Photon Management*, Ning Wu (Colorado School of Mines)

Potential New Areas of Interest

- *Extension.* Thus far, photon management is mainly aimed for enhancement of short circuit current. There are exciting opportunities to explore photon management to reduce photon entropy loss to increase open circuit voltage.
- *Integration.* Integrate photon management together with electrical transport to fully engineer the structure to enhance solar cell efficiency as a whole. In addition, there are significant opportunities to integrate the materials in the transparent conductor projects with the design and modeling efforts in the photon management projects. For example, transparent electrodes may be designed as an efficient structure for light management purposes. Alternatively, one may incorporate advanced optical design to reduce the loss in transparent electrode while maintaining its electrical properties.
- *Manufacturability.* Photon management will only be viable, if it can be implemented in a cost effective way. Study the integration of new photonic structures and transparent electrodes into practical scalable solar cell manufacturing.

BAPVC Annual Project Report
Project Title: Perfect TCO for full spectrum PVs
PI: Wladek Walukiewicz
E-mail: w_walukiewicz@lbl.gov

Summary:

They have studied indium-doped cadmium magnesium oxide (CdMgO:In) alloys for the transparent conductor and electron emitter applications in thin film PV technologies. The study shows that alloys with about 40% of Mg are UV transparent with doping controlled conductivity making the alloy suitable for transparent contacts and electron emitter applications with a large bandgap of 3.5eV and electron density of 1 x 10^{20} cm^{-3}. In addition, they observed that adding MgO to CdO greatly improves the stability of CdMgO:In in highly corrosive environment.

Key Accomplishments:

The purpose of the study was to search for a large gap conductive material that could be used as a transparent contact and/or electron emitter in thin film PV technologies. A series of $Cd_{1-x}Mg_xO$:In thin films with magnesium concentration $x < 0.6$ were grown by sputtering technique. The electrical and optical properties of the materials were characterized using Hall Effect measurement and the UV/Visible/NIR optical spectrometer. The Bandgap and the carrier density vs. Mg content *x* are plotted in the figure 1. The bandgap has large bowing parameter of 3.1eV. It is seen in Fig. 1 that a UV transparent and conducting material with the band gap of 3.5 eV and electron concentration of 1 x 10^{20} cm^{-3} is obtained for the composition x of approximately 0.4.

Using the known locations of the conduction band minimum (CBM) and the valence band maximum (VBM) for the end point compounds and adopting the band gap bowing parameter of 3.1eV allows prediction of the composition dependence of the CBM and VBM. The band edge energies are shown in Fig. 2. Interestingly, it is seen that most of the band gap increase originates from the rapid upward shift of CBM with increasing Mg content. This explains the observed reduction of the electron concentration as the CBM shifts towards and crosses the Fermi level stabilization energy, E_{FS} at about 35% Mg. The large tunability range of the electron affinity from 5.9 eV in CdO to 0.9 eV in MgO allows for matching of the CBM of the alloy with conduction band edges of the absorbers in currently used thin film PV technologies including CdTe, CIGS and CZTS. Thus, as seen in Fig. 2 the CBM of CgMgO alloy with 42% Mg content aligns with the CBM of CdS that currently is the standard electron emitter in thin film PV technologies. However, an obvious advantage of CdMgO is that it has a much larger gap and much better short wavelength transparency than CdS.

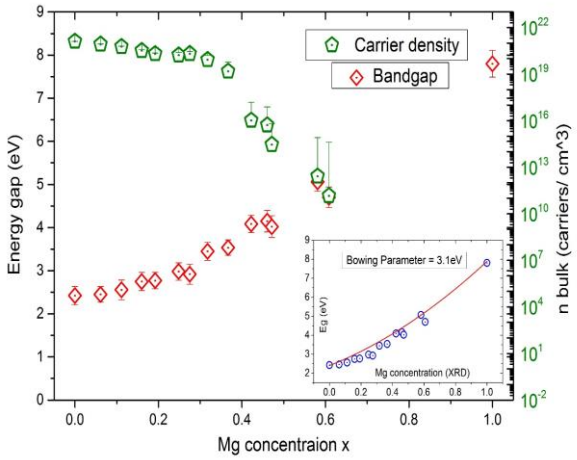

Figure 1: Bandgap (red, left y-axis) and the carrier density (green, right y-axis) vs. Mg content *x*. The inset shows the fitting for the bowing parameter of 3.1eV.

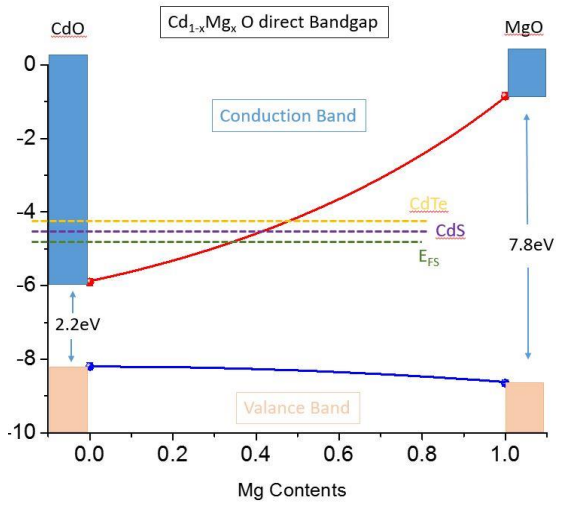

Figure 2. Band-offset diagram of $Cd_{1-x}Mg_xO$:In alloy. Note that at 42% Mg, the conduction band of the alloy matches with that of CdS. The energies are relative to the vacuum level.

In addition, in order to evaluate the effects of alloying on the stability of the thin films, CdMgO films were soaked in water and their electron density was recorded as a function of the soak time. As is shown in Fig. 3 adding of relatively small amount of Mg greatly improves the stability. These preliminary results indicate that the stability could be related to the surface pinning properties of the thin films.

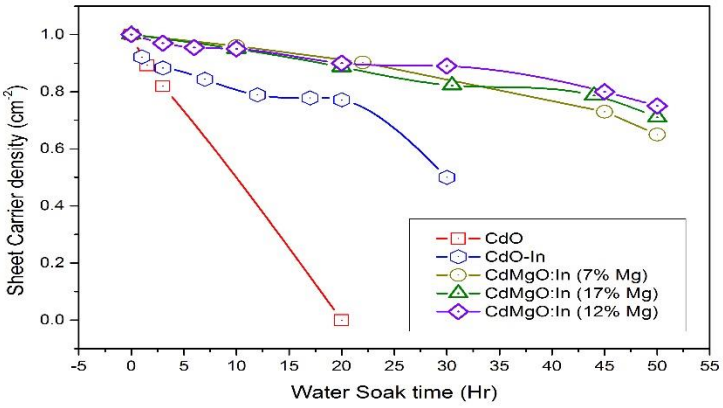

Figure 3: Sheet carrier density vs. water soak time for CdO and CdMgO:In with various Mg contents. Sheet carrier density was normalized with respect to the initial value. i.e. at water soak time = 0 hour.

Future Work:

The research on transparent conductors and electron emitters will continue and will be supported by other funding sources.

BAPVC Annual Project Report

Project Title: Earth abundant p-type transparent conductors
PI: Joel W. Ager, Materials Sciences Division, Lawrence Berkeley Nat. Lab
E-mail: JWAger@lbl.gov

Summary:
P-type transparent conductors based on Cu-Zn-S alloys have been synthesized which have world record combinations of transparency and hole conductivity. A scalable process for the deposition of these materials has been developed, allowing them to be integrated with Si and III-V photovoltaic absorbers. Results have been reported in two refereed journal publications which acknowledge support from BAPVC.

Key Accomplishments:

The conductivity of p-type transparent materials (TCMs) has historically lagged behind that of well-known n-type transparent conductors such as indium tin oxide (ITO), Al-doped ZnO (AZO), and F-doped tin oxide (FTO). Moreover, most of the p-type TCMs reported thus far require processing temperatures in excess of 400 C, which will limit their applications in devices with limited thermal budgets such as many solar cell architectures.

Previous reports have described the development of new p-type TCMs based on the ZnS-Cu_xS system. Here, wide band gap ZnS provides transparency which the Cu_xS provides p-type conductivity, either through doping on the Zn site in the ZnS [1,2] or by forming a Cu_xS-ZnS nanocomposite [3]. Of particular interest for solar cell applications is the scalable chemical bath deposition process we have developed for synthesis of the nanocomposite material, Figure 1. As hole-selective transparent contacts, CuS:ZnS films we have developed equal or exceed the performance of competing room temperature deposited hole contacts such as carbon nanotubes and graphene [3].

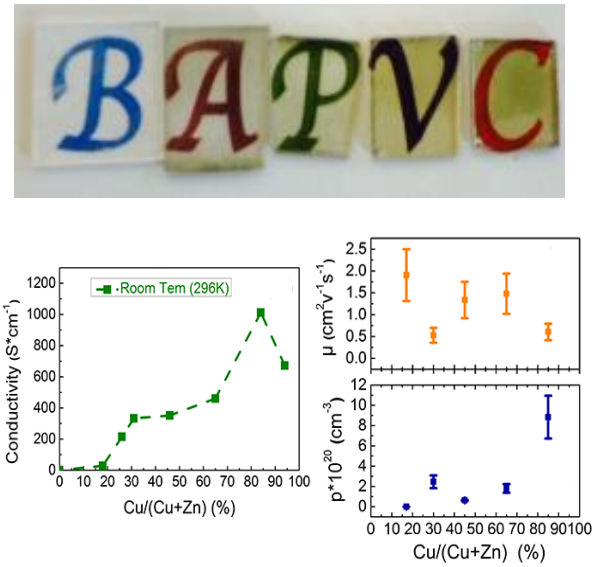

Fig. 1. (top) Transparent 50 nm CuS:ZnS nanocomposite films deposited on glass; the Cu CuS fraction increases from 0-90% left to right. (bottom) Conductivity, mobility, and carrier concentration of the nanocomposite films. Adapted from Xu *et al.*, Nanoletters, 2016.

An efficient PV device using a p-type TCM had not been reported in the literature, in particular with a low temperature process. In collaboration with BAPVC researcher Ali Javey's group, solar cell integration was performed by fabricating n-Si/p-CuZnS and np^+-Si/p-CuZnS structures. Excellent hole collection was found in the n-Si/p-CuZnS cells with 1 sun open circuit voltages exceeding 500 mV.

The chemical bath deposition process would be expect to be conformal, creating the possibility to use it to make hole selective contacts to textured absorbers. Initial work in this area has been successful. Figure 2 shows 1 sun J-V data from a textured n-Si/p-CuZnS structure along with a similar structure made with planar Si. Both structure have an open circuit voltage

>500 mV, attesting to the passivating and hole selective nature of the heterointerface. Moreover, the short circuit current is substantially improved in the textured device due to light trapping.

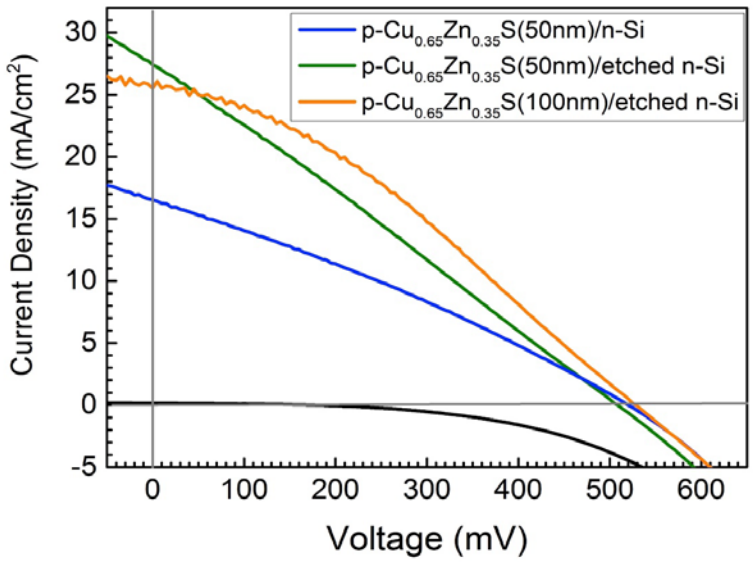

Fig. 2. Current-voltage data from textured Si absorber interfaced with conformal $(CuS)_{0.65}$:$(ZnS)_{0.35}$ made by chemical bath deposition. Data from a planar control is shown as well. With an optimized p-TCM hole contact thickness (100 nm), an open circuit voltage >0.5 V and a short circuit current >25 mA cm^{-2} are achieved. Device size 1 cm x 1 cm, simulated AM1.5G illumination. . Data from Xu, Bullock, and co-workers, unpublished.

The developments in this project eliminate the main barriers preventing the use of p-TCMs in device applications and thus will enable new applications such as thin film tandem solar cells based on abundant elements and, potentially, other applications, such as "invisible" electronics on flexible substrates.

Future Work:

It should be noted that efforts in this area performed by the PI are no longer supported by BAPVC. Future work is concentrating on replacing hole selective contacts in commercial PV stacks and in developing methods for scalable microfabrication of patterned contacts.

References:

[1] Diamond A M, Corbellini L, Balasubramaniam K R, Chen S, Wang S, Matthews T S, Wang L-W, Ramesh R and Ager J W 2012 Copper-alloyed ZnS as a p-type transparent conducting material *Phys. status solidi* **209** 2101–7

[2] Woods-Robinson R, Cooper J K, Xu X, Schelhas L T, Pool V L, Faghaninia A, Lo C S, Toney M F, Sharp I D and Ager J W 2016 P-Type Transparent Cu-Alloyed ZnS Deposited at Room Temperature *Adv. Electron. Mater.* **2** 1500396

[3] Xu X, Bullock J, Schelhas L T, Stutz E Z, Fonseca J J, Hettick M, Pool V L, Tai K F, Toney M F, Fang X, Javey A, Wong L H and Ager J W 2016 Chemical Bath Deposition of p-Type Transparent, Highly Conducting (CuS)x:(ZnS)1-x Nanocomposite Thin Films and Fabrication of Si Heterojunction Solar Cells *Nano Lett.* **16** 1925–32

BAPVC Annual Project Report

Project Title: Optimal Integration of Transparent Electrodes and Photon Management

PI: **Shanhui Fan**
E-mail: shanhui@stanford.edu

Summary:

The objective of this project is to investigate the design and to study the physics mechanism of a metallic nanowire electrode that functions both as a transparent electrode and an anti-reflection layer, with the consideration of the general constraints that the electrode is in electric contact with the semiconductor and is encapsulated.

Key Accomplishments:

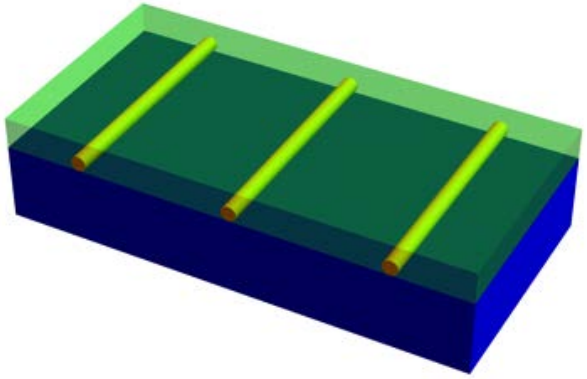

Figure 1. Schematic of the transparent electrode consisting of silver nanowires sitting on a silicon substrate and embedded in a layer of SiN.

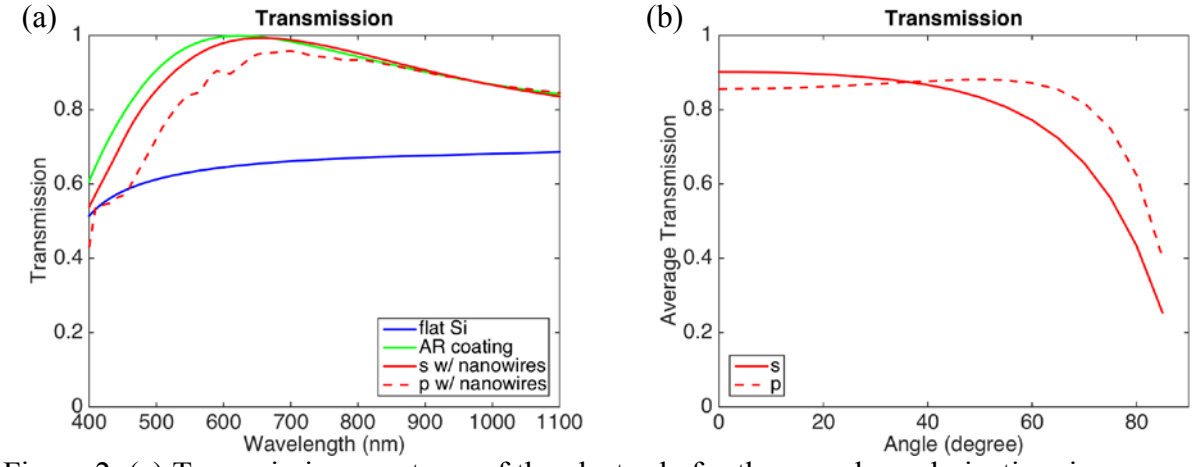

Figure 2. (a) Transmission spectrum of the electrode for the s- and p-polarization, in comparison with the transmission spectrum of a flat silicon/air interface and that of a single layer anti-reflection coating. (b) Angular dependence of the average transmission of the electrode for the s- and p-polarization.

The transparent electrode is a widely used component in solar cells. However, traditional transparent electrode tin-doped indium oxide has limitations such as the lack of abundance of tin. A number of other approaches have been recently explored, including networks of metallic nanowires. Besides the high electrical conductivity and high optical transparency requirements of a high-performance transparent electrode, a practical electrode should also be designed with the consideration of several additional general constraints that the electrode is in electric contact with the semiconductor to extract carriers and is encapsulated to prevent damage.

With these considerations, the optical properties of a nanowire transparent electrode with a generic geometry (Figure 1) are investigated, where periodic silver nanowires are placed atop a silicon substrate and embedded in a SiN layer. Numerical simulation shows that this system can provide broadband anti-reflection, comparable to that of a single layer anti-reflection coating, for both polarizations over most of the absorption frequency range for silicon solar cells (Figure 2(a)). The angular response of this system for both polarizations (Figure 2(b)) also suggests its capability of capturing most diffuse sunlight. This project also elucidates the physics mechanism of this broadband anti-reflection. A Fabry-Perot interference model is developed to take into account of higher order diffraction channels inside the SiN layer and the modification of the reflection coefficient introduced by the silver nanowires. This model is validated using frequency-domain electromagnetic simulations. This work highlights an opportunity of using a nanowire electrode for both carrier collection and anti-reflection purposes.

Future Work:

Future work will aim at further development of transparent electrode for light management. Specifically, numerical works will be carried out to determine the potential of light trapping with such transparent electrode, placed at the semiconductor interface, with an encapsulation layer. And the numerical results will be used to motivate the development of an analytic theory highlighting the fundamental limit of such light management schemes.

BAPVC Annual Project Report

Project Title: Large-Area, Fast and Electric-Field Assisted Continuous Coating for Nanostructured Photon Management
PI: Ning Wu, the Department of Chemical and Biological Engineering, Colorado School of Mines
E-mail: ningwu@mines.edu

Summary
The CSM group built a new flow-coating setup that allowed us to observe the *in situ* dynamics of meniscus movement. We studied the impact of colloidal particle surface property and addition of surfactant on the movement of meniscus.

Key Accomplishments

1. *In situ* observation of the dynamics of flow coating

In order to better understand the flow coating process, the CSM group integrated a customized microscope with the flow coating setup to achieve the *in situ* observation of the meniscus movement during flow coating (**Fig. 1**). By recording the position of the meniscus as a function of time as shown in Fig. 1c, we found that the meniscus underwent a "stick-slip" type motion. During the "slip" period, colloidal particles are deposited uniformly and continually on the substrate, while the "stick" of the meniscus causes the formation of stripes.

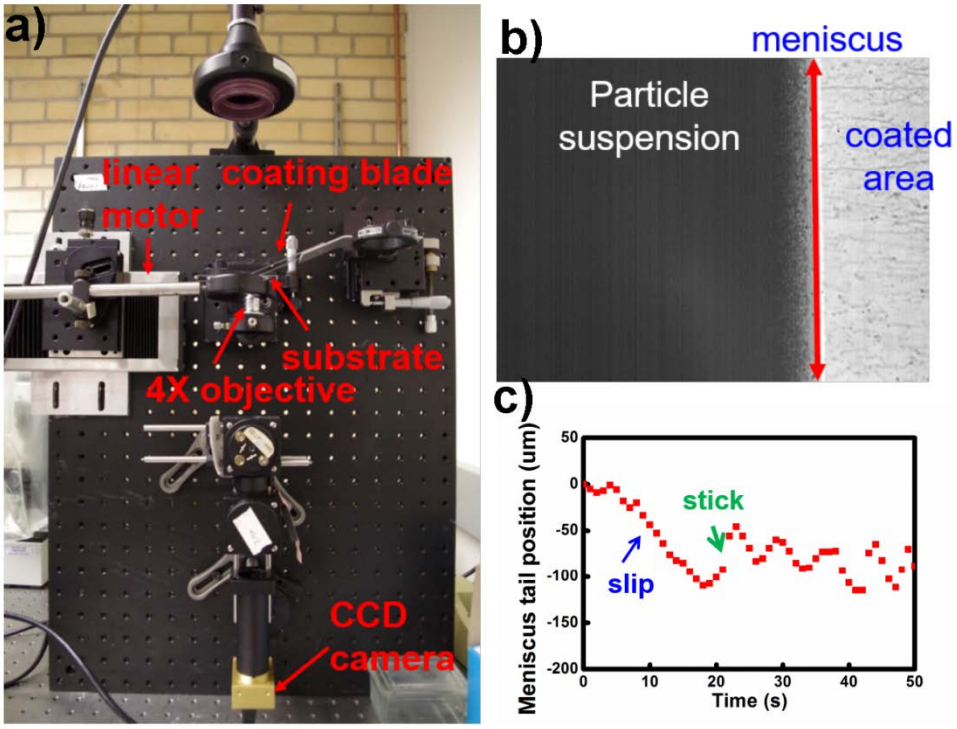

Figure 1 (a) Customized microscope integrated with the flow coating setup. (b) A typical snapshot of the meniscus movement under 4X microscope. (c) Meniscus position as a function of time.

2. The correlation between the length of the meniscus tip and the uniformity of coating

Three batches of colloidal particles were employed in this study: (1) Polyvinylpyrrolidone (PVP) functionalized poly(methylmethacrylate) (PMMA) colloids with rough surfaces, (2) PVP functionalized PMMA colloids with smooth surfaces, and (3) sulfonate-functionalized polystyrene (PS) colloids with smooth surfaces. It can be seen from Fig. 2 that they result in long, intermediate, and short meniscus tails, respectively. Interestingly, we found that the longer the meniscus tail, the smoother movement of the meniscus. As a result, more uniform coating can be achieved by using PMMA colloids with rough surfaces.

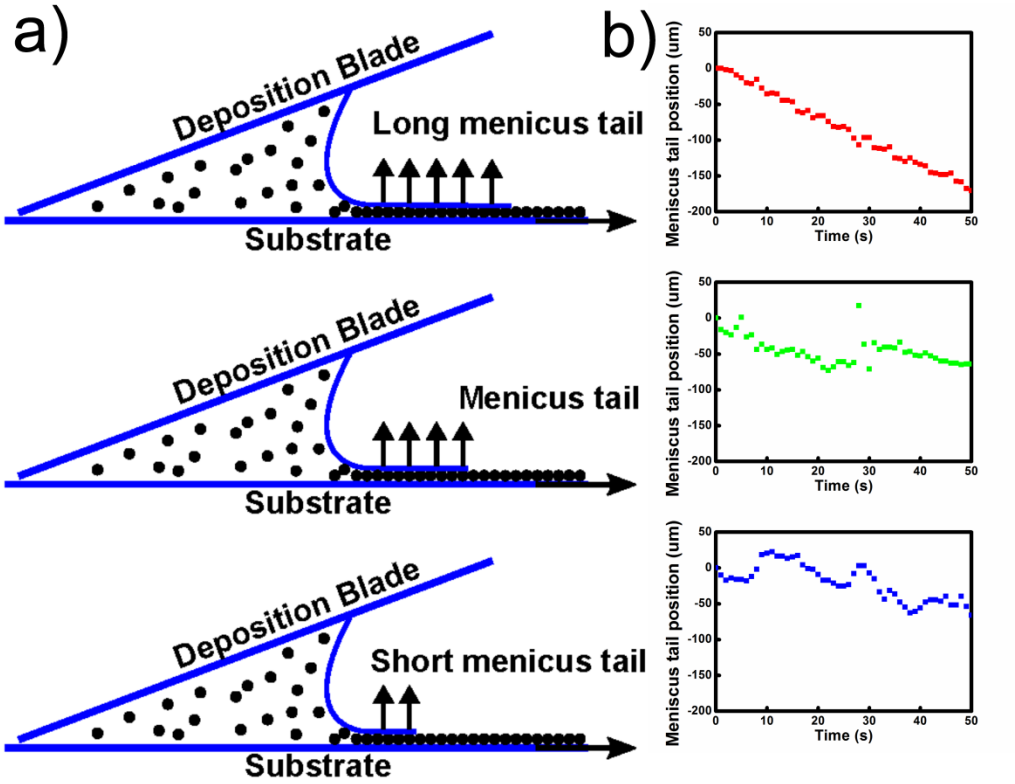

Figure 2 (a) Schematic of meniscus tails with different lengths. (b) The movement of meniscus shows different patterns correspondingly. As a result, the longer meniscus tips facilitates more uniform coating on the substrate.

Future Work

The CSM group plans to keep investigating the parameters that affect the flow-coating quality and improving the electric-field facilitated flow coating technology base on deeper understanding gained from the *in situ* observation.

Thrust: Silicon Absorbers and Cells

Key Challenges

Silicon-based solar cells are the dominant PV technology today with more than 80% market share. The research infrastructure is equally strong. This thrust must focus on those challenges with the greatest opportunities for successful university research. The key challenges which are being addressed to enable high volume manufacturing of high efficiency Si cells are listed below:

1. Commercially viable manufacturing of thin crystalline Si solar cells below 50um
2. Fundamental science of crystal growth and bulk defects for low-cost, high-quality ingots
3. Passivation of thin crystalline Si to meet the high efficiency targets
4. Absorption of all available light within a reduced absorber volume
5. Metallization and packaging of thin Si cells into lightweight modules

Existing Projects in our Thrust

- *High Efficiency Ultrathin Silicon Solar Cells*, Yi Cui (Stanford)
- *Graphene-Thin Insulator-Silicon Heterojunction Solar Cells on Exfoliated Monocrystalline Silicon Substrates*, Sanjay Banerjee (Texas)
- *Defect Identification and Mitigation in High-Lifetime Si Materials: Theoretical Part Characterization of 3d Transition-Metal Impurities*, S.K. Estreicher (Texas Tech)
- *Flash Annealing: A Method for Wafer-Level Processing of Si Substrates to Improve their Material Quality and Extend Ingot Yield, for Very High Efficiency Solar Cells*, Bhushan Sopori, (NREL)
- *Effectively Transparent Contacts for Solar Cells*, Harry Atwater (Caltech)
- *Optical Metamaterials as Antireflection Coatings for Solar Cells*, Mark Brongersma, (Stanford)
- *Laser Wafering*, Stuart Bowden (Arizona State)
- *Materials and Processes for High-Resolution Printed Bus Bars*, Vivek Subramanian (Berkeley)

Potential New Areas of Interest

- Processes for thin Si absorber preparation, such as spalling, epi-lift-off, templated growth, etc.
- Fundamental science of crystal growth and bulk defects for low-cost, high-quality ingots
- Methods for nano-texturing on thin Si surfaces, such as colloidal lithography, nano-imprint, etc.
- Improved passivation of thin crystalline Si foils including passivation of nano-textured surfaces
- Printing contacts on thin Si foils, including liquid precursor development

BAPVC Annual Project Report

Project Title: High Efficiency Ultrathin Silicon Solar Cells
PI: Yi Cui
E-mail: yicui@stanford.edu

Summary:

The goal is to generate high efficiency ultrathin silicon solar cells with an understanding of their device physics and developing manufacturing process. The Cui group at Stanford University has reported progress in the production of < 10 μm monocrystalline silicon at a wafer scale with regular fabrication processability. They have experimentally demonstrated that with novel nanoscale photon management structures, where a 3 μm-thick Si can absorb 58% of the above bandgap sunlight and 7 μm-thick can absorb 86%. They studied the balance between excellent photon absorption and efficient electrical collection in ultrathin monocrystalline-Si solar cells, and demonstrated >80% EQEs at wavelengths from 400 to 800 nm in a sub-10 μm-thick Si solar cell, resulting in 13.7% power conversion efficiency. Furthermore, a thin Si manufacturing technique is explored with metal-assisted chemical etching (MACE), and the fundamental mechanisms of the etching process have been clarified.

Key Accomplishments:

Ultrathin monocrystalline Si cells offer the potential of saving materials, increasing manufacturing throughput, and enabling easy low-weight installation. The Cui group developed wafer-scale free-standing ultrathin monocrystalline Si fabrication with uniform thickness from 10 to sub-2μm by KOH chemical etching (see Fig. 1(a,b)). These ultrathin Si wafers exhibit excellent mechanical flexibility and bendability, as shown in Fig. 1(d,e). Unexpectedly, these ultrathin Si materials can be cut with scissors like a piece of paper, and they are robust during various regular fabrication processing. To demonstrate their processability, the Cui group fabricated planar and double-sided nanotextured solar cells on these free-standing ultrathin Si films. Furthermore, they also experimentally demonstrated a large light absorption enhancement by a double-sided surface nanotexture design on the free-standing ultrathin Si films. Light absorption in 3 μm thick Si film is largely enhanced with a 130% increase in Jsc, achieving 58% absorption of the above bandgap sunlight. The 7 μm thick Si can absorb 86% of the above bandgap sunlight.

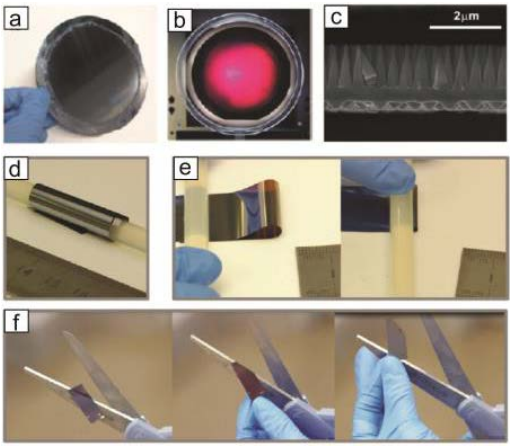

Figure 1. (a) and (b) 4-in. wafer-size ultrathin Si films illuminated by the white light from the backside. (c) SEM image of the cross sections of a double- sided patterned films.(d) A 3 μm thick Si film was wrapped around a plastic rod with diameter of 7 mm. (e) The Si film was folded and then pressed by the plastic rod. The minimum folding radius is around 1 mm. (f) Si cutting process using scissors. Ref. [1]

Despite the exciting success of nanoscale texturing in light trapping, the power conversion efficiencies of nanostructured Si solar cells, however, remain below 19% for thick devices and below 11% for thin devices. The Cui group fabricated a sub-10-μm-thick Si solar cell with a 13.7% power conversion efficiency which utilizes an all-back-contact design to overcome the critical problems of nanostructured devices: Auger and surface recombination. In general, nanostructured solar cells have a highly doped emitter layer at the front, fabricated by high-temperature diffusion processes. Because the diffusion profile of the dopants is dependent on the surface morphology, a nanostructured device tends to have a much deeper junction depth with a higher concentration compared with a planar device. It leads to severe Auger and surface recombination of charge carriers. Another problem of nanostructured Si solar cells is the increased surface area. Considering the fact that the surface recombination becomes more critical to device performance as the absorber becomes thinner, the increased surface area in a thin Si solar cell can lead to a severe decrease of efficiency. The Cui group designed devices with two main advantages: the all-back contact design and the nanocones. Its all-back-contact design prevented Auger recombination loss near the front (see Fig.2), and its nanocone structure minimized the increase in surface area while enhancing the light absorption significantly.

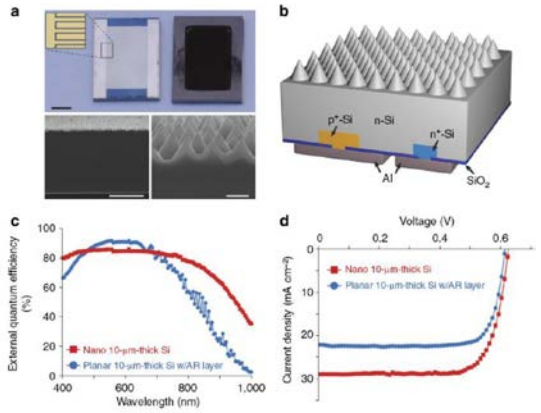

Figure 2. Ultra-thin Si nanocone solar cell. (a) Optical image and SEM cross-sectional views of the 10-μm-thick Si solar cell. (b) Schematic illustration of the device. (c) EQE data of the device and a planar control. (d) J–V characteristics of two devices in c. Ref. [2]

Finally, MACE is explored as a method of scalable production for thin Si because it is an easily scalable, low-cost selective wet etching technique. The final goal is to simultaneously etch thin Si wafers of arbitrary thickness directly from an ingot with little raw Si material loss. Thus far, the Cui group has demonstrated slicing vertically through a wafer of over 300 μm thick to produce long silicon slivers, as shown in Fig.3. To facilitate this goal, the fundamental mechanisms of the etching process were studied and clarified (Ref. [4]). Upon noticing that some of the etched Si looked very dark to the eye, the group further explored and developed a hybrid metal-semiconductor nanostructured interface, producing a structure that absorbs an average 97% of the visible spectrum with a sheet resistance of 16 Ω/□ while 60% of the top-down surface is covered with metal. An example false-color SEM of such a structure is shown in Fig. 3(f). The group continues to explore the applications of ultra high-aspect ratio MACE and this nanostructured interface, attempting to integrate it into a fully functioning Si solar cell.

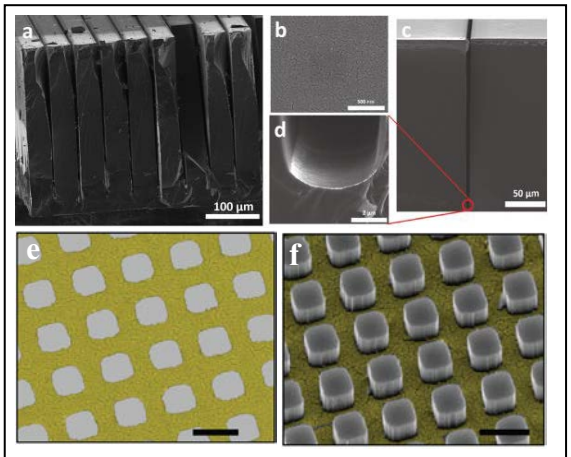

Figure 3. Metal-assisted chemical etching of Si. (a) SEM cross section of 5 μm wide lines etching over 300 μm down. (b) Nanostructure of evaporated metal layer. (c) MACE trench. (d) Zoomed in bottom of trench. (e) False-color SEM of pre-etched metal-patterned Si. (f) Post-etched pillar nanostructured Si. Scale bar is 500 nm for (e) and (f). Ref. [3] + [4]

Reference:
1. S. Wang, B. Weil, Y. Li, K. X. Wang, E. Garnett, S. Fan, and Y. Cui, "Large-Area Free-Standing Ultrathin Single-Crystal Silicon as Processable Materials," Nano Letters 13(4393) (2013).
2. S. Jeong, M. D. McGehee, and Y. Cui, "All-back-contact ultra-thin silicon nanocone solar cells with 13.7% power conversion efficiency," Nature Communications 4(2950) (2013).
3. V. Narasimhan, T. M. Hymel, R. A. Lai, and Y. Cui, "A hybrid metal-semiconductor nanostructure for ultrahigh optical absorption and low electrical resistance at optoelectronic interfaces," ACS Nano 9 (11) (2015)
4. R. A. Lai, T. M. Hymel, V. Narasimhan, and Y. Cui, "Schottky Barrier Catalysis Mechanism in Metal-Assisted Chemical Etching of Silicon," ACS Applied Materials & Interfaces 8(14) (2016)

Future Work:

Future work focuses on the push for higher efficiencies in the 10-20 μm Si solar cell. This goal can be accomplished via two methods: 1) producing a nanostructured heterostructure intrinsic thin-layer (HIT) solar cell; 2) good passivation with an oxide layer and careful surface preparation of ultrathin Si solar cells. The goal is to improve the 13.7% efficiency to 17.5%, and then further to over 20%. 3) Develop scalable and low-cost manufacturable process to generate thin Si with low material loss.

BAPVC Annual Project Report

Project Title: Graphene-Thin Insulator-Silicon heterojunction solar cells on exfoliated monocrystalline silicon substrates

PI: Sanjay K. Banerjee
E-mail: banerjee@ece.utexas.edu

Summary:

Monolayer and multilayer graphene are grown by chemical vapor deposition (CVD) and doped using gold nanoparticles. Together with the low cost, kerf-less mechanical exfoliation of thin silicon foils, graphene-thin insulator-silicon (GIS) heterojunction solar cells are demonstrated on bendable silicon substrates with overall efficiency of 5.4 %. Atomic layer deposition (ALD) of Al_2O_3 was used to passivate the silicon surface and precisely control the tunnel barrier thickness at low temperatures of 200 ˚C.

Key Accomplishments:

The Banerjee group at UT-Austin has demonstrated kerf-less mechanical exfoliation of monocrystalline silicon foils, up to 8 inches in diameter, where the parent wafer can be re-used for subsequent exfoliation, which can substantially reduce the material cost for solar cell applications.

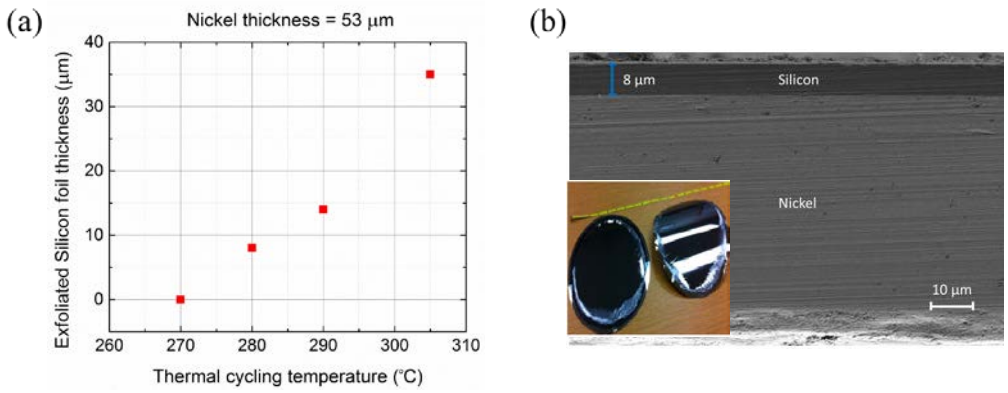

Fig. 1. (a) Exfoliated silicon thickness for different thermal cycling temperatures. (b) Cross-sectional SEM image of exfoliated silicon foil with thickness of 8 µm. Inset: Exfoliation result of 8 inch silicon wafer

Graphene, a 2D honeycomb lattice of carbon atoms, is incorporated with the exfoliated silicon because it is mechanically flexible, optically transparent, and highly conductive. The graphene acts as both the transparent conducting electrode as well as forming the junction in the device. It is p-doped with gold nanoparticles which act as charge transfer dopants when adsorbed on graphene. Large area high quality graphene is synthesized by CVD on copper foil substrate using methane and hydrogen precursor. Fig 2 shows a schematic of the CVD mechanism in (a). The effect of p-doping the graphene is shown in reduced R_S in fig 2(b) and shift in Raman peak position in (c).

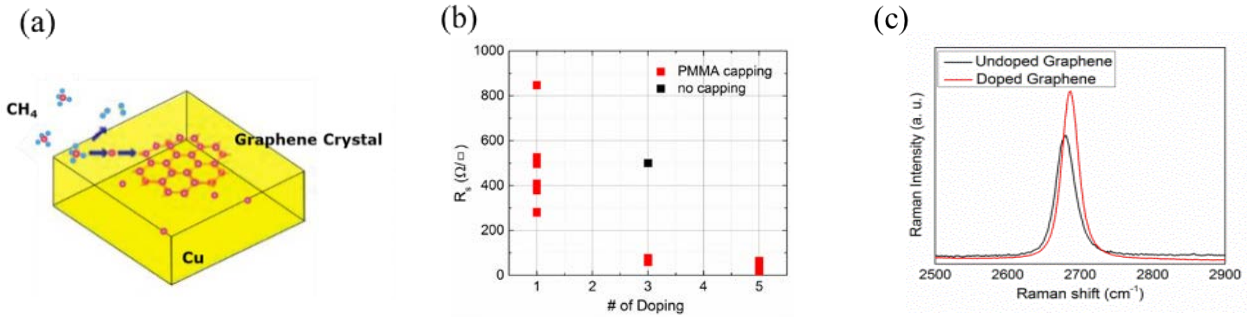

Fig 2. (a) Schematic of graphene CVD with methane precursor reacting at the catalytic Cu surface to form a crystal domain (b) Reduced graphene R_S with increased doping and (c) Raman peak shift due to charge transfer doping

Fig 3 describes the fabrication process for GIS solar cells on thin silicon foil. a-Si:H is first deposited on one side of the silicon to passivate (i-layer) and form ohmic contact (n+ layer) with electroplated nickel. After exfoliation, 1.5 nm of Al_2O_3 is deposited to passivate top surface and create a tunnel barrier for holes. Pre-doped graphene is transferred onto the surface by the conventional wet transfer technique. PMMA remains on the graphene and acts as an encapsulation layer.

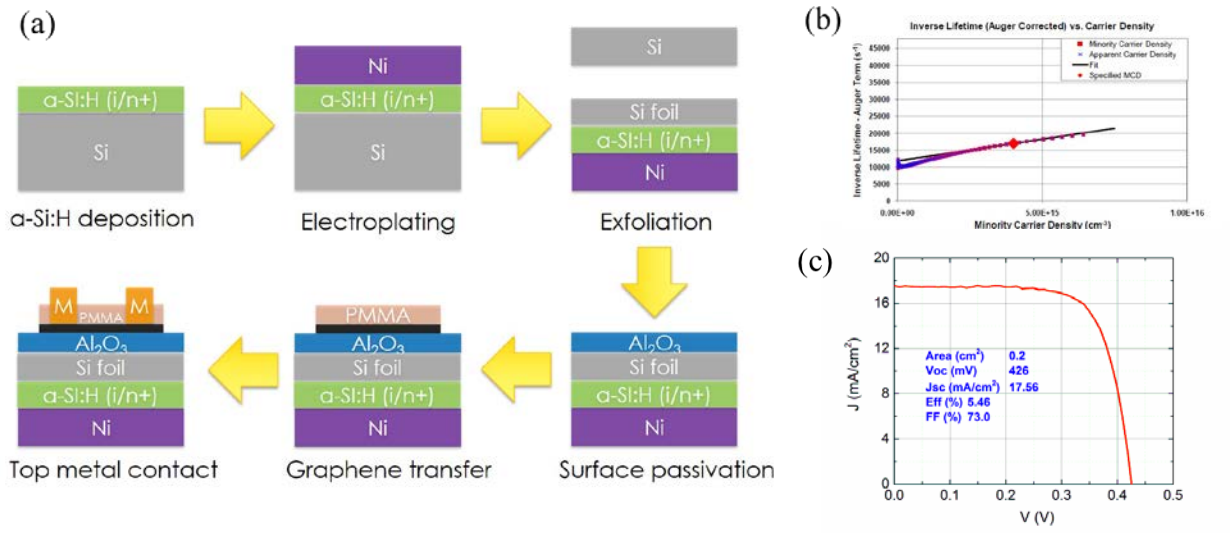

Fig 3. (a) Schematic of fabrication process of GIS solar cell on thin silicon foil (b) Photoconductance measurement result of 1.5 nm Al_2O_3 on silicon (c) J-V characteristics of the GIS cell

Future Work:

Future work will be focused on increasing the overall efficiency of GIS heterojunction solar cells by optimizing the graphene thickness and searching for better thin insulators. The group will conduct a detailed study of optimized graphene layers which balances between light transmission and series resistance. Other insulators such and h-BN and HfO_2 will be considered to further improve surface passivation and to perform as an electron barrier.

BAPVC Annual and Final Project Report

Project Title: Defect identification and mitigation in high-lifetime Si materials: Theoretical part characterization of 3d transition-metal impurities

PI: S.K. Estreicher, Texas Tech University

E-mail: STEFAN.ESTREICHER@ttu.edu

Summary

High-quality Si PV material often contains residual *dilute* 3d-transition-metal (TM) impurities. These TMs can limit the lifetime of minority carriers, especially in p-type Si. Over time, they can diffuse and form small metallic aggregates which contribute to the degradation of cells and modules [1]. The identification of such TM impurities relies on experimental tools such as DLTS or PL which are sensitive down to concentrations as low as $10^{11} – 10^{12}$ (cm^{-3}). But the assignment of DLTS peaks or PL bands to specific TM centers is not always straightforward.

Indeed, only a few gap levels can be assigned with a high degree of certainty to specific TM-related defects, such as the donor level of interstitial Fe (Fe_i) at E_v+0.39eV or the donor and acceptor levels of the {Fe,B} pair at E_v+0.10eV and E_c–0.26eV, respectively. The assignment of other DLTS centers has been called into question or even entirely dismissed. For example, the E_c–0.16eV and E_c–0.29eV, originally assigned to substitutional Co (Co_s), have now been shown to be associated with Co-H complexes [2]. Similar uncertainties are associated with the assignment of PL bands to specific defects. The best-documented example involves the so-called 'copper-pair' defects Cu_{PL} and Cu^*_{PL} which have been demonstrated to be Cu_4 and Cu_3Ag, respectively [3,4]. The latter studies have identified with absolute certainty the defects responsible for numerous (previously incorrectly assigned) PL bands. The experiments [3] were performed in isotopically-pure ^{28}Si samples and the isotopic signatures of the various defects are absolute proofs of their composition. Finally, even well-established migration barriers are sometimes wrong. For example, the migration barrier of Ni_i was recently shown [5,6] to be half of the accepted textbook value.

Further, even when an electrically- or optically-active center can be associated with a specific TM impurity, it is not always clear what can be done about it since important questions remain about its fundamental properties. For example, the migration path and activation energies in various charge (and spin) states of an interstitial TM impurity are not always known; neither is the nature of its interactions with vacancies, strained regions of the crystal, shallow dopants, or hydrogen; nor the electrical activity of the resulting complexes. For example, a lot is known about Fe_i (gap levels, diffusivity…) and Fe_iB_s pairs, but much less about Fe_s or Fe-H complexes. Answers to many questions about Ti, V, Cr, Mn, Co, Ni, and Cu are not experimentally available.

Accomplishments

The goal of the theoretical part of this project is to perform systematic 'first-principles' calculations of the fundamental properties of residual TM impurities in Si. In recent years, this level of theory has become quantitative in many respects and its predictions are much more reliable

than in the past. The stable sites, charge and spin states, electronic states and gap levels, binding and migration energies, interactions with impurities and defects, and other fundamental properties can be calculated. When completed, this study will provide a general picture of the fundamental properties of unwanted TM defects and guide the experimentalist as to how to remove or passivate them.

In recent years, such calculations have been performed in my group for Ti, Fe, Cu, and Ni [5,7-14]. The long-term goal is to complete these studies for all the elements of the 3d-series and provide a consistent set of predictions for all of them. A full report of our final results about V and Co interactions in Si is available in two recent manuscripts. The first, **Vanadium interactions in crystalline silicon,** is published: Backlund, D. J., T. M. Gibbons, and S. K. Estreicher. "Vanadium interactions in crystalline silicon." *Physical Review B* 94.19 (2016): 195210. The second, **Cobalt–related defects in crystalline silicon**, should appear soon.

References

[1] A.R. Peaker, V.P. Markevich, B. Hamilton, G. Parada, A. Dudas, A. Pap, E. Don, B. Lim, J. Schmidt, L. Yu, Y. Yoon, and G. Rozgonyi, Phys. Stat. Sol. A **209**, 1884 (2012)

[2] L. Scheffler, V. Kolkovsky, and J. Weber, Phys. Stat. Sol. A **209**, 1913 (2012)

[3] M. Steger, A. Yang, T. Sekiguchi, K. Saeedi, M.L.W. Thewalt, M.O. Henry, K. Johnston, H. Riemann, N V. Abrosimov, M.F. Churbanov, A.V. Gusev, A.K. Kaliteevskii, O.N. Godisov, P. Becker, and H.-J. Pohl, J. Appl. Phys. **110**, 081301 (2011)

[4] A. Carvalho, D.J. Backlund, and S.K. Estreicher, Phys. Rev. B **84**, 155322 (2011)

[5] S.K. Estreicher, D.J. Backlund, C. Carbogno, and M. Scheffler, Angew. Chemie **50**, 10221 (2011)

[6] J. Lindroos, D.P. Fenning, D. Backlund, E. Verlage, A. Gorgulla, S.K. Estreicher, H. Savin, and T. Buonassisi, J. Appl. Phys. **113**, 204906 (2013)

[7] N. Gonzalez Szwacki and S.K. Estreicher, Physica B **401-402**, 171 (2007)

[8] M. Sanati and S.K. Estreicher, Physica B **401-402**, 105 (2007)

[9] M. Sanati, N. Gonzalez Szwacki, and S.K. Estreicher, Phys. Rev. B **76**, 125204 (2007)

[10] S.K. Estreicher, M. Sanati, and N. Gonzalez Szwacki, Phys. Rev. B **77**, 125214 (2008)

[11] S.K. Estreicher, M. Sanati and N. Gonzalez Szwacki, Sol. St. Phenom. **131-133**, 233 (2008)

[12] N. Gonzalez Szwacki, M. Sanati, and S.K. Estreicher, Phys. Rev. B **78**, 113202 (2008)

[13] D.J. Backlund and S.K. Estreicher, Phys. Rev. B **82**, 155208 (2010)

[14] D.J. Backlund and S.K. Estreicher, Phys. Rev. B **81**, 235213 (2010)

BAPVC Annual Project Report

Project Title: Flash annealing: A method for wafer-level processing of Si substrates to improve their material quality and extend ingot yield, for very high efficiency solar cells.

PI: Bhushan Sopori and Ajeet Rohatgi
E-mail: bhushan.sopori@nrel.gov

Summary:
N-type Czochralski (CZ) silicon, used for very high efficiency Si solar cells, have long starting minority carrier lifetime (MCLT) that can vary over the axial length of each ingot. However, because CZ wafers often have high O and C concentrations, some of the O occurs in the form of oxygen precipitate nuclei (OPN), which ripen during cell fabrication processes to cause oxygen precipitation and swirl defects, with concomitant large decrease in the MCLT. Thus, it is difficult to fabricate very high efficiency solar cells on the wafers from entire Si ingot. A Flash Annealing (FA) process was developed to dissolve OPNs prior to wafer processing and prevent any precipitation during cell fabrication. Flash annealing consists of rapidly heating the wafers in an optical furnace to a temperature between 1200 and 1250 °C in oxygen ambient. The total process time is less than 2 minutes. Flash annealing was applied to a large number of wafers, taken from 2 different ingots (with different material quality). The results showed:

- The MCLT of all wafers reached 3.2 ms (corresponding to bulk MCLT ~ 5 ms) representing the highest MCLT of the wafers. The highest quality wafers remained unchanged.
- FA wafers were placed through critical cell fabrication steps of B diffusion and oxidation. It was found that FA prevented formation of swirl defects and MCLT degradation.
- Detailed analyses of oxygen before and after FA showed that FA led to an increase in dissolved O concentration that corresponded to dissolution of 10 ^{13} cm^{-3} of OPNs.

Key Accomplishments:

1. Wafers taken from different locations along the axial length of two ingots, A &B as illustrated in Fig. 1, were FA by the optimized process. See table 1 for the starting wafer properties. **The MCLT of all wafers improved to the highest value of wafers in ingot A (see Fig. 2).**

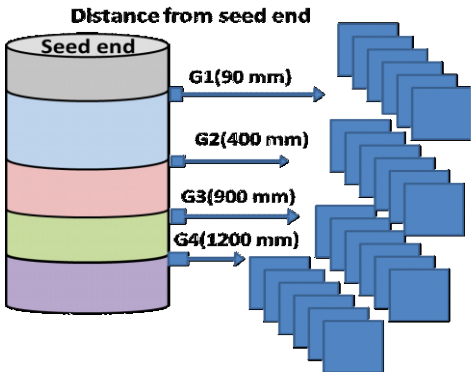

Fig.1. Illustration of wafer selection format from two ingots.

Table 1. As-grown parameters of wafers in ingots A &B

Wafer group	Ingot A			Ingot B		
	O (ppma)	C (ppma)	MCLT (μs) (ingot)	O (ppma)	C (ppma)	MCLT (μs) (ingot)
G1	15.1	0.46	4765	15.9	0.98	1825
G2	12.4	0.49	4992	13.9	1.05	1701
G3	12.6	0.53	4043	14.0	1.37	1478
G4	12.6	0.75	3201	13.8	1.04	1304

2. The researchers have shown that the increase in MCLT was due to dissolution of OPN. The confirmation was made in several ways: (a) FTIR analyses showed that flash annealing

results in an increased (2 x 10^{17} cm^{-3}) in the dissolved oxygen concentration; (b) The injection level dependence of MCLT was fitted with a two-defect model, which gave an estimated density of OPN equal to 2 x10^{13} cm^{-3} (see Fig. 3 for other parameter values). This density of OPN corresponds to ~ 2 x 10^{17} cm^{-3} atoms of oxygen (verifying gain in dissolved O due to OPN dissolution).

3. We have verified that flash annealed wafers do not degrade during solar cell fabrication.

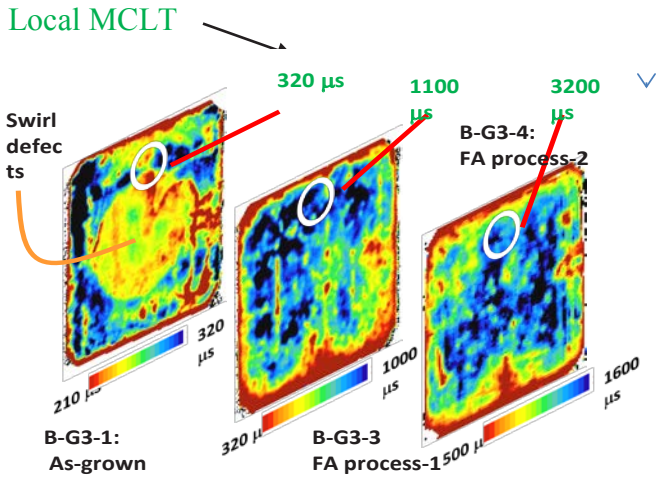

Fig. 2. MCLT maps and local values for sequential wafers from a lower quality ingot [B- G3]. Wafers are as-grown and Flash Annealed by two different process conditions

The local MCLT was measured by Sinton tool before mapping with Semilab tool (using I-E passivation).

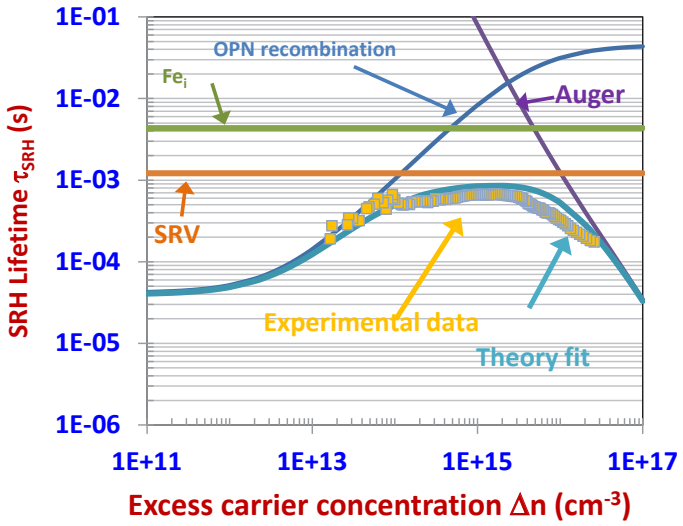

Fig. 3. Example of fitting the injection level dependence of MCLT, using two-defect model and $1/t_{eff} = 1/t_{SRHO} + 1/t_{Fe} + 1/t_{SR} + 1/t_{Aug}$

Best fit: S_{eff}=7, $Fe_i = 3X\ 10^{11}$, OPN density=2 X 10^{13} cm^{-3}, Ec-Et = 0.2eV, $\sigma_n = 10^{-19}$ cm^2

OPN density, when be converted into concentration of dissolved oxygen ~ 2 x 10^{17} cm^{-3}

Note: An important feature of the FA process is that it is inherently a very clean process that does not require an expensive HCl cleaning of the furnace or wafers. In addition, because the wafer temperature during the annealing is highly uniform, there is no generation of defects that can degrade the wafer quality.

Future Work:

Two groups of wafers, consisting of annealed and unannealed sequential-wafers, are being prepared for fabricating solar cells and determining improvement in the cell efficiency due to FA process. These cells will be analyzed in detail to establish the mechanism(s) of efficiency improvement.

BAPVC Annual Project Report

Project Title: Effectively Transparent Contacts for Solar Cells
PI: Harry Atwater
E-mail: haa@caltech.edu

Summary:

The Atwater research group developed effectively transparent contacts and demonstrated record transparency (99.9 %) in optical simulations and experiments. Significant short circuit current density enhancement (~2 mA/cm^2) was observed by replacing conventional contacts with effectively transparent contacts. Due to the low series resistance silicon heterojunction solar cells with effectively transparent contacts yield fill factors of > 80%.

Key Accomplishments:

Effectively transparent contacts (ETCs) were incorporated in silicon heterojunction solar cells by imprint lithography with silver paste. Scanning Electron Microscopy (SEM) images are shown in Fig. 1b and c. Figure 1 a shows current-voltage characteristics of silicon heterojunction (SHJ) solar cells with three different front contacts: 70 nm indium tin oxide (ITO) and flat contacts, 70 nm ITO and ETCs and only 70 nm ITO. While significant short circuit current is lost with flat contacts, the ETCs yield the same short circuit current as a cell with only ITO due to their almost perfect effective transparency. Furthermore, high fill factor (>80%) is obtained.

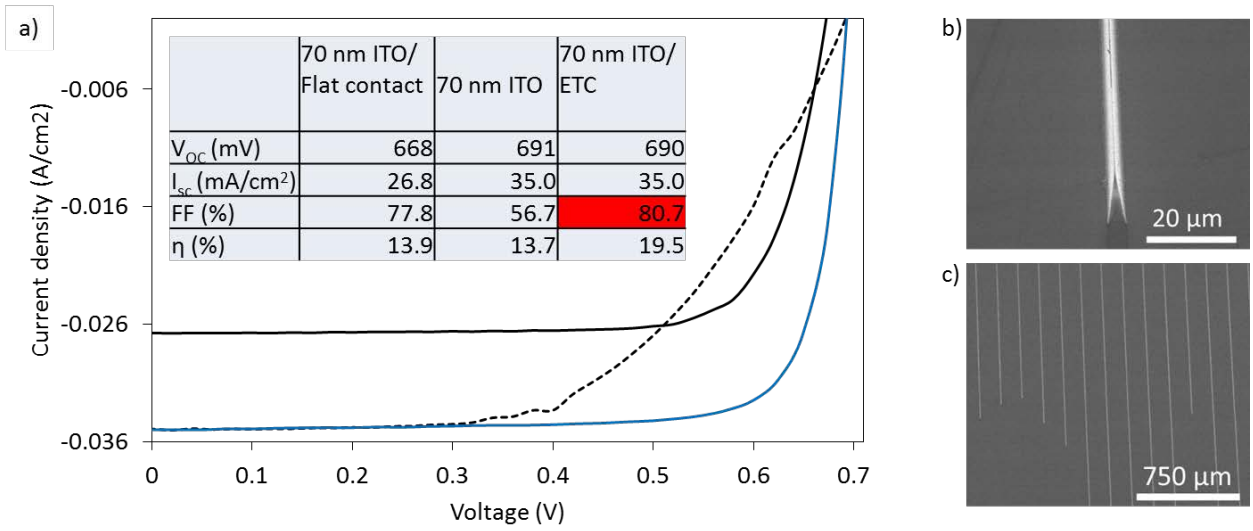

Figure 1: a) Current-voltage characteristics of silicon heterojunction solar cells with flat (standard) contacts, ETCs and only ITO. b) and c): SEM images of ETCs.

ETCs show high performance over a wide range of angles of incidence as determined by optical simulations and experiments. Figure 2a shows data from an experiment where the angle of incidence was varied at a wavelength of 600 nm.

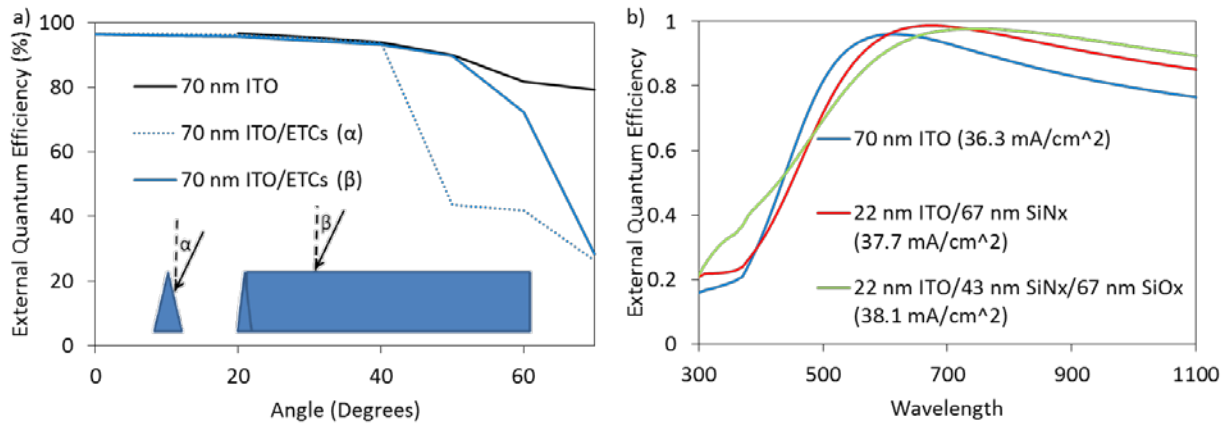

Figure 2: a) Angle dependence of external quantum efficiency of SHJ solar cells with ETCs compared to cells with only ITO. b) Simulated external quantum efficiency of SHJ solar cells with optimized antireflection coatings.

ETCs can also replace transparent conductive oxides due to their very close spacing (here 80 μm). In SHJ solar cells with only 22 nm ITO up to 77.3% fill factor was obtained. This opens the door for optimized antireflection coatings consisting of earth abundant materials. Furthermore, antireflection coatings can be optimized for low reflection and low parasitic absorption. Figure 2b shows the simulated external quantum efficiency of SHJ with three different antireflection coatings. With these materials short circuit current density enhancement of 2 mA/cm^2 can be achieved compared to a conventional ITO layer – which is in addition to the transparency gain from ETCs.

Future Work:

In future the team will combine light management strategies developed at Caltech, ASU, Stanford and MIT in order to obtain high efficiency heterojunction solar cells with low cap-ex and low manufacturing cost.

BAPVC Annual Project Report

Project Title: Optical metamaterials as antireflection coatings for solar cells
PI: Mark L. Brongersma
E-mail: brongersma@stanford.edu

Summary:
Metamaterials are artificially engineered materials offering the unique opportunity to tailor their optical properties and functionalities. Brongersma group previously demonstrated that a traditional quarter wavelength-thick silicon nitride antireflection (AR) coating for silicon substrates can be replaced by an array of silicon nanoparticles that support optical, Mie resonances. Under the BAPVC program, they demonstrated that the particle-based AR coatings can be made more broadband than a single layer AR coating by placing differently-sized Si nanoparticles on the surface at subwavelength distances.

Key Accomplishments:
Under the BAPVC program, the Brongersma group has provided a detailed understanding of the antireflection properties of optically-resonant semiconductor nanostructures. The scattering from such nanostructures can cancel the reflection from a high refractive index substrate. In this period of the program, we designed and fabricated more complex arrays of particles to extend the spectral bandwidth and achieve functionality otherwise impossible to obtain using the traditional single layer coating. It was previously established that a scattering particle cancels part of the scattered light from the substrate at its resonant wavelength. Here, it was shown that particles of different sizes that feature different resonant frequencies can be organized on a surface to cancel reflection at multiple wavelengths. The optical resonance frequency of a particle depends on the size, materials choice, and shape. It was shown how a bimodal array consisting of two particle sizes atop a semi-infinite silicon substrate can provide more broadband antireflection.

Two different samples were simulated, optimized, and fabricated. One has same-size nanopillars and the other having a bimodal distribution of sizes (see insets of Fig. 1(a)). Simulated and measured reflection data for unpolarized light are reported in panel (a). It was possible to control and change the farfield spectral features of light reflected from silicon with a high degree of flexibility by using carefully designed silicon nanopillars with a pillar height of approximately a quarter-wavelength. In particular, it was possible to engineer the number of minima in the reflection spectrum by designing the size distribution of the pillars, and move their spectral position changing the pillar sizes. Very low reflectivity at one or two wavelengths in the visible range was obtained. The physics behind the operation of such structure is highlighted in Figure 1(b). On the left, the magnitude of the magnetic field in the monomodal array is plotted at 560 nm. Here, the resonant properties of the pillars determine a minimum in the reflection spectrum whose position matches the resonant wavelength of the nanostructure. On the other hand, the middle and right panels show that the two sizes of pillars in the bimodal array resonate at different wavelengths (431 nm and 590 nm, respectively) leading to the two observed minima in the reflection spectra.

The ultimate goal of an antireflection coating is to increase the amount of light transmitted into the substrate. For this reason, the average reflection in the visible spectrum (400 nm - 800 nm) between the metasurfaces and an 68 nm-thick uniform SiN layer was compared. The monomodal pillar array exhibits an average reflectivity of 7%, consistent with the traditional

approach. On the other hand, the bimodal array outperforms the continuous layer. Its calculated spectrally averaged reflectivity is as low as 4%. The presented structure was design to maximize light transmission at the solar peak wavelength and in the blue-side of the visible spectrum, where silicon absorption is higher. Further reflection reduction can be achieved by including more pillar sizes or shifting their resonances, as needed.

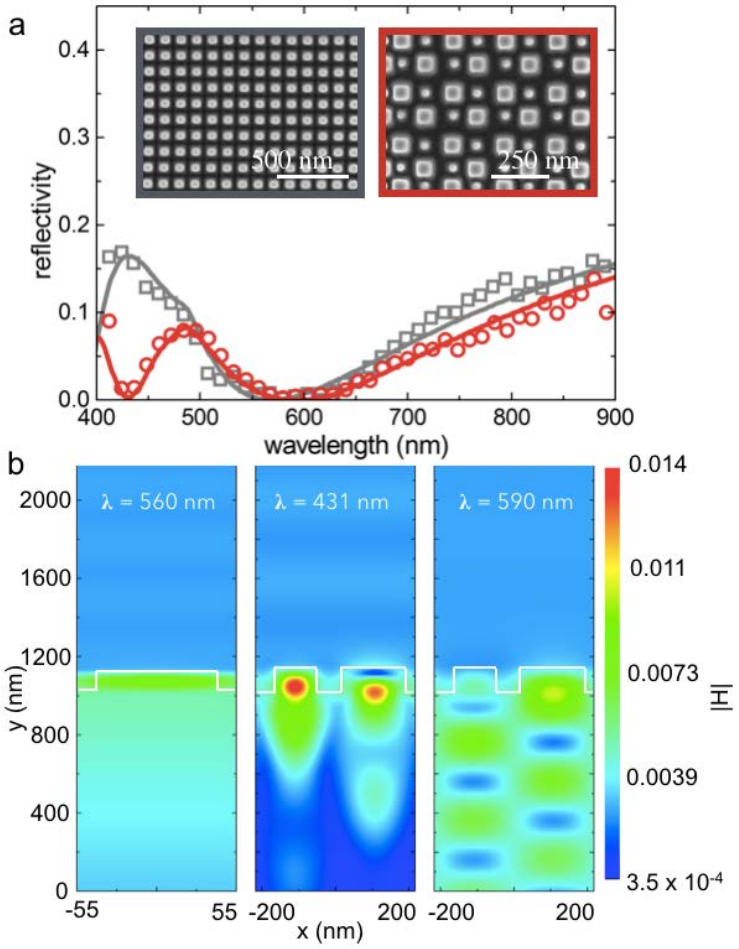

Figure 1. (a) Calculated (continuous lines) and measured (dots) reflection spectra of a patterned silicon wafer with a monomodal (grey) and bimodal (red) array of 3D particles. (Inset) Top view SEM images of the fabricated samples. Pillars in the monomodal sample are 70 nm-tick and 80 nm-wide, repeated over a period of 110 nm. In the bimodal sample, thickness is fixed at 77 nm, while pillar sizes are 52 nm and 93 nm, respectively. In this case, period is 217 nm. (b) Map of the magnitude of the magnetic field along a cross section of the device structures. Field is shown at 560 nm (left) for the monomial array; 431 nm (middle) and 590 nm (right) for the bimodal array.

Future Work:

The group is currently exploring more complex structure involving a plurality of particle sizes. We are also working with other BAPVC groups at Arizona and Caltech to implement these coatings in economic silicon heterojunction solar cells.

BAPVC Annual Project Report

Project Title: Laser Wafering
PI: Stuart Bowden
E-mail: sgbowden@asu.edu

Summary

To achieve the goal of 'laser wafering' the group at ASU has set up a laser with nanoseconds pulse width and variable wavelength (670nm-2600nm) and run experiments to create a damage plane at controlled depth of the sapphire wafer. The damage plane in sapphire was characterized with optical microscope and lift off was attempted on the sapphire wafer across the damage plane.
In addition to the experimental work, the group has performed theoretical investigation to understand the laser material interaction.

Summary of Key Accomplishments:

To realize the goal of 'laser wafering', a laser of fixed pulsed length (6ns) and variable wavelength (670-2600 nm) was set up at Solar Power Lab in ASU. Although the initial goal of the project was to implement the process in silicon, preliminary experiments were performed in sapphire due to the simplicity of characterization. Prior to the experiment, some theoretical calculations were performed in order to predict the amount of power needed and the effect of numerical aperture of the optics used for the creation of damage plane. In the theoretical analysis, two different models: 'ray optics model' and 'electron plasma model' were used. Out of these two models; the first one, based on Snell's law, gives rough estimate on the focusing of laser underneath the desired depth of a substrate. On the other hand, more realistic 'electron plasma model based on Keldysh theory accounts for non-linear phenomena such as multiphoton photoionization and impact ionization which are dominant absorption mechanisms of sub-band gap photons. For both models, a TM_{00} Gaussian beam of well-defined beam waist is used. The damage threshold values are 3.5×10^{14} W/m^2 in sapphire and 8×10^{12} W/m^2 in silicon for a nanosecond pulse width laser. From these threshold values and the amount of laser power dumped in at the focus point of the material, the shape and size of the region of permanent

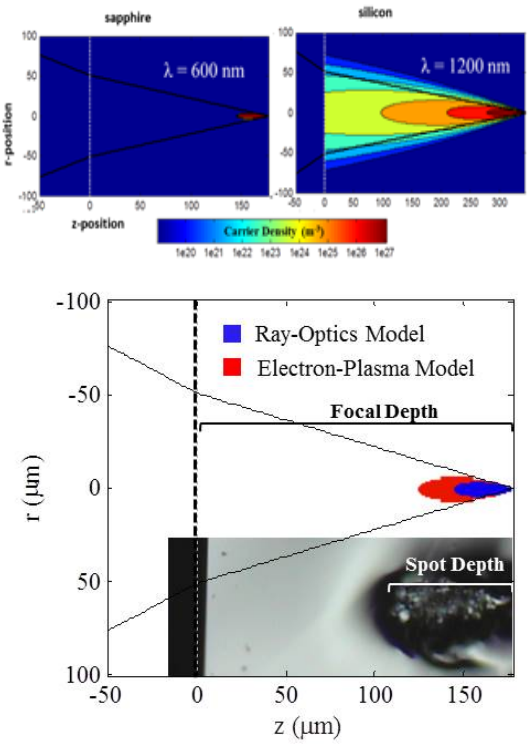

Figure 1. Electron-plasma model results for 600 nm wavelength laser in sapphire and 1200 nm wavelength laser silicon (above) and laser damage size in sapphire compared with theoretical models (below). These results exhibit the matching of our theoretical analysis with the experimental observation.

damage are roughly estimated. The theoretical and experimental observation of the damage spot size and power density are compared in Figure 1. As presented in Figure 1 , for given numerical aperture (N_A=0.5) of the optics, due to higher refractive index of silicon than sapphire, the damage spot size in silicon seems to be comparatively larger than in sapphire.

To achieve the experimental goal on laser wafering, a system was designed to integrate the laser system with a three-dimensional automated stage. Successful dicing of 2" round double side polished sapphire wafers was performed using 667 nm laser light focused 200 μm into the bulk of the material. The optical microscope images of Figure 2 show that the permanent laser damage spots are contained entirely in the bulk of the material without leaving any traces of damage on the surface.

Multiple regions varying subsurface laser damage density and damage plane depth were prepared. Multiple techniques to expose the subsurface damage plane to the etchant were also designed and attempted. One technique used was to laser drill at the corners of the damage region to allow a path for the etchant to the subsurface damage array. The samples were placed in a solution of 49% hydrofluoric acid at room temperature for 4-96 hours. Unfortunately, no change was observed using the optical microscope for the laser damaged material and no successful layer liftoff occurred. This is best explained by the fact that although the material is permanently modified only in a narrow plane in the bulk of the material, at nanosecond pulse lengths, laser damaged material can recrystallize. So instead of forming an amorphous region, a polycrystalline region might, instead, have been formed which is difficult to chemically etch with HF. There would be little to no improvement in etch rate for polycrystalline sapphire vs. crystalline sapphire, meaning that either femtosecond laser damage would need to be used to achieve the extreme stress required to create a fully amorphized , or another liftoff method should be pursued.

Following the failure of chemical assisted layer liftoff, a mechanical liftoff method was pursued with various adhesives. Unfortunately, none of these methods proved successful. The adhesive force between the tweezers edge and the sapphire substrate was not strong enough to overcome the remaining material bonds in the subsurface damage region.

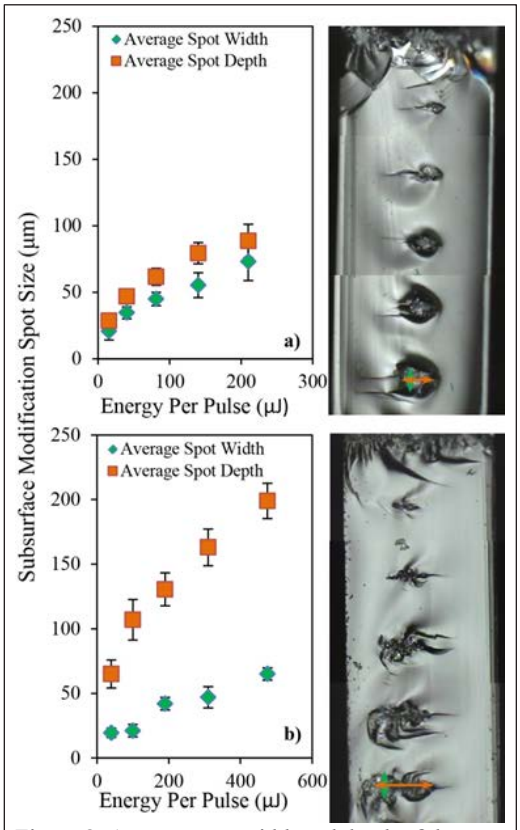

Figure 2. Average spot width and depth of the modified region formed beneath the surface of sapphire from a single laser shot at varying incident pulse energies and optical microscope image of the cross-section of a wafer for a) NA=0.50, and b) NA=0.28 objectives.

Future Work

For future work, a femtosecond pulsed width laser will be used to get fully amorphised plane of sapphire or silicon in the bulk so that it can be etched by HF. Also, to avoid free carrier absorption of laser by silicon or sapphire, the cooling of the sample down to liquid N_2 temperature will be maintained while doing the laser subsurface damage.

BAPVC Annual Project Report

Project Title: Materials and Processes for High-Resolution Printed Bus Bars
PI: Vivek Subramanian
E-mail: viveks@eecs.berkeley.edu

Summary:

In this project, researchers are developing materials and processes for high-resolution bus bars through a combination of development of high-resolution gravure printing and development of advanced nanoparticle conductor inks. In the last year, substantial progress has been made on improving the resolution of gravure printing, with sub-2μm features have been realized, printed at printing speeds of ~1m/s. Additionally, researchers have shown that gravure can be used to print on flexible and rigid glass substrates, and new classes of high-solubility nanoparticle inks have been developed to deliver high conductivity films.

Key Accomplishments:

In the area of high-resolution printing, significant progress has been made, going beyond even our previous world record achievements. Features sizes approaching 1μm have been realized with good line edge roughness and pattern fidelity, while maintaining high printing speeds of ~1m/s. We have used our previously reported understanding of gravure printing to design and build a new gravure printer that is specifically designed to deliver ~1μm resolution, and to be compatible with both flexible and rigid substrates. This tool is shown below in figure 1.

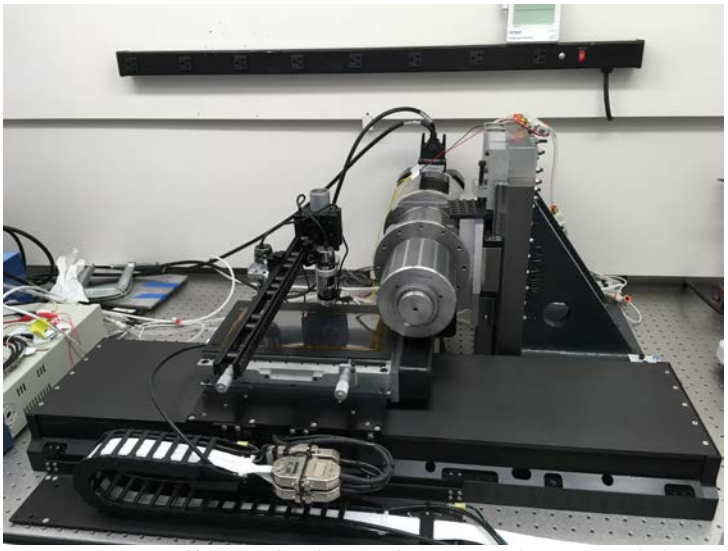

Figure 1: New gravure printer offering high resolution and compatibility with a wide range of substrates.

In addition to developing a new printer, we have also made substantial progress in developing new inks. In particular, it is desirable to have inks with high mass loading to enable rapid printing of the thicker films typically needed for bus bars. This should be achieved without necessitating higher sintering temperatures. We have developed new nanoparticles that offer

high solubility while having low carbon content and low sintering temperature. These have been achieved by using genetic-optimization based machine learning techniques to rapidly optimize new generations of particles tuned to deliver these parameters. Results are shown in figure 2, where we show significant increase in silver mass (i.e., reduction in carbon) and in mass loading (i.e., solubility) over three generations of particle optimization via genetic algorithms.

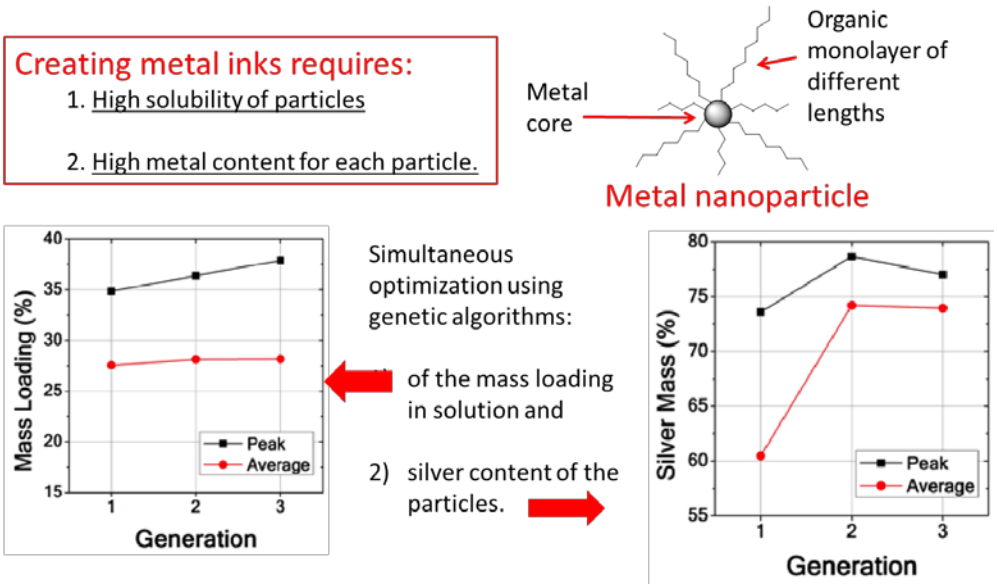

Figure 2: Genetic optimization of nanoparticles for high mass-loading, high-conductivity conductor inks.

Future Work:

We have developed a new printer for continuing development of high resolution gravure printing. This will be used to extend our capability even further, both with respect to resolution, and with respect to printing on rigid substrates.

Thrust: Thin-Film PV

Key Challenges

Thin-film solutions faces four significant challenges: (1) increasing efficiency of modules (particularly decreasing the gap between lab scale champion cells and production modules), (2) reducing direct materials costs, (3) reducing capital intensity of manufacturing, and (4) design and validation for long-term field reliability.

Existing Projects in our Thrust

- *Advanced Materials Characterization*, Mike Toney and Alberto Salleo (SLAC/Stanford)
- *Identifying Problem Areas in CIGSe and CdTe Based PV Devices*, Mark Lonergan (UO)
- *Non-Equilibrium Processing of CdTe Absorbers*, Colin Wolden (CSM)
- *Laser Processing to Improve CdTe Thin Film Photovoltaics Efficiency and Manufacturing*, Mike Scarpulla and Chris Ferekides (Utah/USF)
- *Advanced Evaporation Source Design*, Greg Hanket (IEC)
- *1.7 eV Absorber for Si Based Tandem Solar Cell Applications*, Yong-Hang Zhang (ASU)
- *Fundamental Modeling of Chalcopyrite Solar Cells*, Scott Dunham (UW)
- *Development of Multicolor Lock-in Photoluminescence Methods*, Hugh Hillhouse (UW)
- *In-situ Characterization of Grain Growth in Thin Film Semiconductors*, Delia Milliron (Texas)
- *Sintering CdTe Nanoparticles into Functional Bulk Absorber Layers*, Paul Alivisatos (Berkeley)

Potential New Areas of Interest

- *Theory and Modeling*. Improved collaborative device-modeling resources that, in coordination with materials and device characterization, will inform and guide materials and device development.
- *Materials Chemistry of absorbers*. Improved understanding of defects and grain growth, and their role in metastability, composition, morphology and heterogeneities present both intra-grain and at interfaces and grain boundaries, is critical to advancing device design, process optimization, and performance.
- *Thin Film Device Architecture*. Efforts to optimize heterojunctions, interfaces, transparent conducting layers, carrier-selective contacts, and interconnects are desired. Efforts are also needed to explore means of de-coupling processes, e.g. separating of the "activation" of the absorber layer from intermixing at the CdS/CdTe interface which currently occur simultaneously during the $CdCl_2$ treatment.
- *Device and Materials Stability*. Collaborative research is needed to proactively test innovative device and materials stability under operating conditions (temperature, bias, and light) in order to screen for commercial viability.
- *Device Reliability*. Evaluation of packaged device reliability under combined thermo-mechanical, electro-chemical, and photo-chemical stresses in combination with commercial or BAPVC-developed encapsulants is needed to quickly identify interface adhesion issues and screen for commercial viability.
- *Low Capital Cost Manufacturing*. An expanded focus on developing new low capital cost processing routes to CdTe and CIGS would help thin film technologies compete with crystalline silicon.

BAPVC Annual Project Report

Project Title: Advanced Materials Characterization
PI: Mike Toney & Alberto Salleo
E-mail: mftoney@slac.stanford.edu, asalleo@stanford.edu

Summary:

The Toney Group at SSRL characterizes photovoltaic materials with X-ray techniques. SSRL has developed several in-situ thermal processing chambers that have been utilized on projects with members of the BAPVC. The rapid thermal processing (RTP) chamber has been utilized by the Milliron group to characterize CZTS and CIGS nanoparticles as they transition to sintered films. The in-situ annealing chamber and in-situ Se annealing chamber have been utilized by several projects in the Bent group. An investigation has also been done into the chemical character of the Cl remaining in Cl derived perovskites both in-situ and ex-situ X-ray absorption spectroscopy (XAS). Diffraction and XAS has been utilized to better understand the CuZnS TCOs developed by the Ager group. The work of the Salleo group within BAPVC focuses on using sensitive sub-gap measurements to characterize optical absorption and defects in photovoltaic materials and entire PV stacks.

Key Accomplishments:

The Ager group at LBL is developing $Cu_xZn_{1-x}S$ alloys as a promising p-type transparent conductor. Initial studies by the Ager group suggested that their films were amorphous; however, the Toney group has been able to determine that the films are nanocrystalline and to determine the crystalline structure of these films. X-ray diffraction patterns of $Cu_xZn_{1-x}S$ films are shown in Fig. 1. The XRD shows that the films contain both sphalerite and wurtzite ZnS phases with predominantly wurtzite at x=0.30, which corresponds to a peak in conductivity.

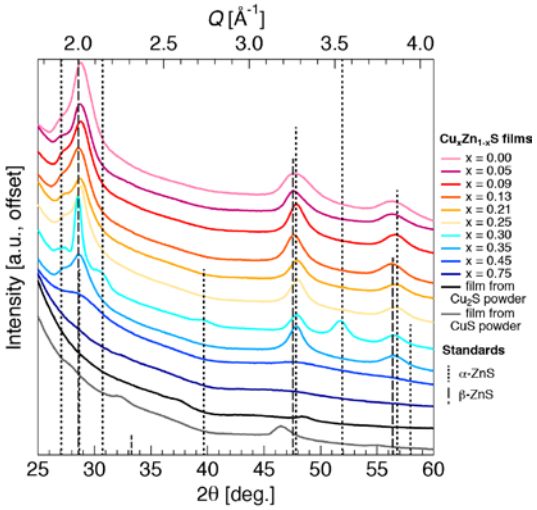

Figure 2. XRD of $Cu_xZn_{1-x}S$ films deposited on quartz at room temperature for $0 \leq x \leq 0.75$. Films contain a mix of sphalerite (β) and wurtzite (α) ZnS, with wurtzite dominant in the $x = 0.30$ film.

Work has been done on hybrid perovskite solar cell absorbers to understand the role that Cl plays in improving the performance of Cl derived $MAPbI_{3-x}Cl_x$ (MA = methyl ammonium) solar absorbers. XAS has verified that Cl remains in the films after typical annealing. Comparing the spectra of Cl of fully converted (to $MAPbI_{3-x}Cl_x$) films to XAS of MACl and $PbCl_2$ standards, we showed that the remaining Cl is not the precursors remaining in the film. Further work is needed to understand where in the film the Cl is incorporating.

Measurements implemented by the Salleo group include: below-gap photocurrent measurements (FTPS) in photovoltaic stacks to characterize defects and locate whether they are

found in the active layer or in other regions of the stack; true absorption (i.e. excluding scattering) above gap using photothermal deflection spectroscopy (PDS) in thin and thick layers; and absorption below-gap in active layers using PDS to characterize defects. In 2014 through the spring of 2015, Salleo group collaborations with BAPVC members on FTPS measurements increased significantly, including ones with GE/First Solar, the University of Oregon (Mark Lonergan's group), the Colorado School of Mines (CSM - Colin Wolden), and 3-Sun.

Publications:

1. "Formation of Nanoscale Composites of Compound Semiconductors Driven by Charge Transfer", W. Gao, R. Reis, L.T. Schelhas, V.L. Pool, M.F. Toney, K.M. Yu, W. Walukiewicz, Nano Lett. **16** 5247–5254 (2016). DOI: 10.1021/acs.nanolett.6b02395
2. "Impact of Conformality and Crystallinity for Ultra-Thin 4 nm Compact TiO_2 Layers in Perovskite Solar Cell", K.E. Roelofs, V.L. Pool, D. A. Bobb-Semple, A.F. Palmstrom, P.K. Santra, D.G. Van Campen, M.F. Toney, S.F. Bent, Adv. Mater. Inter. **3**, 1600580 (2016). DOI: 10.1002/admi.201600580
3. "P-Type Transparent Cu-Alloyed ZnS Deposited at Room Temperature", R. Woods-Robinson, J.K. Cooper, X. Xu, L.T. Schelhas, V.L. Pool, A. Faghaninia, C.S. Lo, M.F. Toney, I.D. Sharp, J.W. Ager, Adv. Elect. Mater. **2**, 1500396 (2016). DOI: 10.1002/aelm.201500396
4. "Chemical bath deposition of p-type transparent, highly conducting $(CuS)_x$:$(ZnS)_{1-x}$ nanocomposite thin films and fabrication of Si heterojunction solar cells", X. Xu, J. Bullock, L.T. Schelhas, E.Z. Stutz, J.J. Fonseca, M. Hettick, V.L. Pool, K.F. Tai, M.F. Toney, X. Fang, A. Javey, L. H. Wong, J.W. Ager, Nano Lett. **16**, 1925–1932 (2016). DOI: 10.1021/acs.nanolett.5b05124
5. "Chlorine in $PbCl_2$-Derived Hybrid-Perovskite Solar Absorbers", V.L. Pool, A. Gold-Parker, M.D. McGehee, M.F. Toney, Chem. Mater. ***27***, 7240–7243, (2015). DOI: 10.1021/acs.chemmater.5b03581.

Future Work:

N/A.

BAPVC Annual Project Report

Project Title: Identifying problem areas in thin film photovoltaics
PI: Mark Lonergan
E-mail: lonergan@uoregon.edu

Summary:

The Lonergan group has collaborated with the Wolden group at Colorado School of Mines to study the effect of different back-contact metals on the evolution of performance, the sub-bandgap density of states (DOS), and impurity concentration distribution of CdTe absorbers subjected to accelerated lifetime testing (ALT). This study suggests that titanium back-contacts suppress the formation of a deep defect band that is correlated with compromised performance as the cells underwent 1-sun ALT. Additionally, the Lonergan group has developed an improved analysis for drive level capacitance profiling (DLCP) that quintuples the precision of dopant and defect density determination in thin-film solar cells without the use of any new equipment or additional measurement time.

Key Accomplishments:

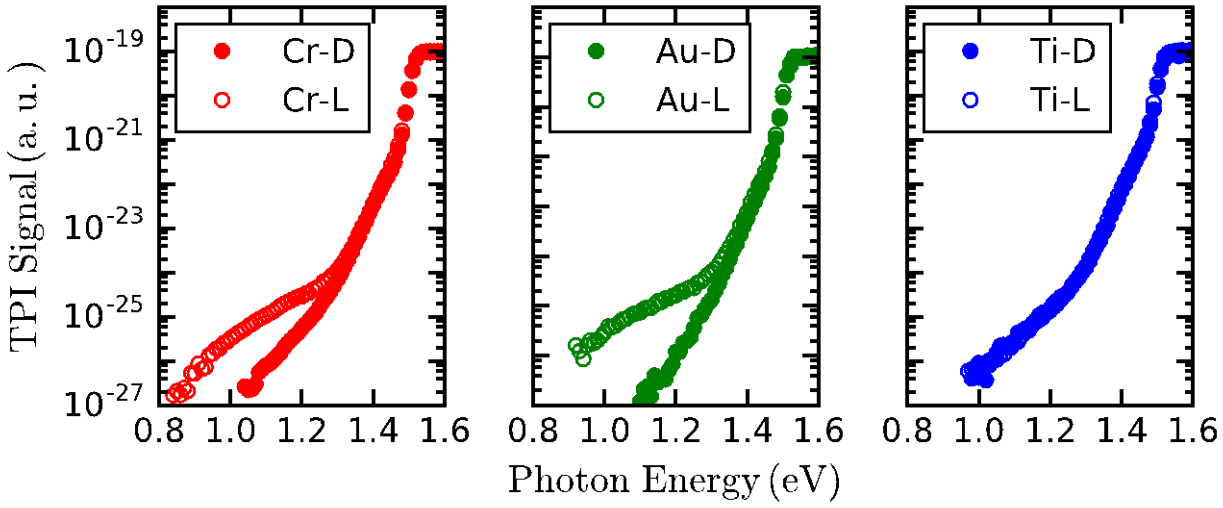

Figure 1. Transient Photocurrent (TPI) spectra for CdTe solar cells with chromium (left), gold (center) and titanium (right) back-contacts. Samples underwent ALT for ~300 hours under one-sun illumination (L) and in the dark (D). While the presence of light in the ALT leads to higher defect densities in the Cr and Au back-contact samples, the Ti back-contact appears to suppress the formation of this defect.

The Lonergan group investigated the effect of different back-contacts on defect evolution in CdTe solar cells following ALT in the dark and under 1-sun light for 300 hours. The TPI spectra shown in Figure 1 suggest that light can enhance defect formation in CdTe absorbers but this action is suppressed by a titanium back-contact. The density of the defect at 1.15 eV was predictive of the short-circuit current density across all six devices.

The Lonergan group also drastically improved the analysis for DLCP, an essential method for accurately measuring, dopant, trap and, interface defect densities in thin-film solar cells. [1] By including previously unused constraints, the number of free parameters used to fit the dependence of the junction capacitance on AC voltage amplitude was reduced from three to two. Applying this analysis to simulations or experimental data results in a five-fold increase in precision as well as improved accuracy. [2] Figure 3 shows experimental data demonstrating this improvement.

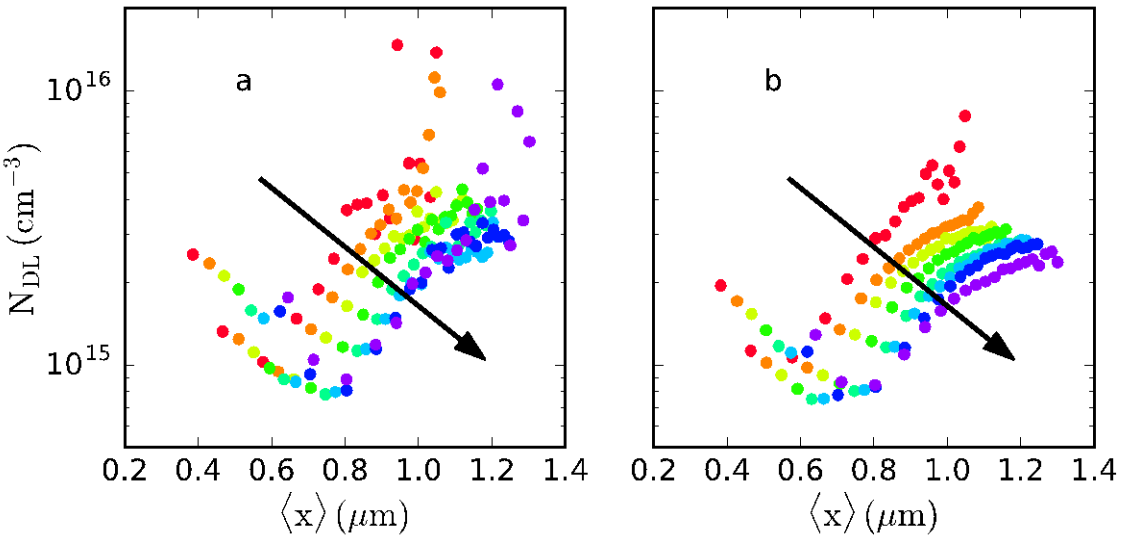

Figure 3. DLCP for a CIGS absorber extracted using the standard (a) and improved (b) analysis. Arrows indicate increasing measurement frequency. The increased precision is most notable at extreme frequencies, which are the most important for isolating defect and dopant profiles.

Because the breakthrough here is simply a change in analysis, the improved method's increase in precision and decrease in measurement time is immediately available to the entire semiconductor device community in industry and academia without any added cost.

Future Work:

The Lonergan group will expand characterization of CdTe with varied back-contacts that have not been subjected to ALT and follow defect evolution in those cells through a prolonged ALT process and publish a paper on the results. The group will also publish the manuscript in preparation regarding the improvements to DLCP and use the improved technique to collect trap density profiles in graded bandgap (Ag,Cu)(In, Ga)Se_2 absorbers to provide insight into the relationship between stoichiometry, trap density, and device performance.

References

[1] J.T. Heath et.al. "Bulk and Metastable defects in CIGS thin films using DLCP," *JAP*, **95**, 1000-1010(2014).

[2] C.W. Warren et.al "An improve method for determining carrier densities via DLCP", manuscript in preparation

BAPVC Annual Project Report

Project Title: Non-Equilibrium Processing of CdTe Absorbers
PI: Colin A Wolden, Colorado School of Mines
E-mail: cwolden@mines.edu

Summary:
There were three areas investigated over the past year. First, we evaluated molecular chlorine (Cl_2) as an alternative to $CdCl_2$ for CdTe activation. It is shown that recrystallization occurs quite quickly (~1 minute), with devices fabricated at promising conditions displayed good rectification and efficiency >11%. The second aspect was the exploring the use of pre-formed $CdS_{1-y}Te_y$ alloy windows as opposed to relying in high temperature interdiffusion. Using this approach we reduced the temperature for CdTe deposition 180 C with no change in device efficiency. Lastly, we studied the impact of the metal layer on device performance an stability with ZnTe:Cu contacted devices. It was shown that titanium was significantly more stable than Cr or Au.

Key Accomplishments:

A critical step in CdTe solar cell production is its activation through exposure to $CdCl_2$. This process results in recrystallization, grain growth, and interdiffusion with the CdS window layer. It has been shown that during this process Cl rapidly diffuses through the film, preferentially accumulating in the CdS window layer and decorating CdTe grain boundaries. $CdCl_2$ activation is capex intensive and has been described as the "the most intricate process in manufacturing. It would be desirable to simplify this aspect of CdTe manufacturing. In this work we explored molecular chlorine as an alternative activation agent. XRD texture coefficient analysis was used to first screen the large process space, and it was found that the process was fast (< 2 minutes) and that oxygen was not required and in fact detrimental. Promising conditions were used for device fabrication and compared with those produced by standard $CdCl_2$ activation. Best device performance was obtained using the minimum Cl_2 exposure that could be reliably delivered in our present system, yielding several devices were fabricated with >11 % efficiency and V_{oc} > 800 mV. It was shown that Cl_2 was equally effective to $CdCl_2$ at generating carriers as their C-V profiles were nominally identical. The Cl_2-activated devices were somewhat inferior in both current collection and open circuit voltage. EQE analysis revealed that the primary deficiency was excessive recombination within bulk CdTe, suggesting that Cl_2 introduces defects into this region. In addition, it suggests that the degree of CdS-CdTe interdiffusion is somewhat attenuated relative to conventional $CdCl_2$ treated devices. In terms of both uniformity and run to run reproducibility Cl_2 activation was superior, reflecting the improved control provided by the gaseous source. These results indicate that Cl_2 has promise as an alternative to $CdCl_2$.

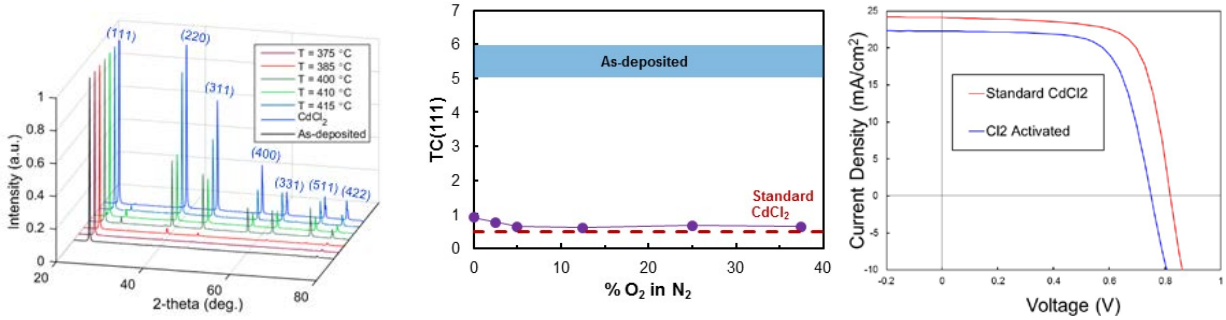

Figure 1. Normalized XRD patterns as a function of process temperature at t = 10 min, 25% O_2, 5 sccm Cl_2/Ar; TC(111) as a function of oxygen fraction at T = 400 ºC, t = 2 min, and 1.5 sccm

Cl_2/Ar ; Comparison of J-V curves obtained using $CdCl_2$ activation and molecular Cl_2 activation.

Oxygenated cadmium sulfide (CdS:O) is an alternative CdTe window layer that delivers improved blue response relative to CdS. Our recent study revealed that CdS:O completely transforms during device fabrication into a layer containing cadmium sulfate clusters interspersed among $CdS_{1-y}Te_y$ nanocrystals. This motivated us to study CdTe solar cells employing pre-formed $CdS_{1-y}Te_y$ alloy windows without sulfate present. The intrinsic properties of alloys deposited by co-evaporation are evaluated and then used in place of CdS in standard device fabrication. Interestingly we find that device efficiency is nominally unchanged despite a 180 Creduction in CdTe deposition temperatures. XRD analysis of interdiffusion with CdTe is performed and the results show that it is largely suppressed in alloy-based devices.

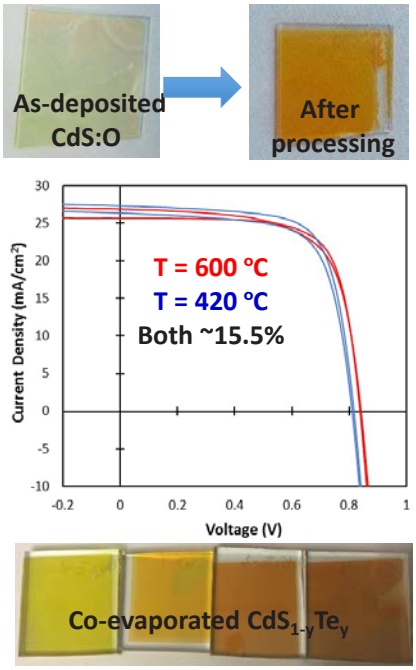

Fig. 2. Photographs of CdS:O before and after device processing, co-evaporated $CdS_{1-y}Te_y$, and selected J-V curves from both devices.

In this work we explore chromium and titanium as more practical alternatives to gold. It was found that comparable performance could be obtained with each metal, but that the optimal Cu loading scaled as one would expect based on solubility. Comparisons of current-voltage and quantum efficiency behavior among devices produced with insufficient, optimal, and excess Cu dosing are used to provide insight into the role(s) of this critical impurity for device performance. Reliability tests were carried out under different stressing conditions and the results show the relation of the degradation with both the metal and the presence of illumination. It was found that Ti-based devices were much for stable, particularly under illumination. Atom probe tomography (APT) revealed that copper does not aggregate and segregate with this contact as was previously observed with gold, and this is suggested to be a key to greater stability.

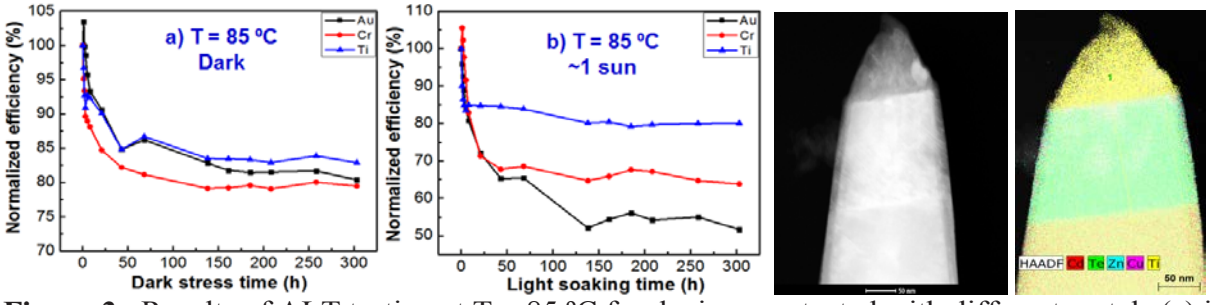

Figure 3. Results of ALT testing at T = 85 ºC for devices contacted with different metals (a) in the dark and (b) under illumination. APT cross section and elemental analysis showing that Cu remains uniformly distributed after RTP activation,

Future Work: Current work focuses on the use of ternary alloys for bot band gap grading and the introduction of external dopants.

BAPVC Annual Project Report

Project Title: Laser Processing to Improve CdTe Thin Film Photovoltaics Efficiency and Manufacturing

PI: Michael Scarpulla, University of Utah
E-mail: scarpulla@eng.utah.edu

Summary:

a) A novel solution-based method from ionic aqueous precursor solutions was developed for CdTe thin-film deposition. Films of 1-5 μm thick were deposited at low temperature (~350 K) and ambient pressure using a spin coater. Following standard $CdCl_2$ treatment, films exhibited nearly phase-pure CdTe (<5 vol. % CdS) with (111) preferred orientation, grain diameters up to 3 μm, and low-temperature photoluminescence signal within a factor of 3 from a CSS reference sample.
b) The nano-chemistry of CdTe grain boundary was investigated to understand the beneficial effect of chlorine treatment and bromine methanol etching on passivating grain boundaries. A Te rich region was observed extending quite far down some grain boundaries. Different behavior is seen at S3 and random boundaries. This work is elucidating the complex details of the back contact in CdTe devices at the nanoscale.

Key Accomplishments:

The group has demonstrated an ambient pressure, low-temperature, solution-based method for depositing the CdTe absorber layer that could be adapted to both glass modules and roll-to-roll processing. Our recent laboratory work has demonstrated the successful deposition on Mo and FTO-coated glass via spin-coating alternating ionic precursor solutions of Cd^{2+} and Te^{2-}. This work was presented at the recent 43rd IEEE Photovoltaic Specialists Conference [1] and a journal paper is in review.

The as-deposited film morphology is nanocrystalline with nearly-stoichiometric composition. Annealing at 400 °C – 430 °C for 30 in forming gas without $CdCl_2$ results in ~200 nm grains giving strong XRD peaks but some loss of Cd during annealing. The same annealing with the addition of a drop-cast $CdCl_2$ film shows development of strong (111) texture and high crystalline quality (majority non-CdTe peaks in Fig. 1 are from FTO and CdS). The films are stoichiometric within the accuracy of EDS measurement. SEM images of these films reveal large CdTe grains but evidence of voids that will have to be eliminated during process optimization. The films exhibit photoluminescence at 13 K that is dominated by donor-acceptor pair transitions from the so-called Z-band believed to be related to oxygen or an intrinsic defect. The PL yield for the solution deposited film is within a factor of three of a reference CSS sample– a qualitative indication of optoelectronic quality suitable for devices. It is believed the defect may be converted with annealing into the more traditional A-centers [2,3] (which dominate the emission from Cl treated CSS films) and we will pursue this goal through process optimization.

Another systematic study of the nano-chemistry of polycrystalline CdTe photovoltaic devices was performed using Transmission Electron Microscopy (TEM). TEM investigations of the GB of CdTe revealed a Te rich layer being formed at the GB. This Te layer is responsible for the inversion of the GB of the CdTe PV device. This leads to creation of a depletion region around the GB effectively screening the GB to act as potential recombination center. This process of GB passivation increases the carrier lifetime in the CdTe layer. Additionally a Te rich layer is also

observed at the back surface of CdTe. This layer aids in creating an ohmic layer for back contact thereby helping to overcome the high work function of CdTe. Figure 2 shows the formation of the Te rich layer in the grain boundary of CdTe.

Future Work:

The group will focus on adapting the deposition process for use in a dedicated spray coater more applicable to high-throughput scaling. In addition, the group will focus on improving the solution-chemistry of the process to use Na and S free reducing agents for synthesis of the Te-precursor solution and investigate the incorporation of dopants (P, As, K) during the deposition process. Finally, the post-deposition $CdCl_2$ will be optimized such that full devices can be built using these absorber layers.

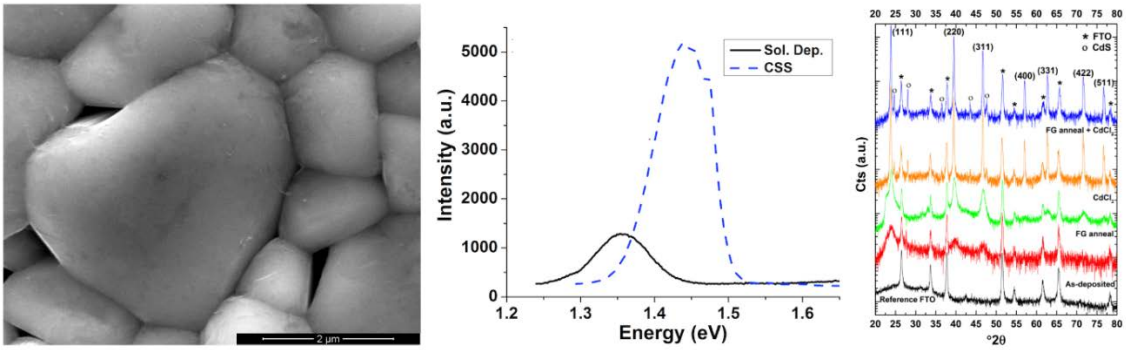

Figure 1. (Left) SEM image of solution deposited film with 2 µm scale bar. (Middle) low-temperature PL spectra from solution deposited and reference CdTe deposited by close space sublimation (CSS). The origin of the PL (Z-band rather than A-centers, as deduced from the spectral shift) accounts for most of the difference in integrated yield. (Right) XRD spectra for film series including as-deposited, forming gas (FG) annealed, and $CdCl_2$ treated.

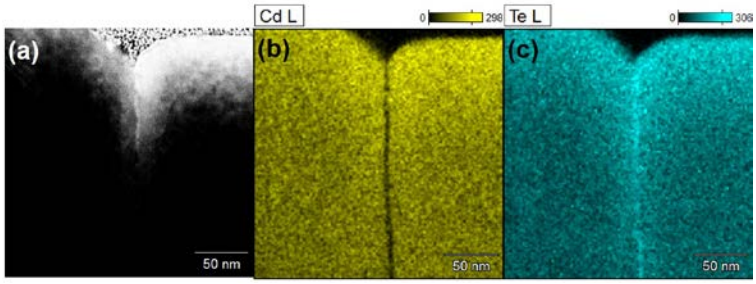

Figure 2. a) TEM image of a CdTe grain boundary at back surface. STEM EDS distribution of (b) Cd and (c) Te of grain-grain boundary interface. The enrichment of grain boundary with Te is clearly observed in (c).

References:

[1] D. S. Pruzan, C. E. Hahn, S. Misra and M. A. Scarpulla, 43rd PVSC Conference Proceedings, Portland, OR, 2016.
[2] C. Kraft, et al., JAP 108 124503 (2010).
[3] S. Vatavu, et al., Thin Solid Films, 515 6107 (2007).

BAPVC Annual Project Report

Project Title: Laser Processing to Improve CdTe Thin Film Photovoltaics Efficiency and Manufacturing

PI: **Chris Ferekides; University of South Florida**
E-mail: ferekide@usf.edu

Summary:
This is a collaborative project between the University of South Florida (USF) and the University of Utah. The aim is to develop high throughput laser-based solar cell processing techniques to improve manufacturability and performance, and lower the manufacturing costs of CdTe thin film PV. Work during year 3 focused on the development of a laser-based process for back contact annealing using a NIR laser (808 nm) donated by Intevac. Preliminary stability experiments were also completed on laser-annealed back contacted cells to determine whether long term-stability could be improved by controlling the amount of Cu used during the back contact formation process. The solar cell structure being utilized for this project is: *glass/TCO/CdS/CdTe/Back contact.*

Key Accomplishments:
For CdS/CdTe solar cells the back contact interface gets activated by means of thermal annealing. Depending on the back contact material the annealing time varies between 20 - 60 minutes. In this study fast contact anneal times - <90 secs – are investigated using a 60 Watt dual diode 808nm laser for the back contact anneal. Two different back contact materials are used for this work: (a) Cu-doped Graphite, and (b) MoN/Mo/Cu. Devices were laser annealed under a stationary beam. Laser power density (LPD) and Cu concentration were varied to study their effect on device performance.

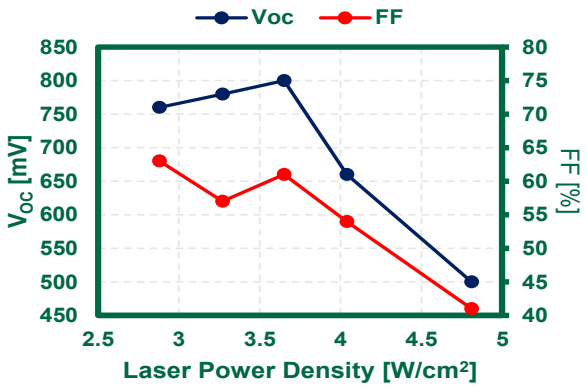

Figure 1. Effect of LPD on device performance

Figure 1 shows the effect of LPD on the V_{OC} and FF of devices with graphite back contact. There is an initial increase in device performance with increasing LPD; however at high LPDs a significant drop in the V_{OC}/FF is observed. SIMS analysis for selected devices suggested that the LPD has a significant effect on Cu diffusion, which is consistent with previous findings on Cu diffusion in CdTe cells. At high LPD Cu diffusion extends deep into the device reaching the CdTe/CdS interface. This can lead to increased interface recombination and therefore the lower performance shown in Fig. 1.

Preliminary Results on Thermally Stressed cells

Cells with laser-processed back contacts were thermally stressed in inert ambient under vacuum at 80 and 100 °C; to-date cells have been stressed for 250 hours. Figure 2 shows the device performance for a device treated at low LPD (3.08 W/cm^2). After an initial drop in V_{OC} and FF the performance improves as the solar cell undergoes thermal stress. The opposite trend was

observed for solar cells treated at higher LPD. These observations are believed to be related to Cu diffusion and Cu-related defects.

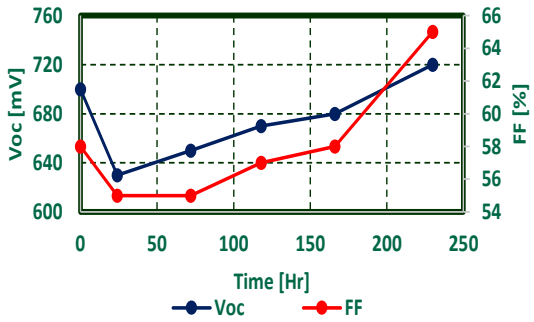

Figure 2. Thermal stability of laser

Figure 3 shows the DLTS spectra for devices with 5 and 10 Å of Cu before and after thermal stress. Pre-thermal stress for the 5 Å Cu device shows a minority carrier trap E1 (E_C- 0.26 eV) possibly a Te_{Cd} defect, and a shallow majority trap H1 most likely an acceptor defect Cu_{Cd}. Post-thermal stress shows the presence of only the minority carrier trap E1. The majority trap –related to p-doping- is eliminated which explains the depleted absorber found with C-V measurements. Higher Cu concentrations introduce a deep level majority trap H2, which is most likely related to Cu defects but further analysis is needed prior to assigning this to a specific defect. The behavior is similar to thermally annealed devices where the increase in Cu was found to result in the formation of deep majority traps.

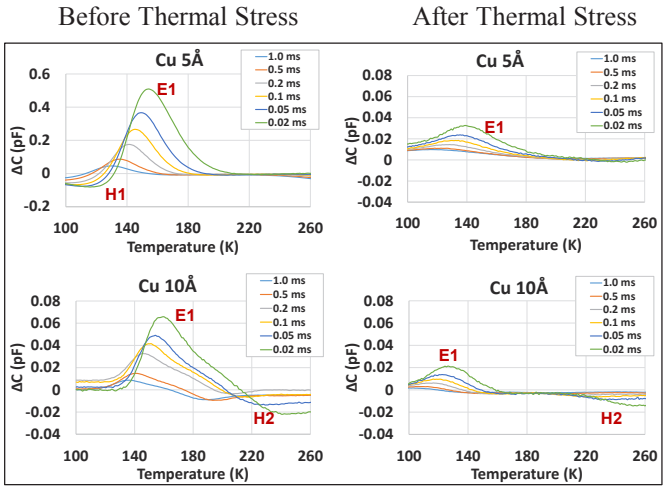

Figure 3. DLTS spectra of LA CdTe devices with different amounts of Cu, before and after thermal stress.

Non-uniformities

Non-uniform heating due to spatial variations in laser intensity continues to be an issue. Small area cells continue to outperform larger ones suggesting non-uniform heating during the laser annealing process.

Best Performance to-date

NIR laser annealing for the back contact process resulted in solar cell performance comparable to baseline thermal anneal process. High V_{OC} (830mV) and FF (70%) were achieved for 90 secs anneal time.

Future Work:

Continue laser (NIR) anneal of back contact/stability work. Focus on identifying defect levels responsible for observed performance and degradation.

Publication:

V. Palekis, S. Collins, M. Khan, V. Evani, S. Misra, M. A. Scarpulla, A. Abbas, J. Walls, and C. Ferekides, *"Near Infrared Laser $CdCl_2$ Heat Treatment for CdTe Solar Cells"*, Proc. 43rd IEEE PVSC, 2016.

BAPVC Annual and Final Project Report

Project Title: Advanced Evaporation Source Design
PI: Gregory M. Hanket, Institute of Energy Conversion (IEC) University of Delaware
E-mail: hanket@udel.edu

Summary:
This project aimed to develop prototype evaporation sources for the inline evaporation of Cu(InGa)Se2 photovoltaic modules. The work involved the modeling, design, and operational characterization of Cu and novel mixed In-Ga vapor evaporation sources. Research over the course of the program included:

- Cu and mixed vapor In-Ga sources of ~1 kg capacity were modeled, designed, and commissioned.
- Source performance was characterized at approximately 15 g/hr effusion rate, including effusion profiles and composition for the mixed-vapor In-Ga source.
- Source stability was characterized against melt depletion.

Key Accomplishments:
The purpose of the program was to investigate various aspects of source design at the pilot scale level. This included the incorporation of nozzle heaters, the use of separate In and Ga melt chambers, and various vapor rarefaction schemes where the degree of mechanical sophistication required a significantly larger volume than in conventional laboratory-scale evaporation "bottles". The larger source size was required to achieve commercially relevant effusion rates and to evaluate power dissipation associated thermal gradients and insulation approaches. Melt volumes corresponding to ~1 kg melt mass were chosen to approximate commercial scale, while being manageable for source depletion studies over the course of days instead of weeks. The source was designed for downward evaporation which enables glass substrate temperatures in excess of the strain point since the glass can be supported from underneath. A single effusion nozzle was used in anticipation of using multiple sources across the width of the substrates in commercial application where an axiallysymmetric design was used to limit thermal non-uniformities to the z-direction. A qualitative depiction of the design approach is shown in Figure 1. Vapor is generated within the centrally-located crucible, flows up into an expansion chamber, radially outward into an annular manifold, then down to and out of the effusion nozzle.

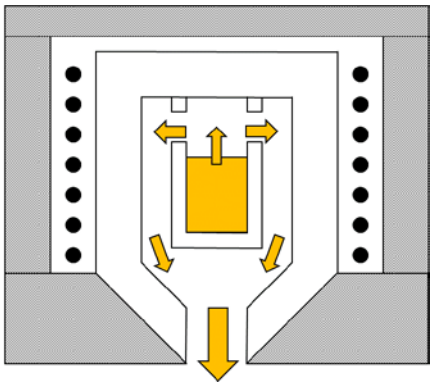

Figure 1. Concept for downward evaporating Cu source.

Thermal modeling: COMSOL software was used to design and model the thermal properties of the source. The most critical aspect of the thermal behavior of the source is the temperature drop at the nozzle entrance and along its length which can result in both condensation and spitting as well as a drop in effusion rate as the source depletes. The temperature profiles of a source with and without nozzle heater are shown in Figure 2. To a first approximation, the operating power of the nozzle is equivalent to the predicted blackbody radiation emanating from the nozzle area at the source temperature.

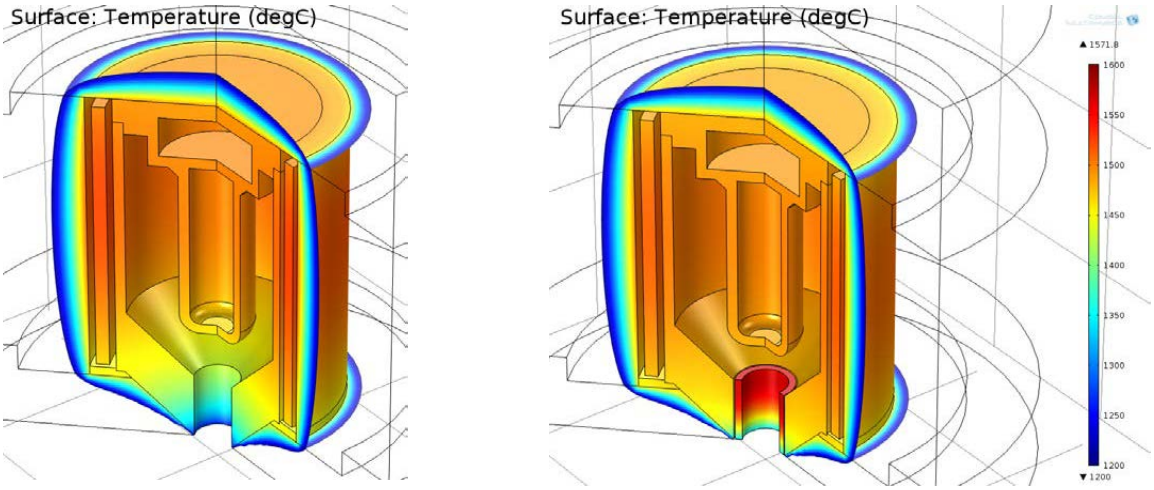

Figure 2. Effect of *in-situ* heater on nozzle temperature profile. The nozzle entrance is 75-100ºC hotter with the heater, mitigating condensation and subsequent spitting.

Copper source operation: Initial results of the Cu source validated the performance of the source with only a limited number of spits. The second issue for Cu source operation is effusion rate stability over time. Effusion rate and deposition profile across the substrate were characterized for melt heights ranging from fully charged to 75% depleted. Effusion rate dropped by only 28% over the course of depleting the melt.

Mixed-vapor In-Ga source design and operation: A mixed-vapor In-Ga source was developed to avoid variations in vapor composition as the substrates translate through a deposition zone over multiple rows of sources. The use of distinct rows of In and Ga sources would yield variations in the incident Ga/(In+Ga) flux at the substrate composition where the use of a mixed In-Ga vapor source can eliminate the flux variation resulting in non-uniform film composition across the substrate. To maintain symmetry, a concentric crucible geometry was developed and is shown in Figure 3. The inner crucible was used for In, and the outer for Ga, as In requires only a single small effusion orifice due to its higher vapor pressure compared to Ga which requires multiple larger orifices. The In orifice was varied in size to achieve the desired Ga/(In+Ga) composition in the deposited films.

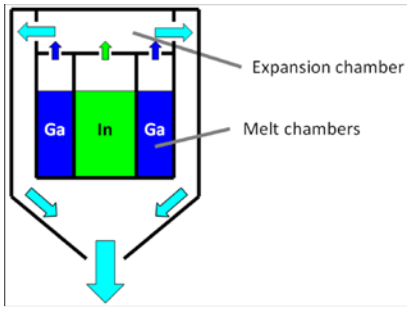

Figure 8. Design approach for simultaneous evaporation of In and Ga to effuse a mixed vapor.

Source effusion and composition stability was evaluated at 15 g/hr (0.25 g/min) effusion rate from full charges (500g In, 480g Ga) down to ~65% In depletion. Film composition and deposition rate were determined from fluorescence (XRF) measurements and the compositional stability over time was within the measurement error. The consistency in composition and effusion rate demonstrates that the use of internal flow restricting orifices is a feasible means of composition control.

Future Work:

This program has successfully demonstrated a novel approach for vapor composition control in continuous manufacturing processes as well as a mechanically and electrically robust source design. Future work needs to further focus on the full elimination of spitting from the sources.

BAPVC Annual Project Report

Project Title: 1.7 eV absorber for Si based tandem solar cell applications
PI: Yong-Hang Zhang
E-mail: yhzhang@asu.edu

Summary:

Prior work in developing high-efficiency monocrystalline CdTe solar cells has been advanced and expanded to include wider bandgap absorbers. High-quality MgCdTe material has been demonstrated with lifetimes > 500 ns. Here, the group has demonstrated a monocrystalline CdTe solar cell with an NREL certified efficiency of 17.1% (active-area of 20.3%) and an open-circuit voltage of > 1.1 V as well as an 11.2% efficient monocrystalline 1.7 eV bandgap $Mg_{0.13}Cd_{0.87}Te$ solar cell with an open-circuit voltage of 1.176 V.

Key Accomplishments:

CdTe solar cell devices with a total-area efficiency of 18.52% and an unshaded area efficiency of 20.3% measured at ASU and an NREL certified total-area efficiency 17.1% have been demonstrated. Finding a more transparent, higher-work-function alternative to p-type a-Si:H is a potentially highly rewarding, but very challenging quest. Possibilities such as ZnTe, CuZnS and MoO_x have all been—and currently are—under investigation with collaborations with several different BAPVC members.

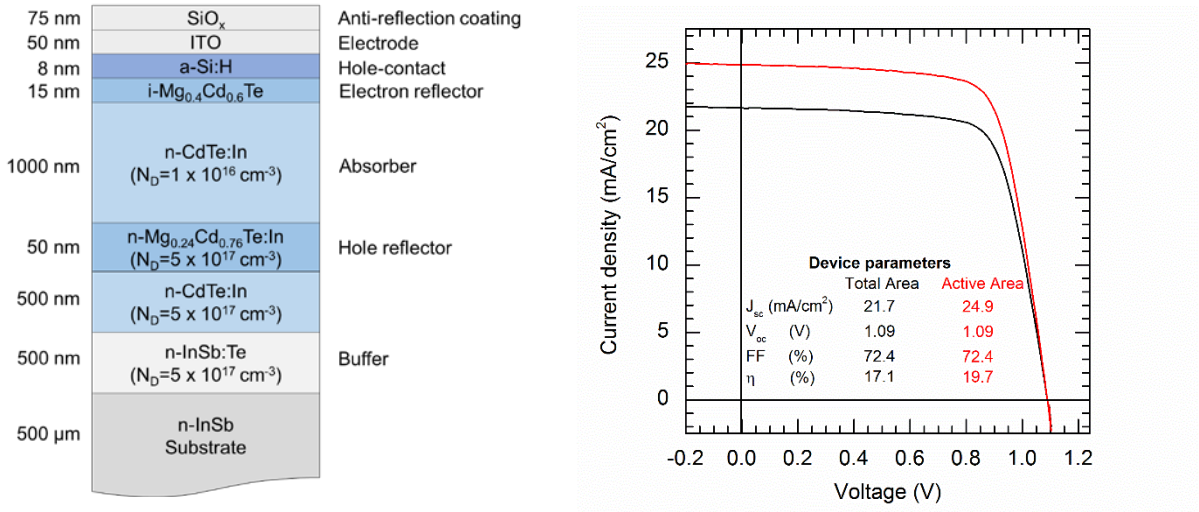

Figure 1 a) Solar cell device structure for a monocrystalline CdTe absorber and b) the device performance of the most efficient cell.

The group has fabricated 1.7 eV $Mg_{0.13}Cd_{0.87}Te$ solar cells with 11.2% efficiency and V_{oc} of 1.176 V. The materials studies have shown that the $Mg_{0.13}Cd_{0.87}Te/Mg_{0.5}Cd_{0.5}Te$ DH has very strong PL intensity and a long minority carrier lifetime of 0.56 μs and calculations show an implied V_{oc} of 1.3 eV is possible based on this material. However, fabricated devices show a V_{oc} much lower than this value and the FF is also low (only 63.5%). It is possible to further increase V_{oc} and FF by employing a different p-type material with higher built-in potential with the n-CdTe layer and by

optimizing carrier transport. The J_{sc} can be further improved by minimizing the reflection and parasitic absorptions and by increasing the absorber layer thickness. To have an efficiency gain in a tandem configuration with Si solar cell (even with 25.6% efficiency), the 1.7 eV $Mg_{0.13}Cd_{0.87}Te$ solar cell efficiency should be as least 13%.

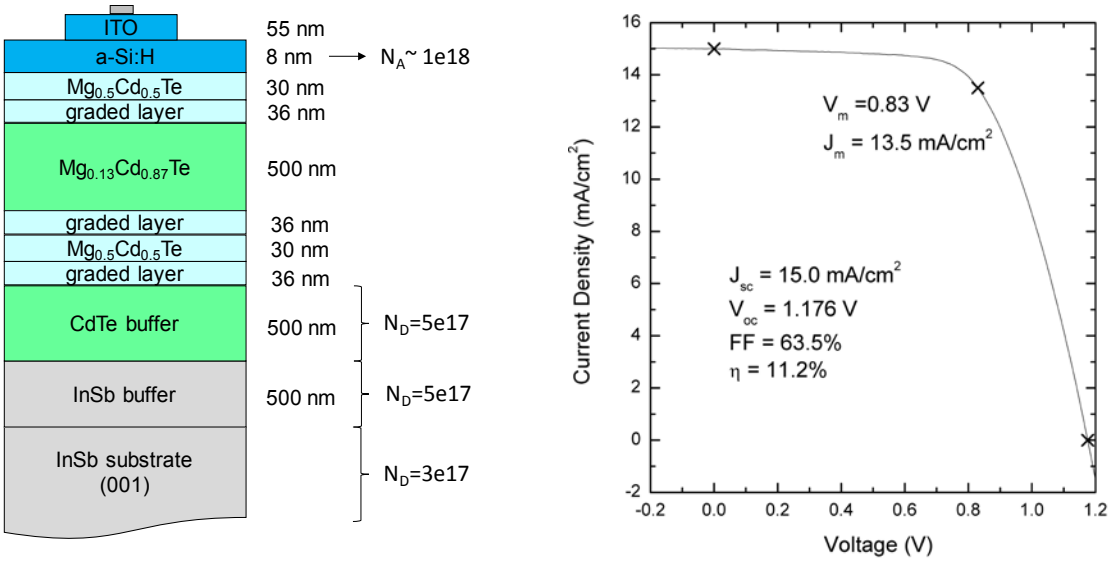

Figure 2 a) Solar cell device structure for a 1.7 eV bandgap absorber and b) the device performance of the most efficient cell.

Future Work:

A new joint project within BAPVC 2.0 between the PI Yong-Hang Zhang, the University of South Florida, and the University of Utah is geared to transfer the double-heterostructure solar cell design to their polycrystalline process. In addition, continued collaboration with First Solar is planned to further develop and optimize both the 1.5 eV and 1.7 eV absorbers, principally using their ZnTe deposition processes.

BAPVC Annual Project Report

Project Title: Fundamental Modeling of Chalcopyrite Solar Cells
PI: Scott T. Dunham, University of Washington, Seattle
E-mail: dunham@ee.washington.edu

Summary:

This project deals with calculation and modeling of the properties of defects in CIGS and CZTS absorber materials. The fundamental goal is predictive models for defect evolution, impurity kinetics and phase transformation in these materials to enable optimization of fabrication processes for maximum cell efficiency and reliability. Toward this end, they use a hierarchy of methods including density functional theory calculations, canonical thermodynamics, Monte Carlo simulations and classical continuum device simulation to connect theory to expected materials and device behavior.

Key Accomplishments:

Fundamental understanding of the complex behavior of impurities and point defects in CIGS ($CuIn_xGa_{1-x}Se_2$) and CZTSSe ($Cu_2ZnSnS_xSe_{4-x}$) under realistic processing conditions is essential for effective applications in thin film solar cell devices. In previous years, the group developed a tool for calculation of the concentrations of intrinsic lattice defects at given CZTS and CIGS stoichiometries. A method was developed that makes use of defect formation energies from ab initio calculations combined with mass action relations between the defects to enable calculation of concentrations of defects in all accessible charge states under a given set of stoichiometric constraints and processing temperature. The method has been extended to allow for use of an arbitrary combination of stoichiometric constraints and chemical potentials in the presence of a range of commonly-present impurities and associated extrinsic defect complexes. In addition, migration barrier heights calculated with the nudged elastic band (NEB) method provide insight into the effect of the local lattice structure on the diffusion of dominant point defects.

They applied this approach to study the complex defect physics that emerges in CIS doped with Na, K and Cd as a function of stoichiometry, and use that understanding to develop predictive models for impurity incorporation. In this application, the fractional compositions of constituent species are fundamental inputs, and the respective chemical potentials are calculated at the given points in composition space. Using this canonical method, they mapped the Fermi level in terms of the [Cu]/[In] ratio, γ, and the normal valence parameter 2[Se]/([Cu] + 3[In]), η. They found that for the Cu-poor region, $\gamma < 1$, the Fermi level in undoped CIS exhibits an n-type plateau for $\eta < 1$, where V_{Se}, In_{Cu}, and Cu_i dominate. For $\eta > 1$, the material is p-type and dominated by V_{Cu} and Cu_{In}. The material is stable against the formation of secondary compounds in transition between n- and p-type due to increase in compensated $nV_{Cu} + In_{Cu}$ complexes.

Upon doping with Na, K and Cd, they find that the n-type plateau shifts to smaller values of η compared due to the suppression of $nV_{Cu} + In_{Cu}$ complexes by Na and K occupying Cu sites. As the material becomes increasingly Cu-depleted toward stoichiometries near the CdS-interface, the increased availability of unoccupied Cu sites leads to dominant concentrations of K_{Cu} and Na_{Cu}. Since the charge states of Cd substituting cation sites depend sensitively on the Fermi level, the relative concentrations of Cd_{Cu} and Cd_{In} varies with the normal valence parameter η.

Thermodynamic analysis suggests that within a reasonable window of processing conditions, a simple mechanism accounts for for the incorporation of Cd in CIS near the CdS interface. Using first-principles NEB to identify the dominant nearest-neighbor transitions for impurity diffusion, they found that Na and K diffuse rapidly compared to Cu and Cd via Cu vacancies at experimentally relevant temperatures. The presence of K led to the greatest enhancement of Cu vacancy diffusion, which suggests that the incorporation of K (as compared to just Na) leads to more rapid diffusion of Cu vacancies to the CdS interface as shown in Figure 1, providing a higher concentration of available sites for Cd.

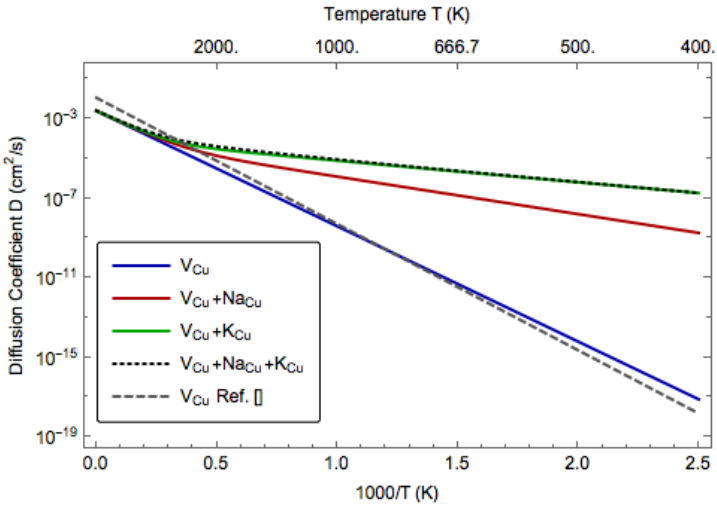

Fig. 1: Calculated dependence of diffusion coefficient of Cu vacancies on presence of extrinsic defects at 0.1 at.%.

One of the goals of this project was to better understand ordering and phase separation in CIGS. Using an extensive database of DFT calculations, the group optimized an energy functional models for use in canonical Monte Carlo simulations which reveal the formation of indium and vacancy-rich regions during lower temperature annealing as illustrated in Fig. 2. The calculated composition maps were then used in continuum simulations of full device structures to analyze the impact on performance. The result that composition variations and phase separation can be expected to degrade device performance, with decreases in open circuit voltage and fill factor dominating over potential small enhancements in carrier collection.

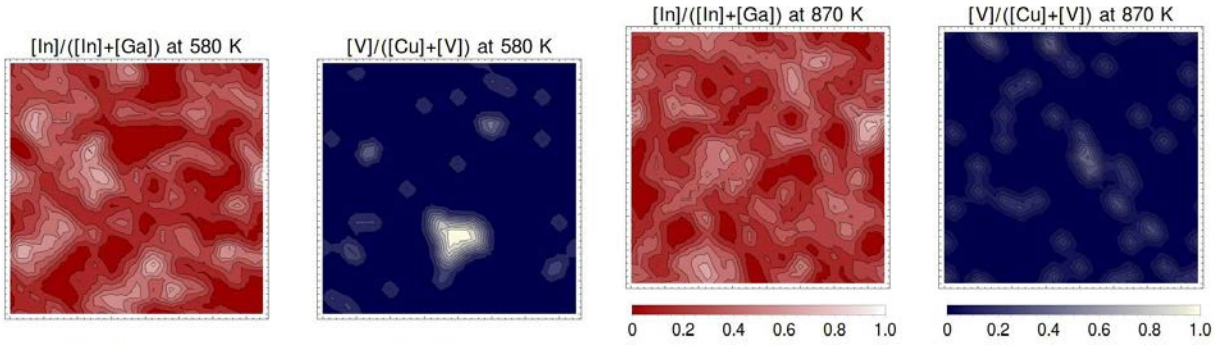

Fig. 2. Contour plot of In fraction after MC simulation at 580K and 870K for systems with an average [In]/[In+Ga] fraction of 25%, and an average vacancy concentration of 2.5% of cation sites.

Future Work:

The project is not funded for the current year, but it is hoped that resources will become available to extend the effort to develop coupled material, process and device models that can be used for optimization of manufacturing processes to enhance performance and reliability while reducing costs.

BAPVC Annual Project Report 2016

Project Title: Development of Multicolor Lock-in Photoluminescence Methods for In-Situ Process Monitoring and Ex-Situ Mapping of Solar Cell Absorber and Interface Quality
PI: Hugh W. Hillhouse
E-mail: h2@uw.edu

Summary:

Existing methods for characterization of photovoltaic absorber or interface quality are either too time consuming or are affected by environmental factors to employ for in-line process monitoring. In this project, we seek to develop a suite of novel lock-in photoluminescence methods that will directly probe material or interface quality in a processing environment. The technique uses a predefined series of optical pulses with varying excitation wavelength or intensity to sequentially illuminate the sample and a reference sample. The emitted PL from both samples are modulated in time due to the excitation pulse sequence and therefore can be collected using a single synchronous photodetection system. By generating specific demodulation signal patterns and inputting them into the reference channel of a lock-in amplifier, a single DC output can be generated that (depending on the demodulation pattern) reveals information about absorber quality, homogeneity, nanoscale potential fluctuations, surface recombination, and surface or interface charging. As a result, the technique will be useful for monitoring materials and devices at most stages of processing. Most importantly, due to the unique optical set-up, lock-in amplification, and demodulation patterns, the sample can be unambiguously assessed without interference from source intensity drift, stray light, fouling, and other artifacts. The technique should be robust and rapid enough to employ in-situ during processing and will have micron-scale resolution so that it can be used to perform ex-situ mapping of cells and modules.

We completed a prototype of the instrument and collected data sets on various semiconductors including GaAs, InP, and CdTe. The difference PL spectra show that the surface of InP is high quality (as expected) while GaAs and CdTe have high surface recombination (see Figure 1). In a six month extension of the project in 2016 we sought to utilize a multichannel lock-in amplifier and a customized optical chopper to develop a more capable and yet significantly less inexpensive version of the tool. However, due to experimental difficulties, we were not able to achieve these advances during the short duration of the extension. We were however able to make significant advances on the analysis and interpretation of steady-state PL from photovoltaic materials (particularly those with sub-bandgap states) in order to get rapid estimates for the steady-state quasi-Fermi level splitting near the surface of a variety of semiconductors. The method has already proved very valuable for materials that change with time, as is see with CIGS upon air exposure and in very environmentally sensitive materials like hybrid perovskites. A publication has been submitted and is under review. A brief summary of the forthcoming publication [1] is below.

Maximum Open-Circuit Voltage from PL Quantum Yield of Semiconductors:

The steady-state quasi-Fermi level splitting near the surface a semiconductor under 1 Sun illumination can typically be estimated from the magnitude of the external photoluminescence quantum yield (PLQY) if the material has no sub-bandgap emission. However, all real materials have some sub-bandgap absorption and emission due to dynamic short-range disorder (thermal motion of atoms), while some important materials exhibit stronger sub-bandgap emission due to longer-range disorder from amorphous structure (a-Si), native point defects (CIGS, CZTS), or a

flexible framework (hybrid perovskites). Here, we show that the external PLQY (which is typically much less than 10% even for excellent photovoltaic materials) is enhanced in materials with sub-bandgap emission, without an accompanying increase in quasi-Fermi level splitting. This is important since the steady-state quasi-Fermi level splitting divided by the unit of fundamental charge is a good upper estimate of the maximum possible open-circuit voltage that could be generated if the semiconductor were used as the primary absorber in a solar cell. Thus, we demonstrate that neither PLQY nor PL peak intensity alone are sufficient metrics for evaluating the potential of a given semiconductor as a photovoltaic material. We present two simple methods that more accurately estimate the quasi-Fermi level splitting in real materials from the PLQY so long as either the bandgap or the wavelength of the peak photoluminescence intensity is known. We validate both methods for chalcopyrites, kesterites, and hybrid perovskites and show that these simple non-contact material characterization methods provide an excellent upper estimate of the V_{OC} that a material is able to produce in a photovoltaic device without fitting PL data to a model, without having to accurately measure the absorption coefficient below bandgap, and without the need for fabricating a device.

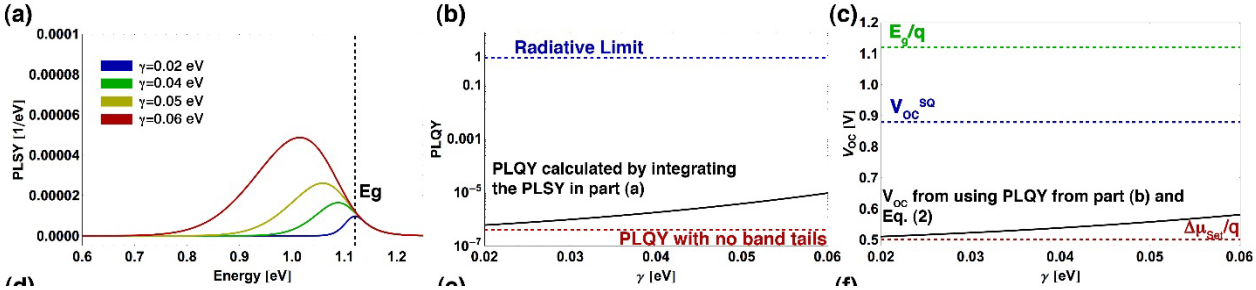

Figure 1. Effect of sub-bandgap absorption on (a) PL spectral yield, (b) the total PL quantum yield, and (c) V_{OC} estimated by reducing the SQ Voc by (kT/q)ln(PLQY). The PLSY curves in part (a) are generated using $\theta = 1.5$, $E_g = 1.12$eV, T = 298.15 K, and $\Delta\mu_{Set} = 0.5$ eV (57% of qV_{OC}^{SQ}). The PLQY in part (b) is calculated by integrating the PLSY curves in part (a). ***The difference between the solid black and dashed red lines in (c) reveals the error incurred by using the (kT/q)ln(PLQY) approach.***

	Δμ from PL fit [eV]	Measured PLQY	ϕ	Δμ from eq. 2 [eV]	Δμ from eq. 10 [eV]	Δμ from eq. 12 [eV]	Voc [V]	PCE [%]
GaAs	0.893	$1.70\text{x}10^{-5}$	0.643	0.903	0.890	0.897	—	—
CZTSSe	0.458	$2.34\text{x}10^{-5}$	0.0867	0.538	0.455	0.463	0.443	8.32
CISSe	0.487	$3.78\text{x}10^{-4}$	0.380	0.517	0.484	0.500	0.487	11.2
CIGSSe	0.664	$7.36\text{x}10^{-4}$	0.540	0.676	0.657	0.675	0.659	13.3
$CH_3NH_3PbI_3$	1.12	$4.88\text{x}10^{-4}$	0.481	1.12	1.10	1.10	1.09	16.1

Table 1. PLQY and estimated Δμ for GaAs, CZTSSe, CISSe, CIGSSe, and $CH_3NH_3PbI_3$. Note the close match between the Voc estimated with eq 10 and 12 (this work) with the measured Voc.

Reference:

[1] J.K. Katahara, I.L. Braly, A.R. Uhl, Z. Yang, A.K.-Y. Jen, H.W. Hillhouse," Determination of Maximum Open-Circuit Voltage from Photoluminescence Quantum Yield of Semiconductors," Submitted.

BAPVC Annual Project Report

Project Title: In-situ Characterization of Grain Growth in Thin Film Semiconductors for Lower Costs, Highly Reproducible, High Efficiency Solar Cells
PI: Prof. Delia J. Milliron
E-mail: milliron@che.utexas.edu

Summary:

CZTS and CIGS nanorods were synthesized and their phase transformations and sintering to make photovoltaic active films were studied. In situ X-ray diffraction and TEM provided critical insights Collaboration with Mike Toney (BAPVC, Stanford) was extremely helpful in advancing the project objectives.

Key Accomplishments:

This project led to the development of a new synthetic strategy for preparation of CZTS nanorod sheets in situ during colloidal synthesis. The 2D sheets contain crystallographically ordered nanorods and could be easily processed from solution into highly textured thin films. The sheet formation process is instigated by the incorporation of antimony as a precursor in the nanorod synthesis reaction. This has the additional, beneficial effect of facilitating nanocrystal sintering during thermal annealing so that large grained CZTS thin films, suitable for photovoltaic active layers, could be prepared. Collaborating with Mike Toney (BAPVC, Stanford), we carried out in situ X-ray diffraction to evaluate the role of the antimony dopant in facilitating grain growth.

The project further studied the transformation from metastable to stable phase CZTS, which was demonstrated by in situ diffraction at variable thermal ramp rates to have a size- and shape-dependent activation energy. The transformation proceeds in a way that resembles classical nucleation and growth. As such, high ramp rates minimize the nucleation rate relative to the growth rate, yielding large grained microstructured thin films in a very short time, circumventing the limitations of conventional sintering methods to make photovoltaic thin films from colloidal nanocrystals.

Future Work:

BAPVC support for this project has ended.

BAPVC Annual Project Report

Project Title: Sintering CdTe Nanoparticles into Functional Bulk Absorber Layers
PI: A. Paul Alivisatos
E-mail: paul.alivisatos@berkeley.edu

Summary:

Sintering semiconductor nanocrystals represents a possible low-cost route to creating functional bulk absorber layers for photovoltaic applications. Here the Alivisatos group highlight the critical aspects of sintering CdTe tetrapods into smooth, dense, polycrystalline films that are capable of yielding >7% efficient solar cells with just 500 nm thick active layers. Despite respectable performance, they find that there is significant room for improvement regarding the current state-of-the-art processing and device structure. Namely, 'optimal' films/devices have exceptionally low photoluminescence yield, grain sizes on the order of 50-100 nm, a metastable ITO/CdTe hole- collecting contact, and CdTe that is not phase pure. Their findings further suggest that this approach to creating functional CdTe absorber layers has much potential beyond the already encouraging results reported in the literature.

Key Accomplishments:

Herein, they highlight several critical aspects of the sintering process that reveal the importance of residual salt and sintering atmosphere on the final grain morphology and CdTe phase purity. They also present stress-induced contact doping and anode barrier lotheyring as possible mechanisms for the forward bias current/light soaking effect. Plausible origins of such effects could be copper diffusion and reaction with ITO or metastable acceptor impurity activation at the ITO/CdTe contact.

State-of-the-art solar cells derived from sintered CdTe nanoparticles typically begin with a solution of CdTe tetrapods (TPs) with their native oleate-based ligands partially exchanged for pyridine. The pyridine exchange process that is typically used is expected to leave ~20% of the surface still covered in oleate, making further ligand removal via a chlorine-salt treatment necessary before sintering. With this ink, films are built upon glass/ITO substrates according to the layer-by-layer procedure illustrated in Fig. 1. Once the desired thickness is achieved (often around 400-600 nm), the device is completed with indium-doped sol-gel ZnO and Al, creating a final layer structure consisting of ITO/CdTe/ZnO:In/Al.

Fig. 2 (a) shows the device performance results for a sintering temperature and atmosphere series, and Fig. 2 (b) shows a SEM device cross section of the optimal 5% PCE 375°C air-sintered cell after several tens of minutes of forward bias soaking. Interestingly, the N_2-sintered film has substantially worse device performance when compared to the equivalent air-sintered active layer despite having better phase purity and a more developed grain structure. This implies that oxygen and/or humidity has an essential role in improving the quality of the CdTe layer and/or ITO/CdTe contact. It is important to note that all of the devices in Fig. 2 they are poorly performing initially (< 2 %), and had to be forward bias light soaked to improve the efficiency; thus, the low performance of all the unoptimal cells can be rationalized in terms of a lack of response to forward bias light soaking.

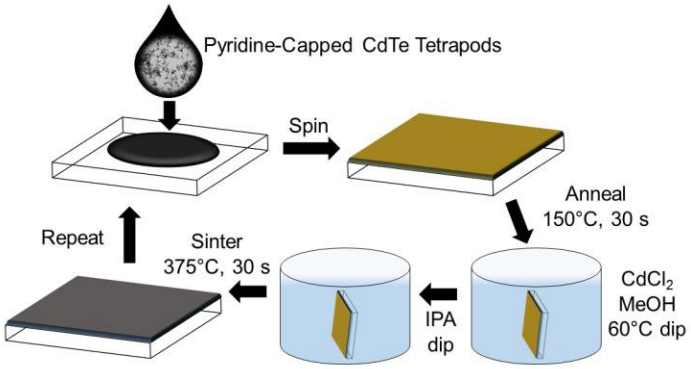

Fig 1. Processing schematic for creating high-quality sintered CdTe films. After treating the pyridine-capped CdTe TPs with $CdCl_2$, a quick IPA dip cleaning is critical for both leaving a small amount of salt on the film to facilitate the sintering reaction and also removing excess salt such that inclusions are not formed.

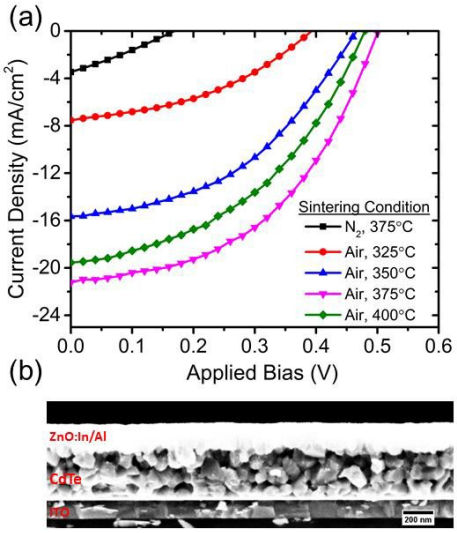

Fig. 2. (a) Effect of atmosphere and sintering temperature on device performance. All devices are sintered for 30 s, consist of 4 layers, and are optimized with a forward bias (light) soak. The optimal sintering conditions in air yield very low performance when done in an N_2 glove box despite better grain morphology and phase purity. The optimal devices at 375°C they are 5% efficient and had integrated EQEs consistent with the J_{SC} values obtained under our solar simulator. (b) Cross-sectional SEM image of the optimal 375°C air-sintered device.

Fig. 3 presents the experimental J-V curves and an attempt at a SCAPS drift-diffusion reproduction of a champion 7.3% 375°C air-sintered device after >90 min of cumulative 3 V forward bias light soaking. They note that this device did not reach 7.3% with initial testing/soaking, but instead reached that level after several days in a N_2 glove box. in order to examine what contact properties could account for such behavior, they used drift-diffusion simulations with the SCAPS modeling software to explore several plausible scenarios. Using the built-in CdTe material parameters, they attempted to reproduce the overall soaked vs. unsoaked effects in terms of two properties of the ITO/CdTe hole collecting contact: 1.) doping near the contact, and 2.) an increase in contact work function. Fig. 3 shows the effect of adding a 5 nm layer at the hole-collecting contact that is p^{++} doped to 10^{19} cm^{-3} and increasing the work function from 4.85 eV to 5 eV. These two changes, along with a photoactivated series resistance, seem to capture all the effects of forward bias light soaking.

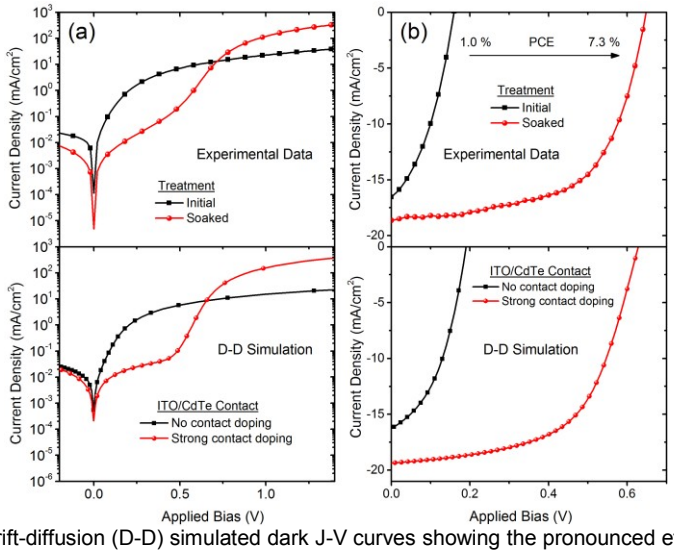

Fig. 3. (a) Experimental and drift-diffusion (D-D) simulated dark J-V curves showing the pronounced effect of forward bias (light) soaking. (b) The same as (a) but for illuminated devices. After several days and soaking treatments, this 4 layer 375°C, 30s, air-sintered device saturates at 7.3% efficiency under 1-Sun illumination. All simulations theyre carried out with SCAPS v3.302.

Future Work: There is no future work planned for this project.

Thrust: Encapsulation and Reliability

Key Challenges

A key challenge for PV module and system reliability is the fact that many of the mechanisms of observed degradation modes are not well understood. This thrust seeks to identify and characterize degradation mechanisms, facilitate the design and standardization of accelerated testing protocols, and provide the fundamentals for the design of improved PV materials and product designs. In particular, we will: (1) characterize the stability and reliability of PV materials and interfaces, including barrier-films and encapsulants; and (2) develop an understanding of the coupled thermo-mechanical, electro-chemical, and photo-chemical degradation mechanisms that determine the reliability and operational lifetimes of PV technologies.

Existing Projects in our Thrust

- *Mechanical Reliability of Module Interfaces and Advanced Perovskite Structures,* Reinhold Dauskardt (Stanford)
- *Network Modeling for Rapid Optimization of Lifetime, Efficiency and CapEx of PERC Solar Cells,* Roger French (Case Western)
- *PV Module Performance and Lifetime Prediction: Inserting New Technologies Without Lifetime Penalty*, Roger French (Case Western)
- *High Sensitivity Mapping of Stress via Anisotropic Optics for Improved PV Manufacturing*, Robert Collins, (Toledo)
- *Improving the Speed and Calibration of Water Vapor Transmission Rate (WVTR) Measurements*, Matthew Reese (NREL)
- *Composite Encapsulation Layers*, Jeffrey Urban (LBNL)
- *Understanding and Improving Durability of Organic Photovoltaic Materials*, Sue Carter (UCSC)
- *Tailoring Electrostatic Interactions to Produce Hybrid Barrier Films for Photovoltaics*, Bernard Kippelen, Samuel Graham (Georgia Tech)
- *A Multiscale, Electro-thermal-optical Reliability Framework: PVRelExpert to Predict Corrosion and PID Degradations for Promising Early Stage BAPVC Technologies*, Ashraf Alam (Purdue)

Potential New Areas of Interest

- Expansion of current work to characterize, model and predict coupled thermo-mechanical and photo-chemical degradation processes in PV technologies to include electro-chemical processes like those responsible for *potential induced degradation (PID)*.
- *Increased interaction with other thrusts* to support reliability and degradation characterization and modeling with particular interests in emerging perovskite, ultra-thin silicon, CdTe and InP PV, along with transparent conductors.
- Development of *multi-layer thin-film mechanics and degradation models* for cell, interconnect, and encapsulant interfaces in PV module packaging technologies, both cell-based and monolithically-integrated.
- Connecting these models with *detailed transport models* for photons, electrons, phonons, and ions in a hierarchical fashion, in order to predict other failure modes.

- *Analysis and development of a database* of thermo-mechanical, electro-chemical, and photo-chemical degradation properties of materials for benchmarking BAPVC innovations, to guide field testing, and inform computer simulations.
- Refinement and redesign of standardized reliability testing capabilities for the broader BAPVC community, re-designing testing for field exposed samples, and calibration/validation of kinetic degradation models and lifetime prediction procedures using in-service and field-exposed data.

BAPVC Annual Project Report

Project Title: Mechanical Reliability of Module Interfaces and Advanced Perovskite Structures
PI: Reinhold Dauskardt
E-mail: dauskardt@stanford.edu

Summary:

Employing a recently developed adhesion metrology, the adhesive properties of encapsulant interfaces in field aged and lab aged silicon solar modules were evaluated. Key mechanisms of mechanical degradation of the bulk encapsulant as well as the glass and cell interfaces were identified and are currently being incorporated into physical kinetics models of delamination. To shield inherently brittle perovskites from mechanical stress and environmental species, a new architecture was develop that partitions planar perovskite solar cells into hundreds of smaller, mechanically isolated, and chemically contained solar cells. The architecture is a promising strategy to improve the long-term reliability of perovskite solar cells.

Key Accomplishments:

The Dauskardt group developed a simple, repeatable metrology for evaluating adhesion energy, G_c [J/m^2], of solar module interfaces (Fig. 1). Unlike previous metrologies (tape, peel and shear tests), the new metrology is independent of bulk mechanical properties of the test specimen, which permits direct comparisons of adhesion for modules of different architectures and aging histories.

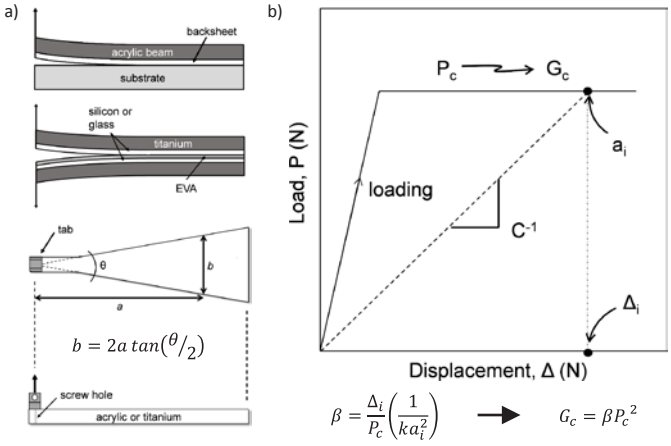

Fig. 1. a) diagram of wedge shaped adhesion specimens. b) load-displacement curve of wedge specimen exhibits constant plateau, from which adhesion energy, G_c, is measured.

The new metrology was employed in several long-term studies of backsheet and encapsulation adhesion in field and laboratory aged PV modules. In a study of EVA encapsulant adhesion in 27-year old historic modules from Sacramento, CA, it was found that modules exposed to sunlight experienced significantly greater adhesive degradation (~90% reduction in adhesion energy between the encapsulant and front glass relative to new material) than modules stored on-site but away from sunlight (~30% reduction in adhesion energy between the encapsulant and cell). The encapsulant exposed to sunlight exhibited poorer UV absorbance and greater de-acetylation. Quantitative analyses of crosslinking and chain scission are in progress, the results of which will aid in modeling the physical kinetics of adhesive degradation.

A survey of historic PV modules indicated that encapsulant delamination often initiates near metallization on the front of solar cells. To determine the reason for this behavior, adhesion of EVA to screen printed silver (cell gridline material) was evaluated. Adhesion energy to silver (950 J/m^2) was nearly half that of EVA to a cell surface (1750 J/m^2), and appeared to drop after just 1000 hours of accelerated aging (1.4x suns, 85°C, 13.5%RH). The results indicate that in addition to chemical and mechanical degradation of the bulk encapsulant and glass/cell interfaces, a complimentary degradation mode (Fig. 2) is delamination at bus bars and gridlines.

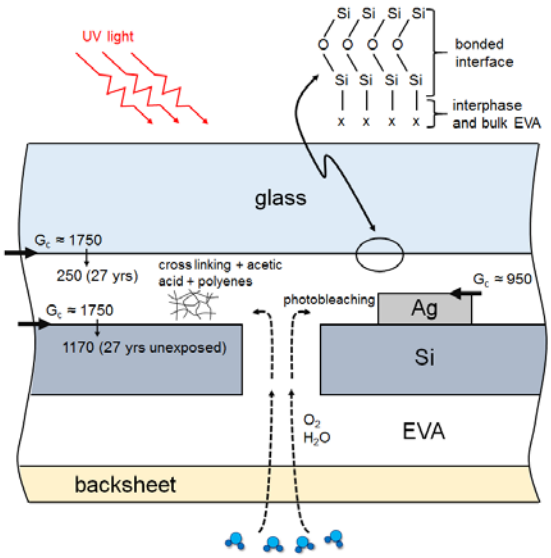

Fig. 2. Illustration of degradation mechanisms in EVA encapsulants. Mechanical degradation of encapsulant and interfaces leads to delamination.

The ionic, salt-like crystal structure of perovskites leads to brittle mechanical properties (G_c ~0.3-1.5 J/m^2), which raises concerns over the long-term viability of perovskite solar cells in field applications. As a solution to overcome the inherent mechanical fragility of perovskites and their susceptibility to cracking under applied loads, the Dauskardt group designed a new architecture that partitions a planar cell into hundreds of smaller, contiguous cells. When infused into a cross-linked polymer scaffold, the cohesive fracture energy of the perovskite layer increased to >10 J/m^2, which is competitive with established solar technologies such as crystalline silicon. The fracture toughness of the typically fragile active layers are greatly enhanced by infusion into scaffolding. Furthermore, the scaffold thickness is tunable, and the spin-coated perovskite forms high-quality films without pinholes in the scaffold (Fig. 3). Scaffolds reinforce perovskite while maintaining high V_{oc} and FF in devices with PCE of 13%.

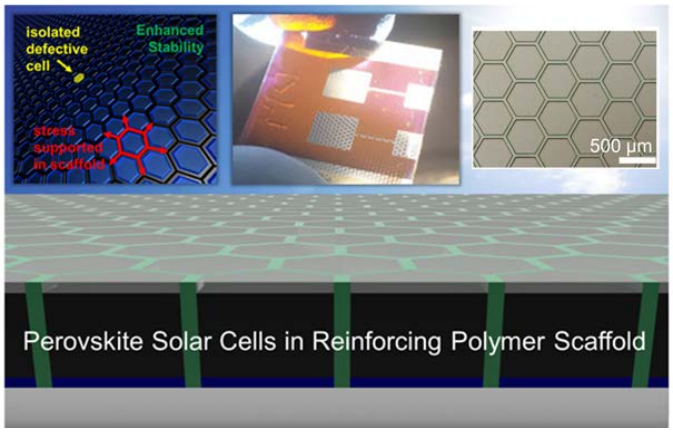

Fig. 3. New cell architecture partitions a planar cell into smaller, mechanically isolated, and chemically contained cells. This approach shields the perovskite from mechanical stress and environmental species.

Future Work:

The Dauskardt group will continue investigating mechanisms of mechanical degradation in PV module materials in order to develop predictive models of module reliability. Long-term field and accelerated lab aging studies of backsheets and encapsulants are in progress, and will be complimented with investigations of potential induced degradation. Perovskite research will focus on optimizing the scaffold geometry and materials, as well as including light management strategies to minimize power conversion losses due to the photoinactive scaffold.

BAPVC Annual Project Report

Project Title: Network modeling for rapid optimization of Lifetime, efficiency and CapEx of PERC solar cells

PI: **Roger French**
E-mail: rxf131@case.edu

Summary:

The research group has partnered with Dupont Silicon Valley Technology Center (DP-SVTC) as a supplier of PERC PV cells and a manufacturer of PV mini modules, and their preparation of the samples for this funded work is underway. The SDLE research center's SPHS100 exposure chamber, with integrated light rack for simultaneous UV and damp heat exposure, has been upgraded to accommodate in-situ data logging, further enabling true multifactor stress testing. Two additional electrical tests, capacitance-voltage profiling and deep level transient spectroscopy, are under development in the SDLE facilities to expand the capabilities of this work for generating insights into performance degradation modes and mechanisms.

Key Accomplishments:

The group's industrial collaborator partners at DP-SVTC are tuning the manufacturing processes for PECVD SiO_2 and AL_2O_3 PERC cells (Figure 1) with which to construct PV mini module samples, and will provide them for exposure studies before the end of 2016. A lifetime and degradation science (L&DS) study has been planned in advance for the samples once they arrive. Measurements are planned involving three well known PV module measurement types utilized in previous L&DS studies of PV modules (confocal raman microscopy, electroluminescence imaging, and I-V curve tracing), as well as new measurement types under development at the SDLE center (capacitance-voltage profiling and deep level transient spectroscopy). Additional lower throughput measurement types, planned for retained samples only, are being provided by other collaborating research groups (quantum efficiency, time resolved photoluminescence, and atomic force microscopy) as part of targeted DOE style studies parallel to the main L&DS study. Planned exposures involve two laboratory test chamber exposures (multifactor 85°C 85% relative humidity with added UV irradiance, and cyclic ASTMG154), outdoor exposure, and an exploratory acetic acid vapor exposure. The unique multifactor exposure chamber, the SPHS100 with integrated UV light rack, has been further developed at the SDLE research center over the past year in preparation for upcoming PV mini module stress exposures. Capacity for in-situ monitoring of PV mini module electrical performance characteristics has been implemented utilizing a Campbell datalogger to measure voltage drops across an array of appropriately sized resistors. This has the added benefit of loading mini module samples under illumination during test, which is a more realistic testing condition than leaving them at an open voltage.

Within the past 6 months, the semi-gSEM analytic technique was successfully applied to an L&DS study on Al-BSF PV mini modules utilizing identical measurement techniques to the majority of those planned for this PERC study. The analysis resulted in a semi-gSEM degradation pathway model detailing a sequence of mechanistic degradation steps, connecting incident accelerated testing environmental stressors to the system level performance response of main interest. The model was mathematically described by a system of equations predicting the progress of each mechanistic degradation process in response to exposure to the accelerated aging test conditions. This successful demonstration of the L&DS study protocol and semi-gSEM analysis technique was applied to similar PV modules with similar measurement types, but alternate exposure conditions will be utilized with this work. (Figure 2).

Future Work:

Minimodule samples with PERC cell construction are planned to be received from the group's DP-SVTC collaborators by the end of 2016, at which time baseline measurements will be taken, and accelerated stress exposures begun. The data gathered from this lifetime and degradation science study protocol will be used both to construct a data block for semi-gSEM analysis, as well as targeted DOE studies for measurement types where data coverage is not as complete (i.e. lower throughput measurements, where only retained samples are measured). The outcome will be semi-gSEM pathway diagrams and a system of equations describing observed degradation pathways in PV modules with PERC cell construction.

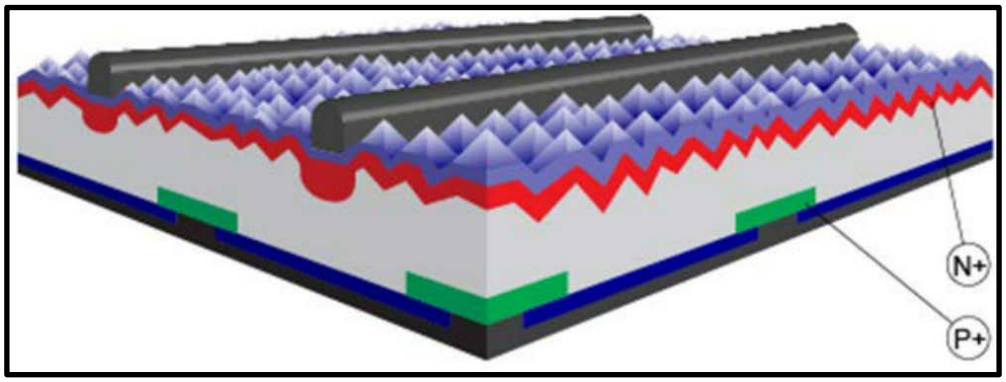

Figure 1: An illustration of the PERC architecture fabricated by the group's collaborators, DP-SVTC. A local back surface field is made through localized contacts of a p+ type base by the Al back contact, and otherwise passivated by an oxide (blue film).

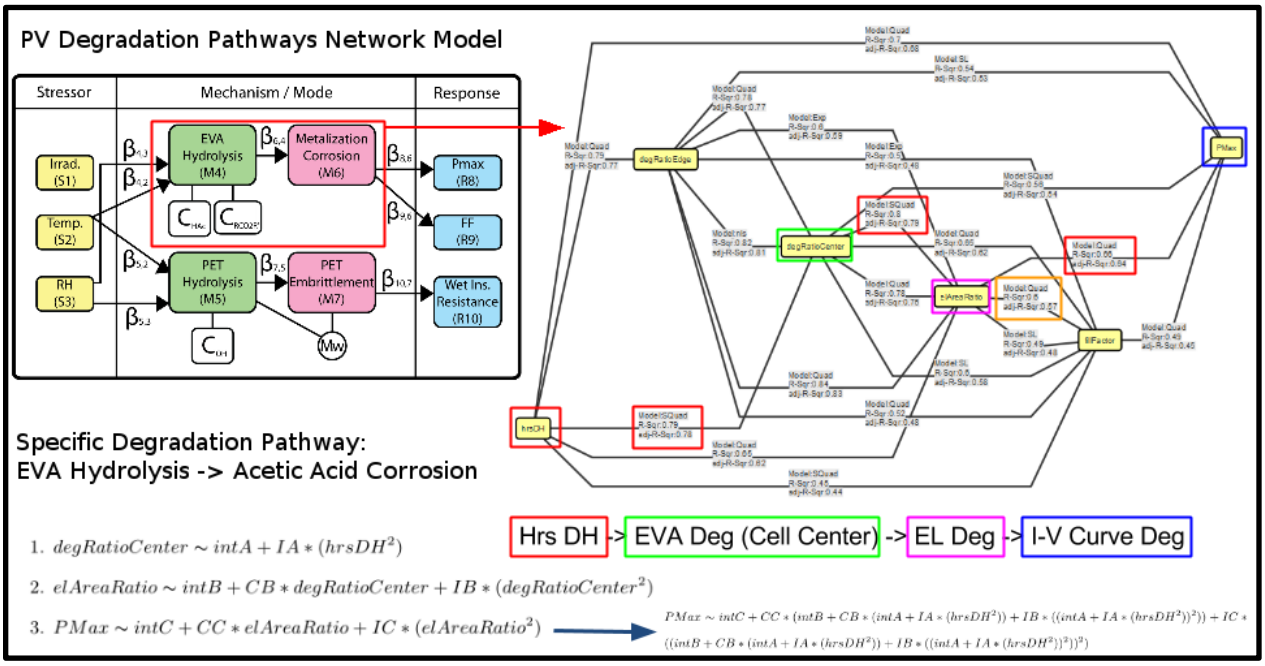

Figure 2: A network of networks model illustrating the multidimensional predictive degradation of a PV module under accelerated aging conditions. While the model shown above was developed for a typical aluminum back surface field (Al-BSF) cell construction, the output of this work will describe the degradation mechanisms of PV modules with PERC cell construction.

BAPVC Annual Project Report

Project Title: PV Module Performance and Lifetime Prediction: Inserting New Technologies Without Lifetime Penalty

PI: **Roger French**
E-mail: rxf131@case.edu

Summary:

The group successfully used their pioneered statistical analytics technique, semi-gSEM, the development of which was supported by BAVPC funds, to identify, confirm, and quantify a degradation pathway for c-Si screen-printed silver PV modules under damp heat testing conditions. This degradation pathway involved the formation of volatile acetic acid byproduct from the hydrolytic degradation of the EVA polymer encapsulant exposed to damp heat (85°C 85% relative humidity), which led to a unique observable metallization corrosion pattern that ultimately coupled tightly to overall module power loss. Each mechanism within the degradation pathway was quantified using spectral, electrical, and image analytics, and a system of equations was derived to model the overall system level module power loss as a functional progression of mechanistic degradation steps.

Key Accomplishments:

A lifetime and degradation science (L&DS) study was successfully completed by the group, capturing a rich dataset describing the degradation modes and mechanisms of PV modules with screen printed silver frontside metallization cell geometry of two gridline sizes. Three measurement types (confocal raman microscopy, electroluminescence imaging, and I-V curve tracing) were used to gather information at 7 time steps along a 3400 hour total dose of exposure to damp heat (85°C, 85% relative humidity) environmental stress conditions. Measurement procedures' variations were quantified with gage R&R and signal-to-noise ratio studies to indicate the number of re-measures needed for each of the three data types per sample each measurement round. Applying these measurement procedures created hundreds of data files per measurement type over the length of the L&DS study, a relatively large data set by laboratory standards. Reusable and extensible R code was written to process the raw datafiles into meaningful results in a pipelined fashion, smoothly scaling with the growing data block as new rounds of measurements were taken. The resulting data set featured three quantified measurement types describing the progression of degradation mechanisms in PV modules under damp heat (Figure 1).

These quantified metrics of unit level and system level performance degradation were related to one another using the semi-gSEM analysis technique. First, a path of statistically strong (on the basis of the adjusted R^2 value) univariate relationships was traced backwards from the system level response of interest, through the unit level mechanisms, ultimately back to the incident stress dose. This network of univariate relationships possessed functional forms which were guided by domain knowledge of known chemical and physical processes. Domain knowledge identified the sequential progression as beginning with damp heat induced EVA hydrolysis and the formation of acetic acid byproduct. This facilitated localized metallization corrosion which eventually caused system level power loss. This explanation for the observed variable trends is described by a system of equations derived from the best fitting functional forms of the strongest univariate relationships. The specific network model developed by this work, which was successfully defended as a PhD dissertation by the graduate student Nicholas R. Wheeler whose thesis was based primarily upon this work, is a sub model within a network of networks describing the degradation modes and mechanisms of PV modules as a whole technology system (Figure 2).

Future Work:

To further publish the findings disclosed in the graduated student's PhD thesis document, a journal article is in preparation and is planned to be finalized and submitted before the end of the year. This represents an important step in the development of Lifetime and Degradation Science study protocols, and the semi-gSEM analysis procedure, which are being utilized to study additional material systems in a similar way to what was exemplified in this work. Among the materials systems being targeted by present and future studies utilizing these procedures are PV polymer materials (PET, Polyacrylates), and PV modules with PERC cell construction.

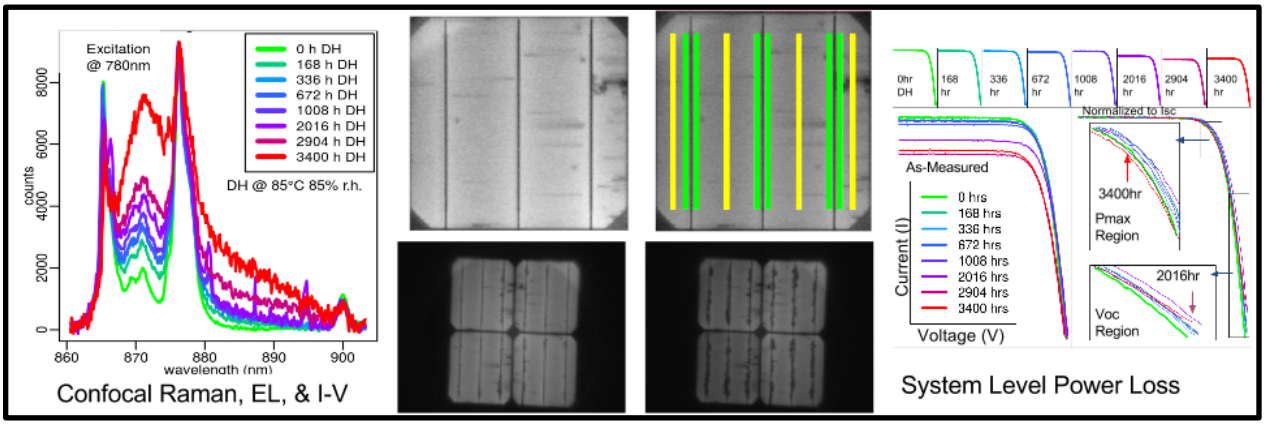

Figure 1: Three measurement types (confocal raman microscopy, electroluminescence imaging, and I-V curve tracing) were used to gather a lifetime and degradation science dataset.

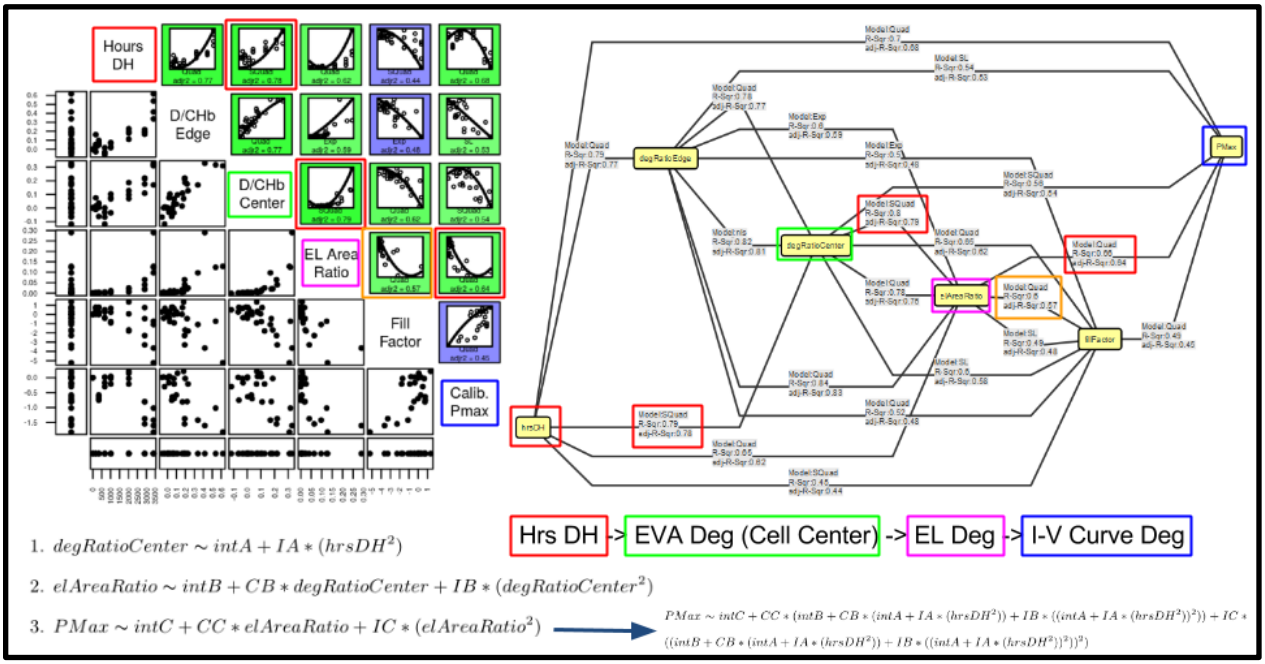

Figure 2: Semi-gSEM analytics was applied to the lifetime and degradation science dataset to produce a degradation path network model, and a system of equations quantifying the mechanistic degradation pathway of acetic acid induced metallization corrosion in PV modules under damp heat stress exposure conditions.

BAPVC Annual Project Report

Project Title:
High Sensitivity Mapping of Stress via Anisotropic Optics for Improved PV Manufacturing
PI: Robert W. Collins
E-mail: Robert.Collins@utoledo.edu

Summary:

Methods for evaluating the stress in various materials prepared and processed in photovoltaics technologies have been developed based on measurement of the polarization change that occurs when a polarized light beam is reflected obliquely from one side of the materials. Calibration of the method for glass panels and Si wafers demonstrates the high sensitivity achievable as a result of (i) the two or more beam passes which probe the stress-induced birefringence, and (ii) the use of a rotating-compensator spectroscopic ellipsometer for high precision, high accuracy detection of the birefringence. An advanced mapping capability for high sensitivity measurement of glass stress has been demonstrated in studies of small samples of Mo-coated glass for Cu(In,Ga)Se_2 (CIGS) technology and full-size (60 cm x 120 cm) coated glass panels for CdTe technology.

Key Accomplishments:

Proof-of-principle results have been obtained in both CIGS and CdTe technologies that demonstrate the ability to map both substrate/superstrate and thin film stresses using a non-invasive through-the-glass optical method that can be integrated into previously-developed in-line spectroscopic ellipsometry instrumentation. The method involves directing broadband light with known polarization properties at oblique incidence to the glass surface and detecting the polarization properties of the light that makes a single reflection from the back glass/film-stack interface and thus two passes through the glass. The measurement geometry and challenges are

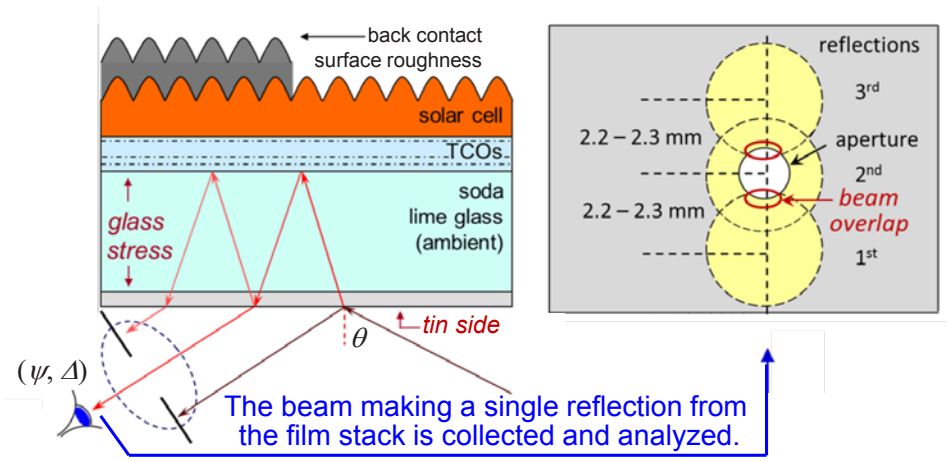

Figure 1: Measurement configuration for non-invasive mapping of stress in 60 cm x 120 cm glass plates coated with transparent conducting oxide and CdTe solar cell layers in the module configuration used by industry. The stress is determined simultaneously with the properties of the films that exist on both sides of the glass. As shown at the right, some light from the first and third reflections may be collected and data analysis corrections for this non-ideality are made.

illustrated in Figure 1. Figure 2 shows example of results obtained on a 60 cm x 120 cm pre-production panel consisting of TEC™/SnO_2/CdS/CdTe. These results are given in terms of the phase shift induced by birefringence over the beam path associated with the two transmissions through the glass, as in the geometry of Figure 1. The phase shift of 50° corresponds to a value of ~ 3 MPa for the projection of the compressive stress vector onto the plane of incidence. A key advantage of the measurement capability is the ability to map the stress simultaneously with the physical properties of films existing on the front and back of the glass. Figure 3 shows a map of the CdS effective thickness for this panel. As shown in Figure 3, the effective thickness accounts for the CdS components in the CdS bulk and the HRT/CdS and CdS/CdTe interface layers.

Future Work:

Future efforts will involve determination of the stress magnitude and its principal axis coordinate system, by applying advanced data collection and analysis methods. The capability will also be developed to measure the profile of the stress throughout the glass thickness, and how the thin films on the surface lead to an unbalancing of this stress and curvature in the glass. Future work will also involve extending the capabilities to wafer Si technologies. In this case, all multiple reflections exiting the wafer will be collected in contrast to the approach shown in Figure 1.

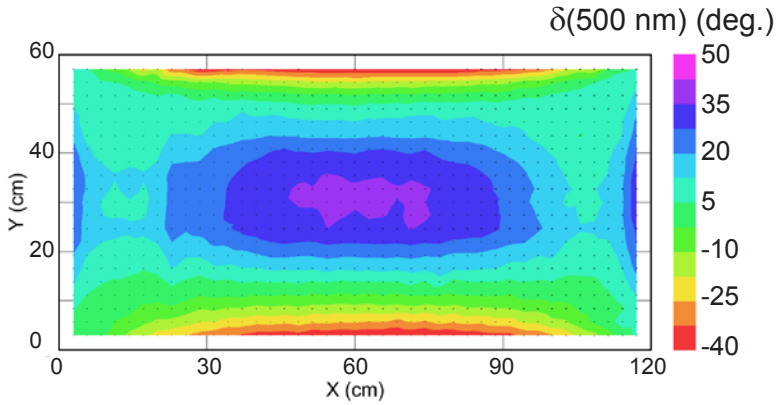

Figure 2: Map of phase shift δ at 500 nm originating from stress-induced birefringence in the glass for a 60 cm x 120 cm TEC™/SnO_2/CdS/CdTe pre-production panel; δ is proportional to the projection of the stress vector onto the plane of incidence which is parallel to the 60 cm side.

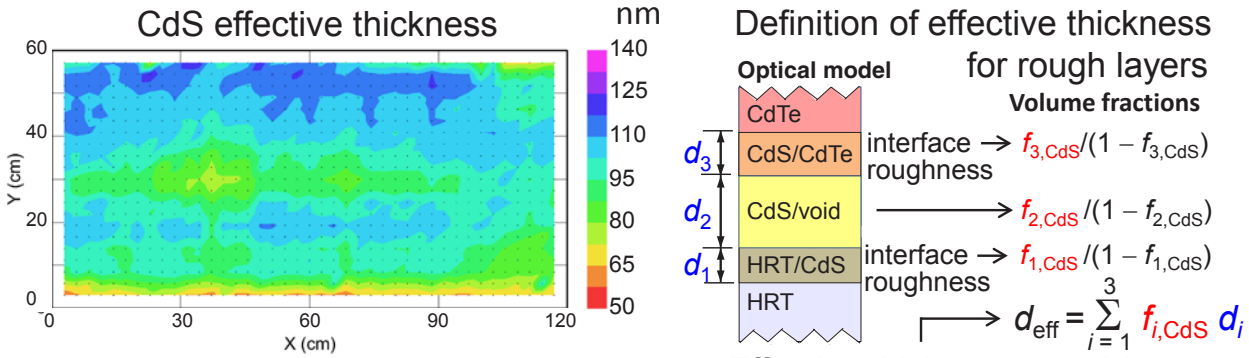

Preproduction TEC/HRT/CdS/CdTe panel provided by: K. Kormanyos, Calyxo USA

Figure 3: Map of CdS effective thickness obtained simultaneously with the Figure 2 stress map.

Project Title: Improving the Speed and Calibration of Water Vapor Transmission Rate (WVTR) Measurements

PI: Matthew O. Reese
E-mail: matthew.reese@nrel.gov

Summary:

This project has developed water vapor transmission rate (WVTR) standards from 0.1 to 10^{-6} g/m^2/day and validated the approach with two independent test methods (NREL's electrical calcium test and MOCON's Aquatran). Previously, no standards were available below 10^{-2} g/m^2/day, even though PV quality moisture barriers require steady state WVTR levels below 10^{-4} g/m^2/day. Furthermore, the group has been identifying routes to speed measurements of high moisture barriers, which can take weeks to months.

Key Accomplishments:

Moisture is well-known to speed the degradation of photovoltaics (PV). PV quality barriers require moisture to be kept out of a module for 20 or more years. Barriers allowing a transmission of 10^{-4} g/m^2/day, would allow the equivalent of ~700 nm thick layer of water over 20 years. For devices with layers a few microns thick, this is clearly too much moisture. Defining and then measuring an acceptable level of moisture ingress, has historically been a challenge. No reference films or standards exist to validate measurements below 10^{-2} g/m^2/day. A variety of barrier materials are being produced and sold by industry, however, with WVTR below 10^{-2} g/m^2/day. While methods have been developed that can measure in this range, calibrations require measurements at high WVTR rates and extrapolating to lower ranges. This may lead to measurement errors or biases that cannot be recognized without standards in the lower ranges. None of these barriers can serve as such standards as they are defect dominated, with no good way of measuring their defect density other than through WVTR measurements.

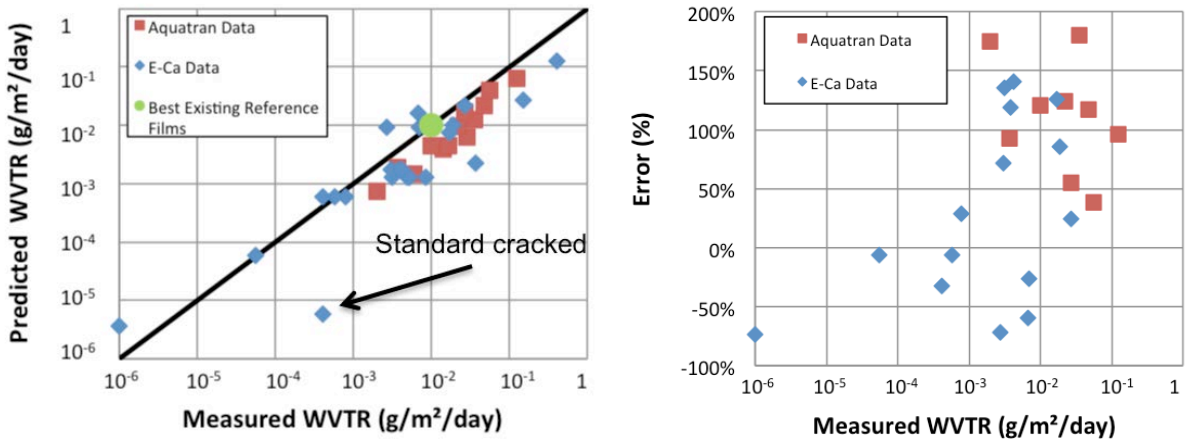

Figure 1: (Left) Predicted WVTR vs. measured WVTR using two independent techniques (NREL's e-Ca test and MOCON's Aquatran). Standards have been demonstrated over five orders of magnitude. (Right) Error between measured and predicted. Most samples, especially with NREL's e-Ca test, are within a factor of two of the predicted value.

This project has developed a method for fabricating water vapor transmission rate (WVTR) standards that is useful over many decades of sensitivity. The method consists of embedding a capillary of known dimensions in an impermeable material such as glass or metal. The capillary is bonded in an impermeable manner using solder or glass frit. Afterwards the capillary is filled with a Fickian polymer with known transport properties. By adjusting the length and diameter of the capillary, moisture transport can be predictably calibrated at various temperatures and humidity ranges.

Figure 1 shows a series of measured values compared to the predicted values as well as measured error from the predictions. Two separate measurement methods were used to obtain this data, the isostatic method (MOCON's Aquatran) and a scavenger method (NREL's e-Ca test). The data suggest that, at present, all measured values are good to within about a factor of two. The group is presently investigating the source of the existing scatter.

The establishment of these standards also generated samples with predictable transients at low transmission rates. By using a Fickian polymer filler material such as polydimethylsiloxane (PDMS), transients for even extremely low transmission rates can be hours to about a day. Having standards with low WVTR values is also enabling for investigations into the cause of measurement-related transients. Figure 2, shows an example of these measurement-related transients for a reference film with high WVTR (~0.1 g/m^2/day). While steady state measurements may ultimately be the same, the time to reach the steady state can vary between measurements. Typically, transients observed for low WVTR measurements take 100 or more hours. Ultimately this work will allow faster measurements by identifying the source of these transients and potentially will allow predictions in quality control situations. At present, the source of some of the measurement transients identified include intermetallic formation between the Ca sensor and "inert" electrode and different surface area of spacers due to surface finish.

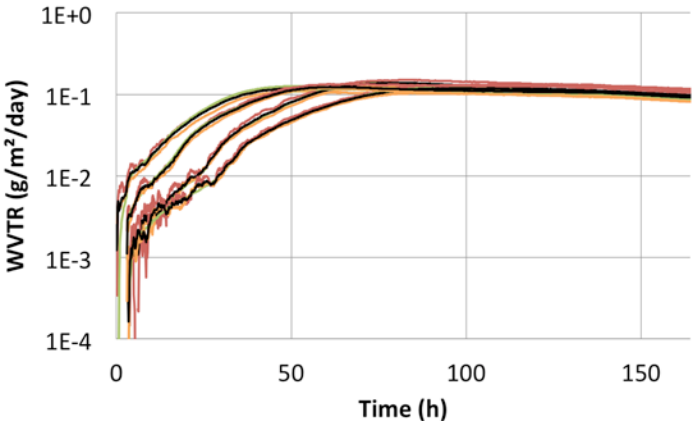

Figure 2: Three independent measurements of same reference film (Aclar) measured at 45˚C/85% R.H. While the steady state WVTR is the same, the transients are not.

Future Work:

Future work will allow a reduction of the measurement error to less than a factor of two between predicted and measured values from WVTR standards. Ultimately, it should be possible to increase confidence to another decimal place (i.e. ~10-20% error). Furthermore, the approach can be used to pair WVTR standards with PV cells/modules to establish threshold requirements for barriers. Additional work will also reduce transients in electrical calcium measurements.

BAPVC Annual Project Report

Project Title: Composite Encapsulation Layers
PI: Jeffrey Urban
E-mail: jjurban@lbl.gov

Summary:
Highly transparent hybrid films based on a water-scavenging metal-organic framework (MOF) and a hydrophobic polymer cyclic olefin copolymer (COC) were made and tested as advanced barrier layers. The incorporation of MOF Nanocrystals (NCs) into the polymer leads to a 10-fold decrease in water vapor transmission, all while maintaining an outstanding transparency over most of the solar spectrum. **(*ACS Appl. Mater. Interfaces*, 2016, 8, 10098–10103)** The group has also developed Graphene Oxide (GO) Composite films based on a simple solution deposition process to continue the strategy achieving better, easier, and cheap materials to displace current options.

Key Accomplishments:
The group has developed highly transparent hybrid films based on a water-scavenging metal-organic framework (MOF) and a hydrophobic polymer (cyclic olefin copolymers, or COC). The incorporation of Metal Organic Framework (MOF) Nanocrystals (NCs) into the polymer leads to a 10-fold decrease in water vapor transmission, all while maintaining an outstanding transparency over most of the solar spectrum. This hybrid encapsulant should offer exceptional barrier performance, mechanical stability, and transparency at lower cost and is schematically shown in **Figure 1.**

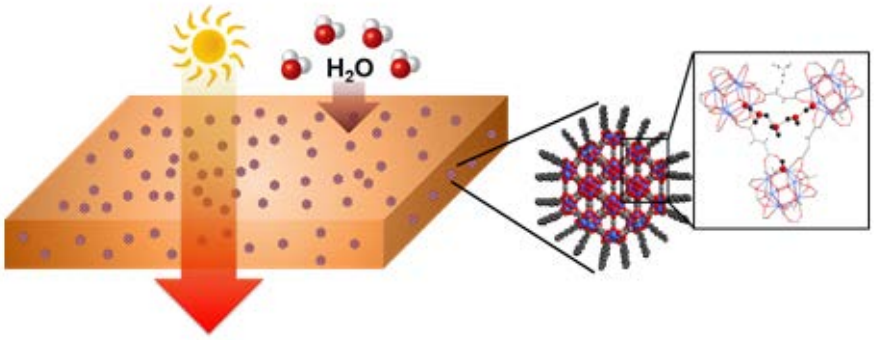

Figure 1. An illustrative cartoon of a hybrid film comprised of the COC polymer matrix and the water scavenging MOF

We have continued to further pursue work on functionalization of the hygroscopic inorganic NC MOF and achieve polystyrene (PS) functionalized MOFs with even better performance. So far, we have observed promising initial results- great stability in toluene for months shown in **Figure 2**. We will use this platform for further study on low-cost, low-temperature polymer and specially designed MOF systems.

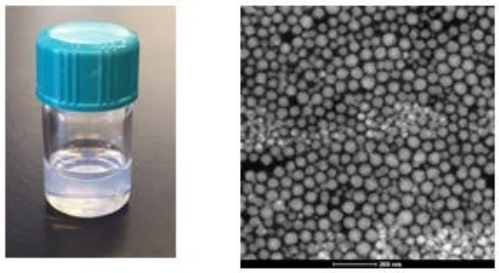

Figure 2. (left) Photograph of polystyrene functionalized MOF after dissolving MOF in toluene for months; (right) SEM images of polystyrene functionalized MOF

An in-situ polymerization method was adapted to synthesize Graphene Oxide (GO) nanosheets with covalently grafted polystyrene (PS) brushes. (Fig. 3) The achieved materials could be dissolved in hydrophobic solution and coated on substrate via solution-based deposition shown in Figure 3. The grafted polymer brushes can not only insure the solubility of GO composite films in organic solvent, but also enhance the protection against water and oxygen. The resulted composite film showed excellent transparency, making it a promising material for encapsulation.

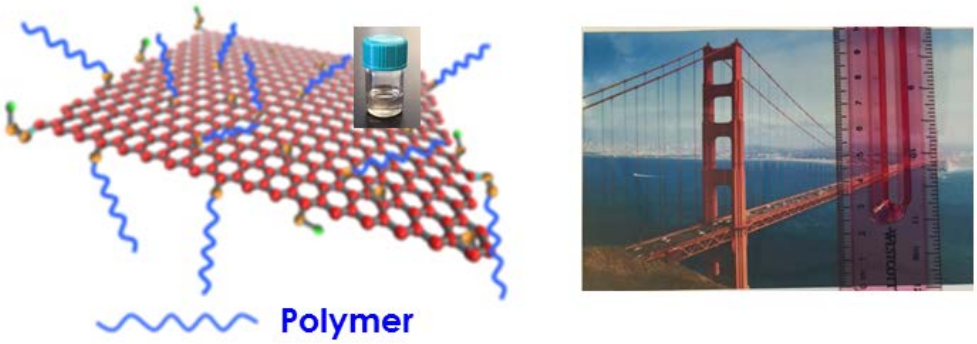

Figure 3. (left) Scheme of Graphene Oxide nanosheets with covalently grafted polymers Red: Carbon, Yellow: Oxygen, Green: Hydrogen, Blue: Grafted Polymer Insert: Photograph of PS-GO dispersed in toluene; (right) Photograph of PS-GO composite films showing transparency.

Future Work:

The group will continue to study the COC/MOF hybrid films by investigating bonding/failure mechanisms in collaboration with Professor Dauskardt at Stanford University. The film has been adapted on coating the semiconducting polymers (P3HT, PCDTBT) from Professor Salleo' s group. Further study will be focused on testing the FTPS of the devices with and without encapsulation for better understanding how the barrier can increase the stability of semiconducting polymers. WVTR of GO based films will be tested to continue our strategy achieving better, easier, and cheap materials.

BAPVC Annual Project Report

Project Title: Understanding and Improving Durability of Organic Photovoltaic Materials
PI: **Sue A Carter**
E-mail: sacarter@ucsc.edu

Summary: Our project was focused on developing methods and models to understand and quantify the durability of organic materials used in photovoltaic modules. These materials included organic adhesion or encapsulation materials and perovskites. For the encapsulation materials, aliphatic TPU had the longest lifetimes (>20 years with no yellowing) but EVA combined with PET yielded similar performance at substantially lower cost. MAPbI3 perovskite materials were found to be stable under light in oxygen/moisture free environments, and PV's made from $MAPbI_3$ were furthermore shown to have greatly enhances stability when TPU was used as an encapsulent.

Key Accomplishments:

The ability of encapsulation materials to limit degradation of PV cells were tested by adding a dye, namely Red Lumogen LR305, to the encapsulant and testing how the PL and the absorption of that dey changes under different accelerated aging conditions . As can be observed in **Fig 1**, both TPU and EVA/PET with UV absorbers performed well unde 15 years of accelerated aging, but EVA with no UV absorbers rapidly failed. This was due to degradation of the polymer host that occurs in a narrow UV window between 360 and 390 nm. Encapsulants that filter out solar irradiation at energies above 400 nm are sufficiently to achieve encapsulation stability, leading to only a small reduction in power efficiency. Lifetimes exceeding 20 years were achieved for LR305 in a PMMA host with UV absorbers under solar irradiation condition and ambient (air) conditions. A Photothermal Deflection Spectroscopy technique optimized for UV-absorbing encapsulation materials was further developed so that early states of the degradation process, resulting in absorption from mid-gap states, could be evaluated as an early detection for aging in encapsulation materials.

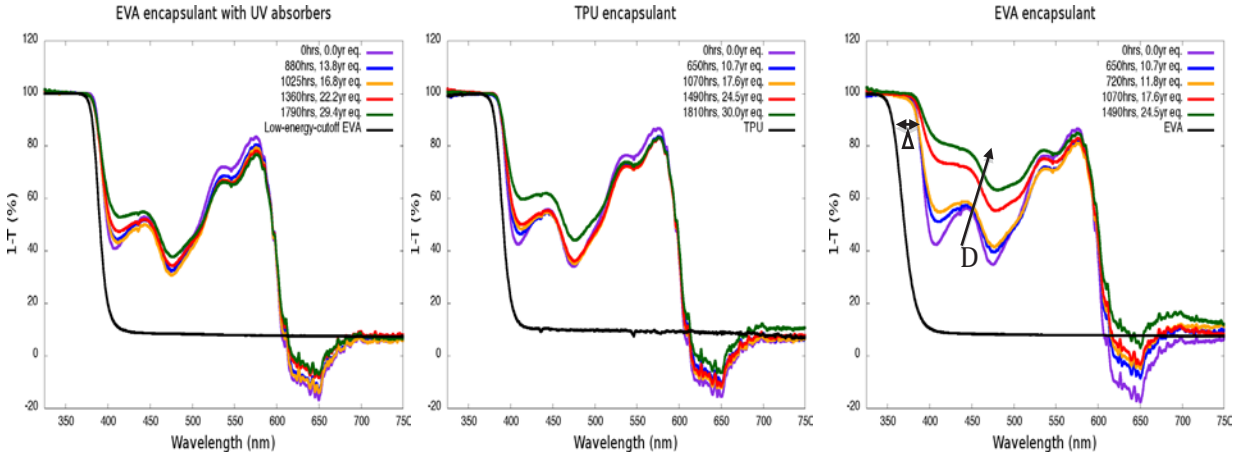

Fig 1: Combined Absorption and Photolumiescence (observed as negative absorption) for different encapsulation materials.

Under dry conditions, the perovskites based on ($MAPbI_3$) were shown to degrade only in the presence of both light and oxygen (they are stable in the absence of oxygen), which together induce the formation of halide anions that generate free radicals which deprotonate the methylammonium cation (**Fig. 2**) and form the highly volatile CH_3NH_2 molecules that escape and leave pure PbI_2 behind. Significant fractions of locally ordered PbI_2 were observed in perovskite films prepared on TiO_2, even when XRD revealed no PbI_2. Finally, perovskites solar cells based on $MAPbI_3$ were shown to be considerably more stable under encapsulation with the TPU films identified above due to the reduction in catalytic activity at the TiO_2 surface[1]; however, degradation leading to device failsure still occurs if temperatures exceed 60 ^oC.

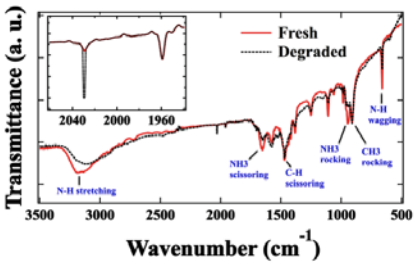

$$CH_3NH_3PbI_3 \rightleftarrows PbI_2 + CH_3NH_3I,$$

$$2CH_3NH_3I + \frac{1}{2}O_2 \xrightarrow{h\nu} 2CH_3NH_2 - H_2O + I_2,$$

$$CH_3NH_3I + CO_2 \xrightarrow{h\nu} CH_3NH_2 + HCO_2 + \frac{1}{2}I_2.$$

Fig 2: FTIR showing amine forming and degradation route for $MAPbI_3$ in dry air.

Future Work:

Our future work will be focused on evaluating degradation mechanisms and routes to improving durability and reducing cost of encapsulation and backsheet materials used in PV packaging. Measurements to be used for these studies include photothermal deflection spectroscopy, FTIR, and high resolution HRSTEM, to study absorption by mid-gap states, chemical changes in the organic material, and microcrack formation, to compliment mechanical and adhesion measurement taking by our collaborators. A variety of common and newer encapsulation and backsheet materials, with different amounts and types of UV absorbers, will be studied to quantify degradation rate for these different materials. Impact of the more stable packaging materials on overall PV efficiency and cost will also be evaluated. The goal will be to determine the early-stage degradation mechanisms for encapsulation materials and develop a path forward to increase lifetime and reduce cost (by ~20%), while maintaining or improving overall module power efficiency.

[1] G. Abdelmageed, L. Jewell, K. Hellier, L. Seymour, B. Luo, F. Bridges, J. Z. Zhang, and S. A. Carter, Mechanisms for Light Induced Degradation in MAPbI3 perovskite thin films and solar cells, Applied Physics Letter, 2016 (in press).

BAPVC Annual Project Report

Project Title: Tailoring Electrostatic Interactions to Produce Hybrid Barrier Films for Photovoltaics
PIs: Bernard Kippelen and Samuel Graham, Georgia Institute of Technology
E-mail: kippelen@gatech.edu; sgraham@gatech.edu

Summary:
In this program, the Kippelen/Graham groups at Georgia Tech have developed barriers coatings using a combination of vacuum deposition methods (PECVD and ALD) that were tested on various photovoltaic systems ranging from crystalline Si to organic photovoltaics. Encapsulation of devices has been achieved by using either a direct deposition process of the barrier layers onto the device or by using indirect methods where the barrier is laminated to the device structure. During the past year, barriers with various structures including ALD nanolaminates, and PECVD/ALD hybrid structures have been studied and characterized in terms of effective water vapor transmission rate measured during damp heat testing. All of these structures were tested using optical Ca tests. High performance was achieved through control of the mechanical properties and film architecture.

Key Accomplishments:
Development of Hybrid Multilayer Barriers deposited at Room Temperature for Direct Encapsulation of Photovoltaics
The direct encapsulation of organic photovoltaics was investigated through the use of barrier layers deposited near *room-temperature* by plasma-based techniques, namely plasma enhanced-chemical vapor deposition (PE-CVD) and plasma assisted-atomic layer deposition (PA-ALD). The objectives of these studies were to: (i) develop a better understanding of the infiltration of PA-ALD precursors used for the deposition of TiO_2 and Al_2O_3 films within the free volume of the polymeric bulk heterojunction as a function of process temperature and organic layer morphology; (ii) develop a rational strategy for the design of multilayer barriers synthesized at near room temperature by PA-ALD and PE-CVD; and (iii) study the shelf stability of directly encapsulated organic polymeric photovoltaic devices in air.

The PA-ALD layers were deposited directly on P3HT:ICBA films and on Si wafers, used as reference at a temperature as low of. Layers of TiO_2 and Al_2O_3 with a thickness of 20 nm were deposited by means of PA-ALD on top of P3HT:ICBA layers at different temperatures (30 - 80 °C) and on films with various morphologies and free volume. XPS depth profile measurements were performed in order to study the depth of penetration of the precursors used for the deposition of the oxide barrier layers by PS-ALD. The smaller dimension of the precursor trimethylaluminium (TMA) used to grow alumina compared to the precursor tetrakis(dimethylamino)titanium (TDMAT) used to grow TiO_2 films allows a deeper penetration of the former within the organic matrix, creating an intermixed hybrid interface between the two materials. The penetration is enhanced at higher temperature, suggesting an increased diffusivity together with a pore broadening in the organic layer.

Next a barrier structure comprising TiO_2 (10 nm)/Al_2O_3 (30 nm)/SiN_x (400 nm/Al_2O_3 (10 nm)/TiO_2 (10 nm) processed near room temperature was engineered in order to efficiently

encapsulate organic photovoltaic devices (OPV) with general structure ITO/PEIE/P3HT:ICBA/MoO_3/Ag, as shown in Figure 1. The TiO_2 and Al_2O_3 layers were processed at 30 °C using PA-ALD and SiN_x at 25 °C ICP PE-CVD. The shelf lifetime at room temperature was then monitored over a period of 1,400 h. Pristine OPVs and devices after encapsulation, after an air exposure of 6 h, were found to display statistically identical performance with average open circuit (V_{OC}) values of 765 ± 4 mV, average short–circuit current density (J_{SC}) values of 9.0 ± 0.5 mA/cm^2, average fill-factor (FF) values of 0.44 ± 0.02 yielding average power conversion efficiency (PCE) values of 3.0 ± 0.3% under 1 sun of simulated AM1.5 solar illumination. Figure 1 shows displays the evolution of the photovoltaic parameters as a function of time exposed to air and under room-light conditions. OPV devices display an average degradation of their PCE values of 12% after 1,400 h in air. Remarkably, the best device (shown by the dashed line in Figure 1) exhibits unchanged (within statistical variations) PCE values after 1,400 h in air. Although statistically the PCE values displayed by this device lie beyond one standard deviation from the average PCE values on the set of samples studied, the stability of this device reveals the potential for the proposed multilayer barrier design to yield OPVs with excellent stability if defects can be avoided during fabrication.

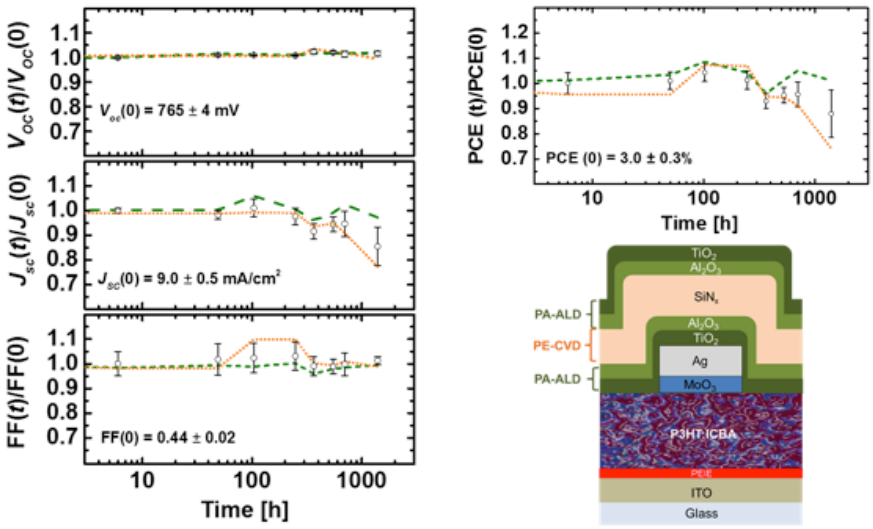

Figure 1. Average values (symbols) and standard deviation (error bars) of normalized photovoltaic performance parameters of 6 encapsulated OPVs as a function of time exposed to air. Dash lines and dotted lines represent temporal evolution for the best and worse OPV device, respectively. Bottom-right panel is a schematic of an encapsulated OPV device.

These results show the viability of room temperature deposited barrier in ensuring long-term device performance and can be considered an important step forward toward the realization of low cost and low energy encapsulation of organic photovoltaics and potentially other photovoltaics material platforms.

Future Work: Future efforts will build on previous successes of our ALD and PECVD based barrier films to package perovskite solar cells (work underway with 3M, NREL, CSIRO) and to study the mechanical reliability of the barriers when integrated into PV module architectures. These experiments will include adhesion and fracture dynamics to predict module reliability.

BAPVC Annual Project Report

Project Title: A Multiscale, electro-thermal-optical Reliability Framework: PVRelExpert to predict Corrosion and PID Degradations for Promising early stage BAPVC Technologies
PI: Muhammad Ashraful Alam
E-mail: alam@purdue.edu

Summary:

The group has developed a physics-based electro-thermal-optical modeling framework (PVRelExpert) to predict the implications of PID, corrosion, and delamination on module performance. The framework developed can be easily adapted to explore other reliability issues, such as yellowing and cracking. The issues can be studied either as individual modes or as correlated degradation processes. This predictive forward modeling capability has enabled a transformative capability of inverse modeling of solar farms so that one can predict the lifetime of solar cells at any geographic location in the world and adapt module design for local weather conditions.

Key Accomplishments:

PVRelExpert uses module structure, material constants, environmental conditions, physics-based, technology-specific compact model for a solar cell to predict the performance/lifetime of solar module and solar farms. Fig. 1 shows an example of the performance prediction of a solar module under test condition where PID-induced stress and moisture-induced corrosion are the main degradation mechanisms. The model accounts for temperature activated moisture diffusion, generation of acetic acid, and acid-induced metal corrosion/delamination, degradation of series resistance, and finally time-dependent loss of power output. One of the most important feature of PVRelExpert is its ability to account for spatial distribution of degradation. Specifically, spatially resolved temperature profile identifies degradation susceptible regions (see Fig. 2) and the simulation of fully interconnected module precisely predicts overall degradation of cell performance. A simulator, such as PVRelExpert will identify geography-specific design challenges – the modules in hot-humid regions of India must be defined differently than the hot-dry regions of Africa. Therefore, PVRelExpert will be useful for calibrating test protocol using simulation results and field performance data as shown in Fig. 3.

Future Work:

In collaboration with BAPV partners in industry, national labs, and academia, we anticipate generating PVRelExpert in three important ways:

1) Include other physics-based degradation modes (e.g. yellowing, cracking, etc.) so that we can predict the correlated degradation of solar modules.
2) Couple PVRelExpert with world-wide weather information so that we can predict the performance of the any new solar cell technology across the world.
3) Use PVRelExpert as an inverse modeling tool to predict the lifetime of existing farms and use the information to help manufacturers to improve climate-aware cell design.

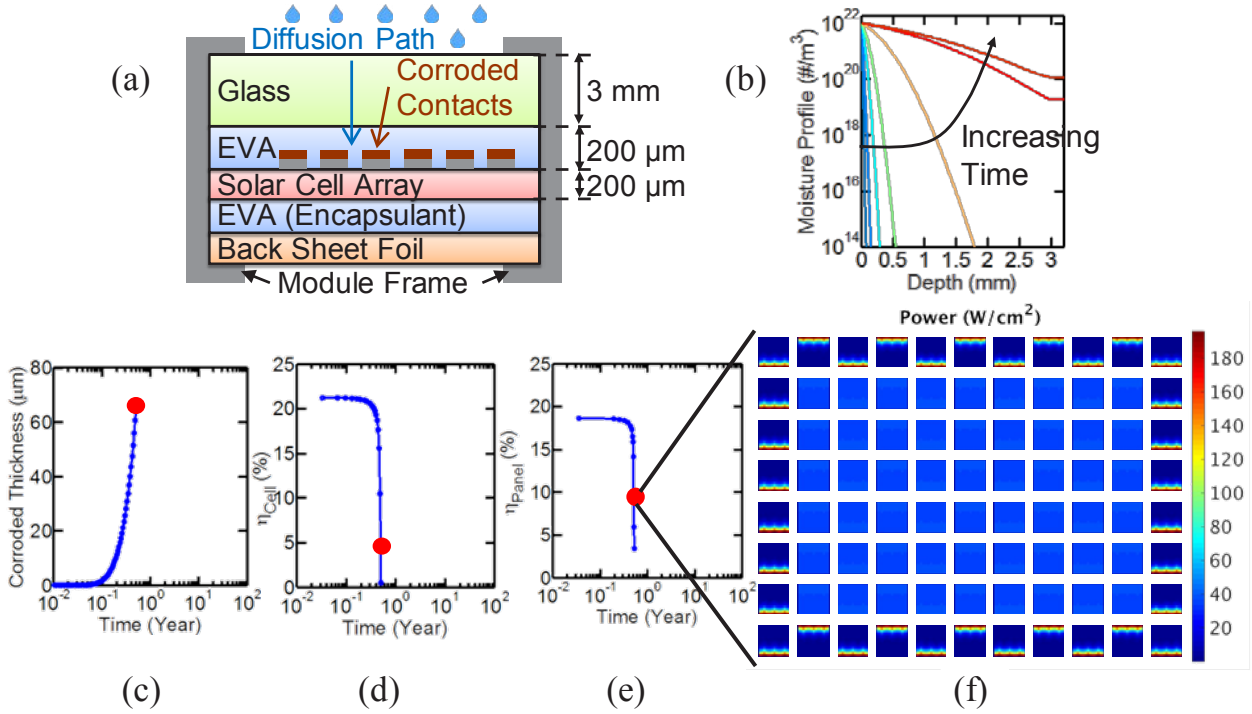

Fig. 1. Prediction of performance of a module undergoing corrosion in 85C, 85% relative humidity condition. (a) Structure of module and moisture diffusion path (b) Moisture profile at interface of corroded contacts and EVA (encapsulant) (c) Corroded Thickness, (d) Cell level performance, (e) module level performance as a function of time (f) Spatially resolved output power of module.

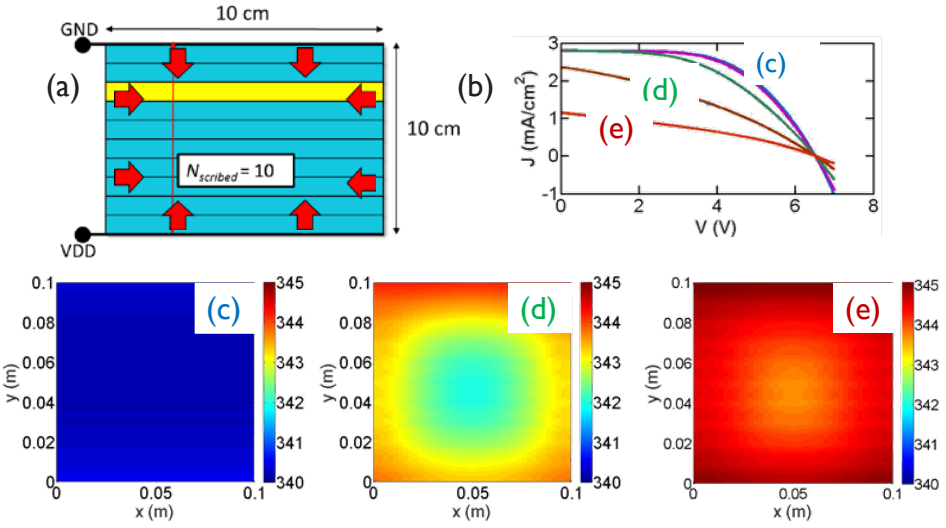

Fig. 2. Spatially resolved temperature profile identifies degradation susceptible regions. (a) Geometry of module, arrows indicate the corrosion direction (b) Evolution of J-V curve in time (c), (d), (e) Spatially resolved temperature profile of module.

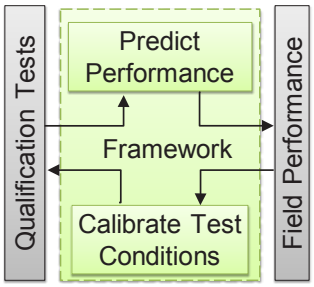

Fig. 3. Interaction of framework with tests and field data to help modifying the tests

References

H. Tsai, W. Nie, J.-C. Blancon, C. C. Stoumpos, R. Asadpour, B. Harutyunyan, A. J. Neukirch, M. A. Alam, G. Gupta, J. Lou, P. M. Ajayan, M. J. Bedzyk, M. Kanatzidis & A. D. Mohite "High-efficiency two-dimensional Ruddlesden–Popper perovskite solar cells." Nature 536, no. 7616 (2016): 312-316

P. Bermel, R. Asadpour, C. Zhou, and M. A. Alam, "A modeling framework for potential induced degradation in PV modules," SPIE Conference, 2015, vol. 9563, p. 95630C–95630C–8.

"Physics-Based computational modeling of moisture ingress in solar modules: Location-specific corrosion and delamination, " R Asadpour, RVK Chavali, MA Alam, Photovoltaic Specialists Conference (PVSC), 2016 IEEE 43rd, 0840-0843.

"Optimum filler geometry for suppression of moisture diffusion in molding compounds," W. Ahn, S. H. Shin, R. Asadpour, D. Varghese, L. Nguyen, S. Krishnan and M. A. Alam, IEEE International Reliability Physics Symposium , 2016.

Reza Asadpour, Raghu V. K. Chavali, M. Ryyan Khan, and Muhammad A. Alam, "Bifacial Si heterojunction-perovskite organic-inorganic tandem to produce highly efficient (ηT* ~ 33%) solar cell," *Appl. Phys. Lett.*, vol. 106, no. 24, p. 243902, Jun. 2015.

X. Sun, R. Asadpour, W. Nie, A. D. Mohite, and M. A. Alam, "A Physics-Based Analytical Model for Perovskite Solar Cells," *IEEE J. Photovolt.*, vol. 5, no. 5, pp. 1389–1394, Sep. 2015.

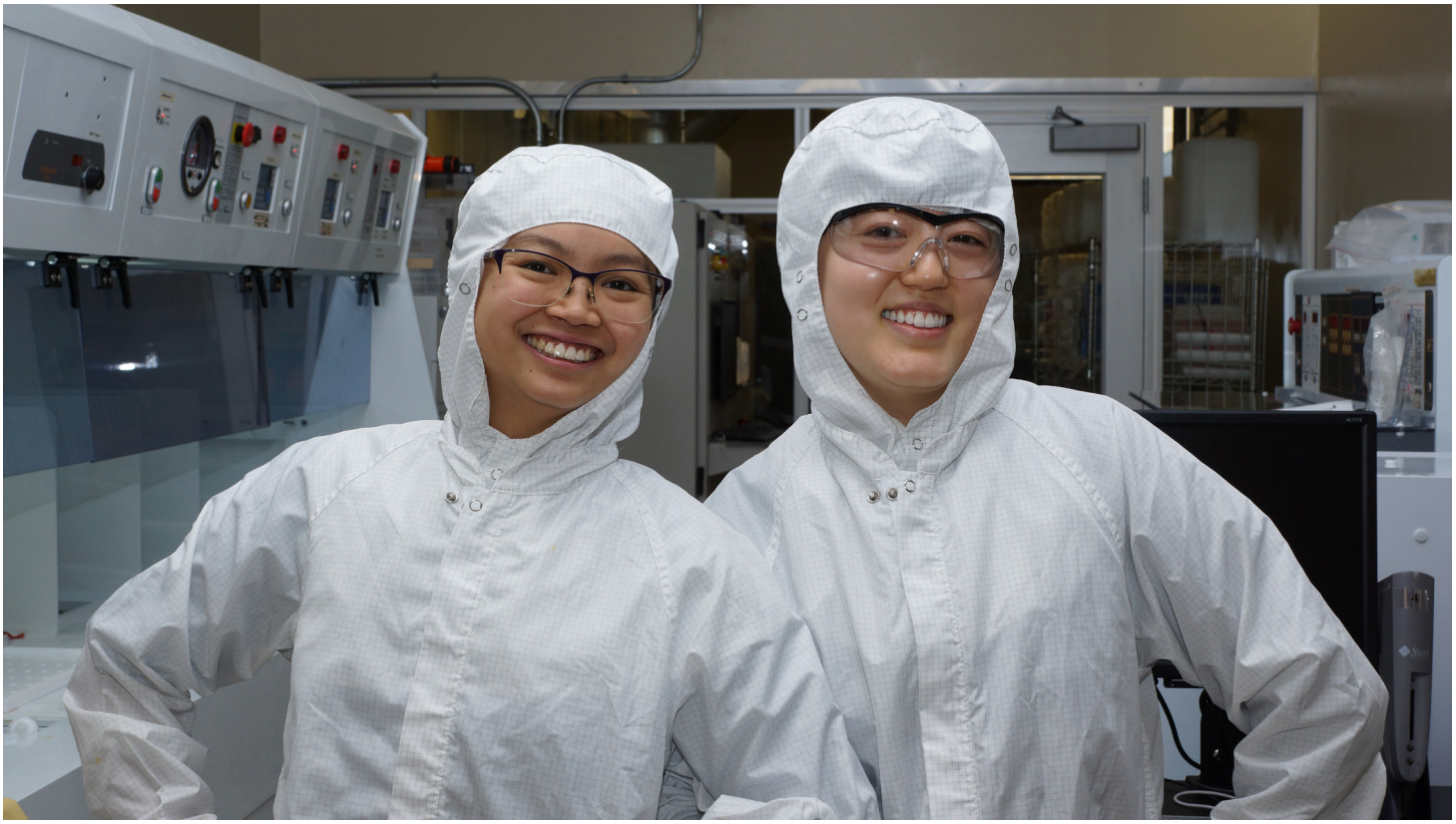

Bay Area Photovoltaic Consortium

McCullough Building

476 Lomita Mall

Stanford, CA 94305-4045

http:/bapvc.stanford.edu